STUDY OF PETROPHYSICAL PARAMETERS AND MULTIPHASE FLOW BEHAVIOR OF POROUS MEDIA

Submitted by:

Jam Muhammad Kashif

2012-MS-PET-06

Submitted to:

Dr. Muhammad Khuram Zahoor

Associate Professor

DEPARTMENT OF PETROLEUM & GAS ENGINEERING
UNIVERSITY OF ENGINEERING & TECHNOLOGY LAHORE
PAKISTAN

2017

Dedication

In the name of *ALLAH*, I bear witness that there is no god but *ALLAH*, the Lord of all Worlds.

I dedicate this dissertation work to my beloved parents for their unending care and encouragement. I also dedicate this research work to my teachers, without their guidance, it would not have been able to do this.

Acknowledgment

First, I would like to thank Almighty Allah for His countless blessings and compassion, who gave me the strength for the completion of this work.

I wish to thank my supervisor Dr. Muhammad Khurram Zahoor, who helped me in this research work and write-up. I also acknowledge for his countless hours of reflecting, reading, encouraging, and most of all patience throughout the entire process.

I would also like to thank OGDCL for their kind support.

Abstract

Datta sandstone of Potwar Sub-basin of Pakistan has significant role with reference to hydrocarbon potential. The fields of Toot, Meyal, and Dhulian produces around 1500 million barrels of oil. Datta formation is disseminated in the western part of Salt Range in Surghar, Shinghar, Shaik Budin Hills in Marwat Range and western Khisofr Range. Datta formation is also present in Kala-Chitta, Hazara and Samana Ranges. Due to the complexity of Datta formation, it is important to investigate/ evaluate its petrophysical characteristics and multiphase fluid flow behavior. In this study petrophysical properties were estimated and later, correlations have been developed between core and log data. Further, the porosity and permeability maps have been generated, which are used for flow rate calculations.

Petrophysical study through wireline log interpretations and lab analysis has produced conclusive results for evaluation of hydrocarbon potential in the formation. Porosity map show trend of porosity which ranges from 0.324% to 20%. Permeability map shows the trend of permeability which ranges from 0.0035 md to 1284 md. This study shows that, for per unit pressure drop, flow rate ranges from 2.95 to 790 (cc/sec) for oil and 1.56 to 347 cc/sec for gas.

Nomenclature

A = Core sample cross-sectional area, cm^2

a = Factor of Tortuosity

a = F and ϕ plot intercept

b = Gas constant for specific type of porous media

F = Factor of formation resistivity, R_o/R_w, fraction

GR_{log} = Formation gamma ray values API

GR_{min} = Gamma ray minimum values (clean sand or carbonate) API

GR_{max} = Gamma ray maximum values (shale) API

h= Height of capillary, cm

I_{GR} = Index of gamma ray API

k = Core sample permeability, md

K_L = Liquid permeability, md

K_g = Gas permeability, md

K_a = Air or gas permeability, Darcy's

L = Length of core sample, cm

m = Exponent of cementation

n = Exponent of saturation, slope of RI versus S_w plot

p_1 = Pressure of fluid at upstream, psig

p_2 = Pressure of fluid at downstream, psig

p_a = Atmospheres absolute pressure, psia

P_{nw} = Non-wetting phase pressure, psi

Pw = Wetting phase pressure, psi

P_1 = Initial reference volume absolute pressure, psia

P_2 = Extended absolute pressure, psia

P_a = Sample chamber initial absolute atmospheric pressure, psia

p = Average pressure flowing through the porous media, psia

p_1 = Pressure at initial reference volume, psig

p_2 = Pressure at final system, psig

P_b = Standard reference pressure for mass flow meters,= 1.00 atmospheric

Q_b= Volumetric flowrate referenced to Pb, cubis centimeters per second

q = Fluid flow rate, cm^3/sec

q_a = Absolute pressure at gas flow rate, cm^2/s

R_w = Resistivity of formation brin, ohmmeters

R_t = Formation true resistivity, ohmmeters

R_o = 100% brine saturated core sample true resistivity, ohmmeters

R_w = Formation water resistivity, ohm-meters

R_t = Resistivity of deep log values generates through True formation resistivity, ohmmeters

r_1, r_2 = Radii of curvature of interface, cm

r_t= Radius of capillary tube, cm

S_w = Brine saturation in formation, fraction

T_{1r} = Reference volume absolute temperature at $P_{1,}$ ^oC

T_{1c} = Sample chamber absolute temperature at $P_{1,}$ ^oC

T_{2r} = Reference volume absolute temperature after P_2 is steadied, ^oC

T_{2c} = Sample chamber absolute temperature after P_2 is steadied, ^oC

U = Viscosity, centipoises, of gas at its average flowing temperature and pressure in core

V_g = Volume of grain, cc

V_c = Volume of sample chamber, cc

V_r= Volume of reference chamber, cc

V_v = Volume through valve displacement (at closed to open position), cc

z_1 = z-factor of gas at P_1 and T_1

z_2 = z-factor of gas at P_2 and T_2

z_a = At T_1 and atmospheric pressure z-factor of gas

$\Delta\rho$ = Difference in wetting and non-wetting phase density, kg/m3

ϕ = Porosity of core sample, fraction

ϕ_{Sonic} = Porosity of sonic log , fraction

$\phi_{Density}$ = Density derived porosity, fraction

Δt_{matrix} = Travel time of interval in matrix, ft/sec

Δt_{log} = Travel time of interval in formation, ft/sec

Δt_{fluid} = Travel time of interval in formation fluid, ft/sec

ρ_{matrix} = Matrix density, g/cm^3

$\rho_{bulk(log)}$ = Log values of formation bulk density, g/cm^3

ρ_{fluid} = Density of fluid, g/cm^3

μ = Fluid flowing viscosity, centipoise, Cp

Table of Contents

List of Figures

List of Tables

Chapter 1 : Introduction

1.1 Introduction

Datta sandstone of Potwar Sub-basin of Pakistan plays a significant role for hydrocarbon potential. The fields of Toot, Meyal, and Dhulian produce around 1500 million barrels. Datta formation is disseminated in the western part of Salt Range in Surghar, Shinghar, Shaik Budin Hills in Marwat Range and western Khisofr Range. Datta formation is also present in Kala-Chitta, Hazara and Samana Ranges. The lithological study of Datta formation (Jurrasic) represents that it consists of sandstone with a streak of shales. Datta Sandstone has essential characteristics and acts as a source and reservoir rock. Datta formation has been confirmed as proven reservoir by previous exploration and research studies in Toot field of Potwar Sub-basin. The field is present in the Attock District of Punjab Province in northern Pakistan. The aerial extent of this field covers 122.67 km^2. The field was discovered in 1968 and in year 1986, production of Toot field reached up to 2400 barrels of oil per day, with 12% to 15% recoverable resource, this area contains 60 million barrels oil as probable.

Due to the complexity of Datta formation, it is important to evaluate its petrophysical characteristics and multiphase fluid flow behavior. The objective of the study is to develop correlations of petrophysical parameters and porous media flow behavior for the Datta sandstone and use these correlations to suggest development options increase the production rates. Understanding of fluid flow behavior through porous media has great importance and involvement of exploitation of hydrocarbon. Significant technical applications related multiphase flow and multicomponent displacement in porous media occur in the petroleum industry. Multiple flowing phases naturally exist in hydrocarbon reservoirs.

1.2 Problem Statement

Petrophysical and fluid flow behavior of Datta formation of different wells/location will be useful to conclude the fluid rock physics and fluid flow behavior of porous media. Petrophysical study through wireline log interpretations and lab analysis has produced conclusive results for evaluation of oil and gas potential in the formation. Similarly, fluid flow behavior of the formation will be evaluated through relative permeability, capillary pressure, and resistivity analysis. Rock-fluid properties will help to understand reservoir behavior of Datta formation in different wells/location.

1.3 Objectives of the Study

In this study, rock-fluid characteristics, fluid behavior and the hydrocarbon potential of Datta formation will be evaluated.

a. To investigate the petrophysical characteristics of Datta formation.
b. To develop correlation between core and log data
c. To predict/investigate the trend of petrophysical properties of Datta formation.
d. To investigate the fluid flow behavior of Datta formation.

1.4 Methodology

1.4.1 <u>A brief description of research flow:</u>

The research will be carried out by going through the following phases:

1. Literature Review.
2. Collection of wireline log and core data from OGDCL/and other sources
3. Interpretation of wireline log data through commercial software
4. Integration of core and log data for establishing correlation
5. A study of Oil-water and Gas-oil Relative permeability analysis
6. A case Study of Multiphase Fluid Flow Through Porous Media
7. Results and discussions.
8. Conclusions and recommendations.

1.4.2 <u>Theoretical studies</u>

Theoretical studies will be carried out in the light of the literature. References are given at the end of this proposal summary and extending the knowledge by including more references while conducting these studies.

1.5 Utilization of Research Results/Expected Results

This study will establish petrophysical trend and correlations of Datta formation of Potwar Sub-basin of Pakistan. Fluid flow through porous media will develop the better understanding to increase both the production rates and reserves of the field. This study will give better insight for conducting simulation studies in future. Effect of various parameters (i.e. porosity, permeability, relative permeability and capillary pressure) will also be checked. Successful studies may help to improve the modeling and designing of surface production facilities, tubing design. In fact, the Formation has an excellent potential for hydrocarbons. Therefore their applications will be helpful for the future exploration of petroleum.

Chapter 2 : Geology and Petroleum System

2.1 Geological Setting

The study zone lies in the Kohat-Potwar geological region, a part of upper Indus basin figure (2-1). Upper Indus basin area bounds by Parachinar-Murree fault in the north and Surghar and the Salt Range thrust bound in the south. The borders of east and west area are set apart by the Jehlum and the Kurram fault accordingly. Partition of this area on the basis of tectonic can be described as Soan syncline, northern Potwar deformed zone, the Salt Range, the Kohat Plateau, the Bannu depression and the Trans-Indus ranges (Khan et al., 1986). Shallow continental shelf environment is composed of silica-bearing rocks and carbonate minerals (Wandrey, et al., 2004b). The late Proterozoic and the Salt Range Formation of the Precambrian spread over with organic-rich shales, sandstones, embedded carbonates as a basement of metamorphic rocks (Shah et al., 1977; Iqbal and Shah., 1980).

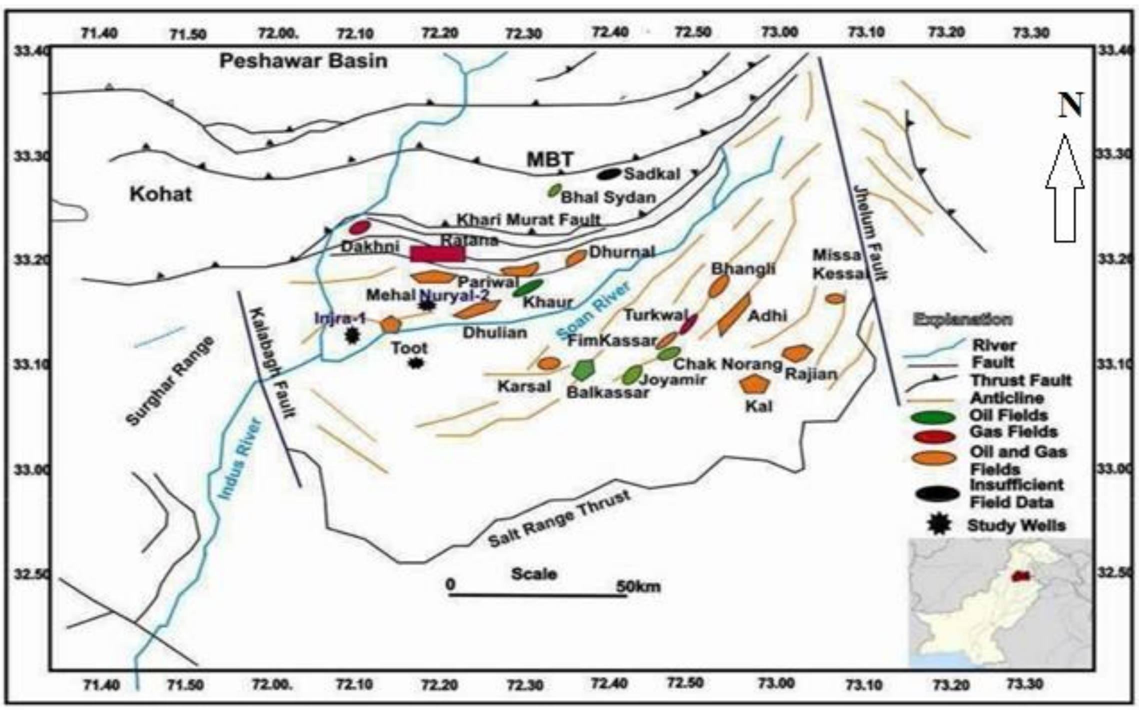

Figure 2-1: Study area geological and location map (modified after Raza., 1992).

The Datta Formation is the essential elements of the western Kala Chitta Range, comprising of the following complicated facies:

- Clays, claystone with subordinate bauxitic lenses within the Upper Part

- Quartzose sandstone, hematitic sandstone and ironstone in the bottom with laterite

Fireclay is present within the top of the Datta formation, and it includes these lithosome's (red ironstone to hematitic sandstone, white quartzite sandstone, white to gray and purple clay and bauxite) in a parallel pinch-out relationship. Vertically, the lithosome's have extraordinarily gradational to the broken relationship. The quartzose sandstone is overlain using white to cream clay with sand to silt-sized quartz grains inside the lower part. With the span of time, occasional quartzose sand over clay or of red sandstone with clay is not unusual. Ironstone to ferruginous sandstone has very current affiliation inside the subject region. (Muhammad Kaleem., 2005). Datta Formation (Jurassic) is chalky to darkened dullin frequently chocolate, solid, huge fine arranged, quartzose, fine to coarse grained, subangular to subrounded randomly micaceous with good visible porosity. On the other hand, Shale is gray to red chocolate, multicolored hard, brittle, noncalcareous, bituminous and carbonaceous with a mark of gymnosperm plants.

2.1.1 Structure

Toot structure is a lightly dipping pericline, with an aerial extent of 6x8 km^2. It has a comparatively steeper south-eastern flank (dipping angle of 6^o-7^o) and a very mild north-western flank (dips 2^o-3^o). Axis of the structure on ground runs from NE to SW and finally bends to the west. Updated seismic data shows that Toot structure at a depth of Eocene horizons is a latitudinal extending anticline in the choice to meridional one. Some N-S trending faults of small vertical and lateral extent additionally complicate the structure specifically to the west of the main fault.

2.1.2 Stratigraphy

By flush cutting, electronic logs and correlation of neighboring wells established the stratigraphic succession. Generally, all horizons drilled were according to geological drilling order with minor variations in thickness and depths. Stratigraphically two most significant unconformities have been encountered within the well or wells. Firstly, Datta formation of lower Jurassic is truncated unconformable due to Hangu formation of Paleocene. Secondly, Kohat formation of center Eocene is overlain at once through Fateh Jhang area of lower Miocene.

2.2 Petroleum System of Upper Indus Sub-basin

Potwar sub-basin has different ages. Total petroleum structures (TPS) arye shown in figure (2-2). These TPS are divided into Precambrian to Permian, Jurassic to Cretaceous, Eocambrian to Miocene and Paleocene to Eocene for exploitation of hydrocarbon reservoirs. It is complex to identify a specific boundary between two separate TPS due to the existence of large fault structures and distortion. Further, it may allow hydrocarbon to migrate from the source rock.

2.2.1 <u>Source Rock</u>

In the focused region of research, main source formations of hydrocarbon are Precambrian Salt Range, Nammal and Patala of Jurrasic and Paleocene age. However, some different capability source rocks have been playing a distinct part or role in the basin (Qadri, 1995).

2.2.2 <u>Reservoir Rocks</u>

The main reservoirs of the research area under consideration are Datta sandstone (Jurrasic) and Sakesser limestone (Eocene). Other sandstone and carbonates reservoir of Miocene, Paleogene, Jurrasic, Permean and Cambrian are deposited in this region (Shah et al., 1977; Iqbal and Shah, 1980). The thickness of lower Jurassic age is +115m and lithology data represent sandstone with a streak of shale.

2.2.3 <u>Traps and Seals</u>

The main hydrocarbon producers of Potwar Sub-basin to the current scenario are upturned faulted anticlinal fold, pop-up structures or traps of block faults. The research area shows that anticline characteristics observe the trend setting as east-northeast to west-southwest and about similar to the plate destruction region. In this area Shale of Datta, Chichali and Lumshiwal formation acts as a seal. (Jaswal et al., 1997).

Chapter 3 : Petrophysics and Multiphase Flow of Porous Media

3.1 Petrophysical Properties

The petrophysical analysis from core samples is used for reserve estimation and exploitation of new discoveries. The standardization of wireline log data with results of core analysis leads to development of correlation, valid for one or specific reservoir. The present work advances this standardization/ confirmation procedure to the pore size level by bringing in core analysis and log interpretation. The main petrophysical parameters which are discussed in this study are porosity, permeability, water saturation, capillary pressure, resistivity and relative permeability.

3.2 Core-Log Data Integration Model

To develop considerable and assertive approach for reservoir characterization, exploitation and reserve estimation have been envisioned through the integration of core and log data. Uncertainty associated with formation evaluation is reduced through laboratory analysis and log data interpretation. Hydrocarbon potential zone and complexity of the formation could be defined from core data and the larger scale investigation of log data. For the integration purpose, laboratory study of a core sample has been developed to measure a variety of rock property-es such as porosity, permeability, and water saturation.

3.2.1 Routine Core Analysis

It is the type of analysis, performed on core samples taken from reservoir, during or after drilling. Measurements obtained from routine core analysis are porosity, permeability, grain density, fluid saturation, permeability and lithology (API RP40).

3.2.1.1 Porosity:

Porosity controls fluid storage and connectivity of the pore structure regulate fluid flow and migration through geological formations, as well as correlations between particular minerals and bulk properties of rock (Lawrence et al., 2015). The ratio of pore space volume to bulk volume is named as porosity, which can be mathematically expressed as: (Ahmed, T., 2001).

$$\text{Porosity } (\phi) = \frac{Pore\ Volume}{Bulk\ Volume} \qquad or,$$

$$\text{Porosity } (\phi) = \frac{Bulk\ Volume - Grain\ Volume}{Bulk\ Volume} \quad (3.1)$$

Effective porosity is calculated from the interconnected pores, which is the focused porosity for Reservoir Engineers. Due to deposition and geologic process original porosity changes to induced porosity form (Ahmed, T., 2001). Compaction and overburden pressure of rock decreases porosity with the increase of depth (Dullien., 1992). The porosity of sandstones varies from 10-40%, whereas, limestone and dolomite porosity ranges from 5-20%.

3.2.1.2 Permeability and Klinkenberg Effect:

The ability of the rock, to allow the hydrocarbons to flow through them is called permeability (Ahmed, T., 2001). Permeability can be calculated by using the following equations:

Permeability (Non-compressible Fluids):

$$K = \frac{q \times m \times l \times 1000}{(p_1 - p_2)A} \quad (3.2)$$

Permeability (Compressible Fluids):

$$K_a = \frac{q_a \times p_a \times \mu \times L \times 1000}{(p_1^2 - p_2^2)A} \quad (3.3)$$

Klinkenberg effect may occur, due to slippage of gas molecules with the pore walls (Wu, et al., 1998). Due to this effect permeability correction is required. In this regard, liquid permeability (k_L) is linked with gas permeability (k_g) as follows:

$$K_l = \frac{k_g}{(1 + \frac{b}{p})} \quad (3.4)$$

3.2.2 Wireline Log Interpretation and Techniques

Wireline log evaluation is the most important techniques for petroleum geosciences. It can be used to generate iso-pacheous maps and to evaluate rock properties like geological description, pore volume, and liquid flowability. The logs may be helpful in identification of prospective areas and to assess well intervals for hydrocarbon production.

3.2.2.1 Spontaneous Potential Log:

Spontaneous potential (SP) log measurements give valuable information during well log interpretation. Mostly log suite contains SP log while running into the well. SP log is used to investigate gross lithology (i.e., reservoir vs. non-reservoir)). This log is also used for the correlation of different zones between the wells (Doll, H.G., 1950).

3.2.2.2 Gamma Ray Log:

Gamma Ray (GR) is a method of measuring naturally occurring gamma ray radiations to characterize the formation type. The gamma ray tool allows to distinguish between shales and non-shales. Rocks containing potassium feldspars, micas, glauconitic, or uranium-rich waters in sandstone, gamma ray shows high value, while, in uncontaminated sandstone (less shale content) its value goes down (Blanchard et al., 1953). Gamma ray index measurement is carried out by the equation given below.

$$I_{GR} = \frac{GR_{log} - GR_{min}}{GR_{max} - GR_{min}} \tag{3.5}$$

3.2.2.3 Porosity Logs:

Porosity logs calculate porosity of the reservoir rock. They are subdivided into following categories (Gaymard et al., 1968):

i) Sonic log

Sonic log is a measure of formation's capability to transmit seismic waves. This capacity of reservoir rock varies with lithology and rock texture, mostly decreases with increase of effective porosity. Wyllie time-average equation is applied for porosity calculation in sonic log:

$$\phi_{Sonic} = \frac{\Delta t_{log} - \Delta t_{matrix}}{\Delta t_{fluid} - \Delta t_{matrix}} \tag{3.6}$$

ii) Density log

Density log deliver an incessant record of a formation's bulk density along the interval of a borehole. Density of minerals (i.e matrix) and the fluid enclosed in the pore space is called bulk density. Porosity from density log can be measured from the following equation:

$$\phi_{Density} = \frac{\rho_{matrix} - \rho_{bulk(log)}}{\rho_{matrix} - \rho_{fluid}} \tag{3.7}$$

iii) Neutron log

Neutron log count hydrogen atoms present in the formation. Mainly this log used to measure porosity of reservoir rock. This log is processed by bombarding high energy neutrons in the formation.

3.2.2.4 __Resistivity Logs:__

Resistivity is the measure of resistance to current passing through rock. The value of resistivity increases on hydrocarbon bearing zone and reduces with saline water in the pores. Resistivity log is applied to evaluate hydrocarbon and water-bearing zones. Resistivity of formation water (R_w) is calculated through resistivity log. Archie equation (3.8) is used to measure water saturation through resistivity and porosity logs data (Archie, G.E., 1942).

$$S_w = \left(\frac{a \times R_w}{R_t \times \emptyset^m}\right)^{\frac{1}{n}} \tag{3.8}$$

3.3 Concept of Multiphase Flow of Fluid through Porous Medium

A partitioning of the total volume of solid matrix and pore space with the latter being filled by one or more fluids is characterized as a porous media. It is important to evaluate the characterizes flow through porous media using petrophysical analysis such as relative permeability, capillary pressure, wettability, and resistivity. Integration of these petrophysical parameters can be helpful to develop multiphase flow model of reservoir rock (Honarpour, et al., 1982).

3.3.1 __Effect of Relative Permeability on Porous Medium__

Relative permeability is described as the ratio of effective to absolute permeability. Single phase fluid flow through a porous medium is descibed as absolute permeability. Moreover, effective permeability deals with the flow of more than one fluid (Cosse R., 1993; Bear J.C., 1972). The figure (3-1) describes gas-water system as given below (*(Honarpour, et al., 1982*):

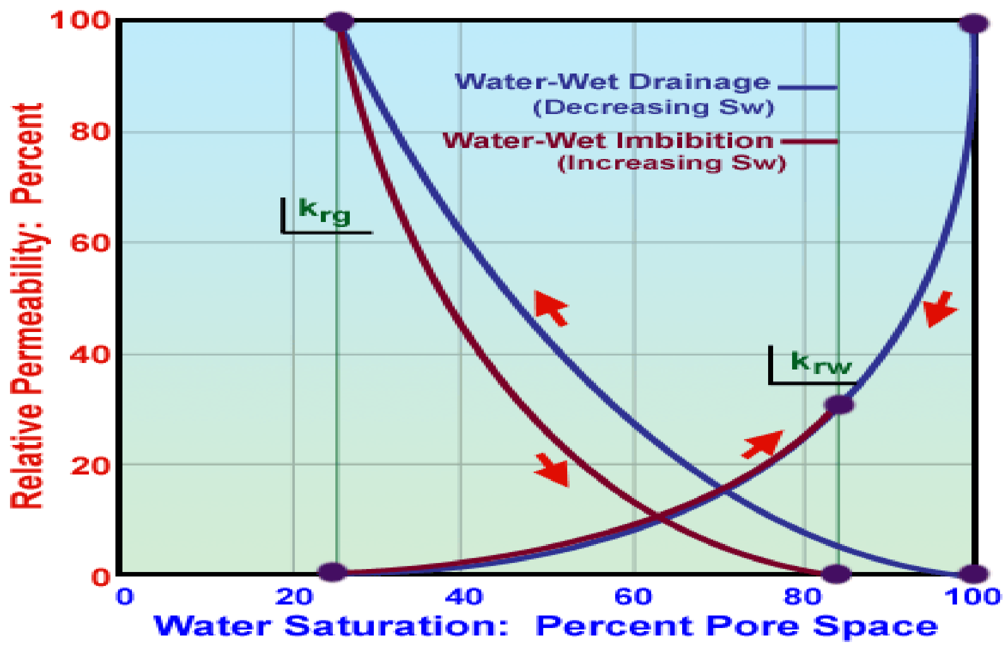

Figure 3-1: Graph is plotted on the data of gas-water relative permeability where water displaced the gas (Honarpour, et al., 1982).

3.3.2 <u>Impact of Saturation On Porous Media</u>

It is fraction of space occupied by gas, oil or water in the pore volume. Oil flow occurred in porous media when saturation exceeds from the critical oil saturation. During injection of gas or water, wetting phase displaced the non-wetting phase the remaining saturation of oil left, termed as residual oil saturation (Ahmed, T., 2001).

3.3.3 <u>Wettability Effect On Porous Media</u>

Wettability is the capability of a fluid to maintain interaction with a solid surface, consequential from intermolecular contact when the two are brought together (Ahmed, T., 2001). As contact angle (ɵ) decreases, system moves towards water-wet. Furthermore, wettability affects the fluid distribution in porous media, for example, non-wetting phase occupies larger pores, while, smaller pores are filled by wetting phase (Buckley and Leverett., 1941).

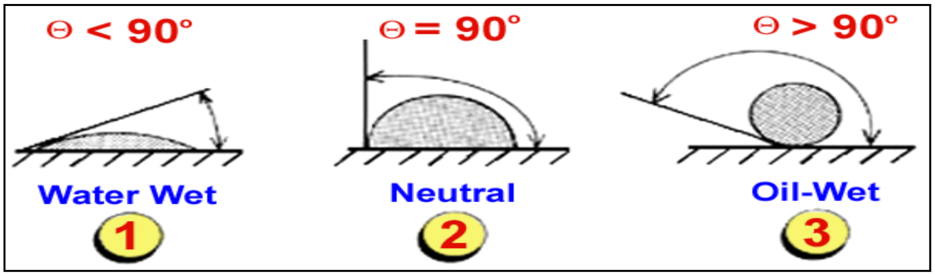

Figure 3-2: Wettability (Contact Angle) (Honarpour, et al., 1982).

3.3.4 Effect of Capillary Pressure On Porous Medium

Capillary pressure (P_c) is defined as the difference in pressure across the interface between two phases. Capillary pressure depends on wettability, pore volume, geometry/ size of pores and interfacial tension. The figure (3-3) represents contact between two immiscible fluids and curvature is resulted due to capillary pressure (Ahmed, T., 2001). The equation (3.9) and (3.10) are used to calculate represents capillary pressure (Alam., 2008).

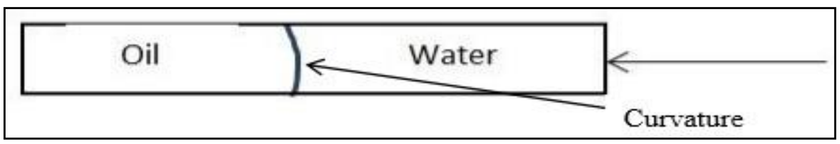

Figure 3-3: Interface between Water and Oil (Alam, 2008)

$$P_c = \frac{2\sigma\cos\theta}{rt} \tag{3.9}$$

$$P_c = \left(\frac{h}{144}\right)\Delta\rho \tag{3.10}$$

Capillary pressure is also known as entry pressure, threshold pressure and breakthrough pressure (Dullien., 1992). Fluid saturation distribution in transition zone depends on capillary pressure and it is used for calculation of transition zone height. Based on capillary pressure data, different saturations in reservoir can be characterized into free water level (FWL), water-oil contact (WOC), transition zone and gas-oil contact (GOC) as shown in figure (3-4) (Ahmed, T., 2001).

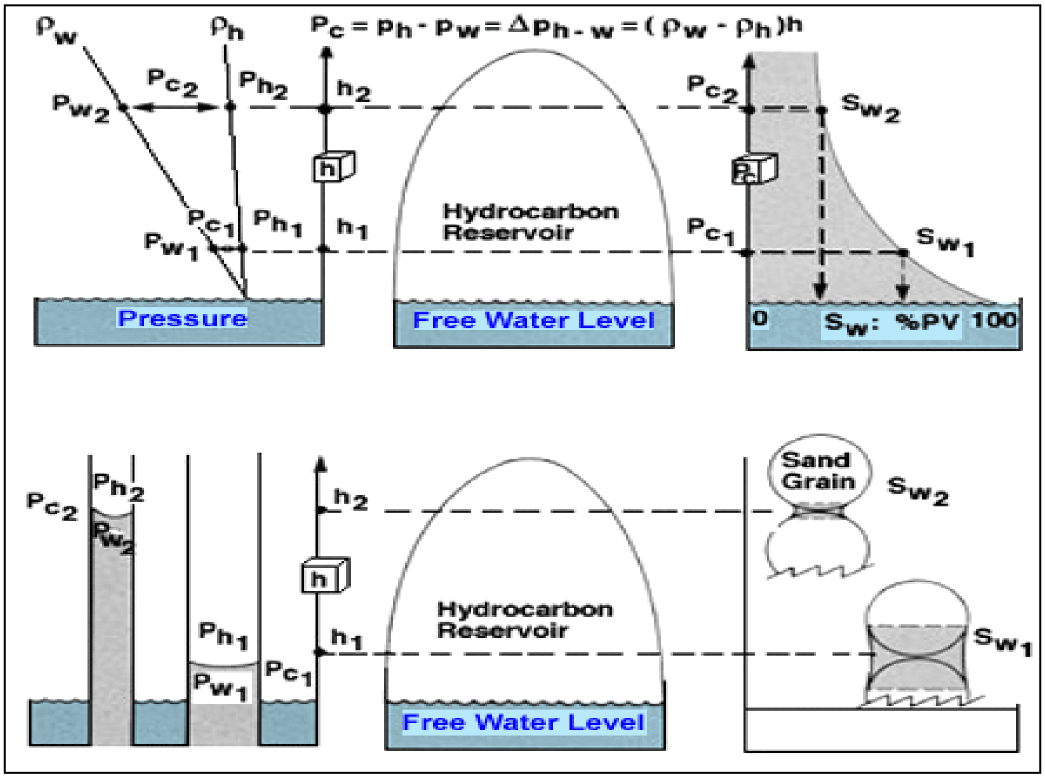

Figure 3-4: Shows the concept of pressure differential among hydrocarbon height and water saturation (Tiab et al, 2004)

3.3.5 <u>Electrical Properties and Formation Factor</u>

Electrical parameters of core sample are measured in the laboratory for calculation of water saturation. Archie defined formation factor (F) in 1942 as the ratio of resistivity of 100% water saturated rock (R_o) to the saturating brine (R_w). Cementation component (m) can be derived from the slope of plotted graph between formation factor and measured porosity (Archie, 1942). The figure (3-5) shows the relationship between formation factors and porosity.

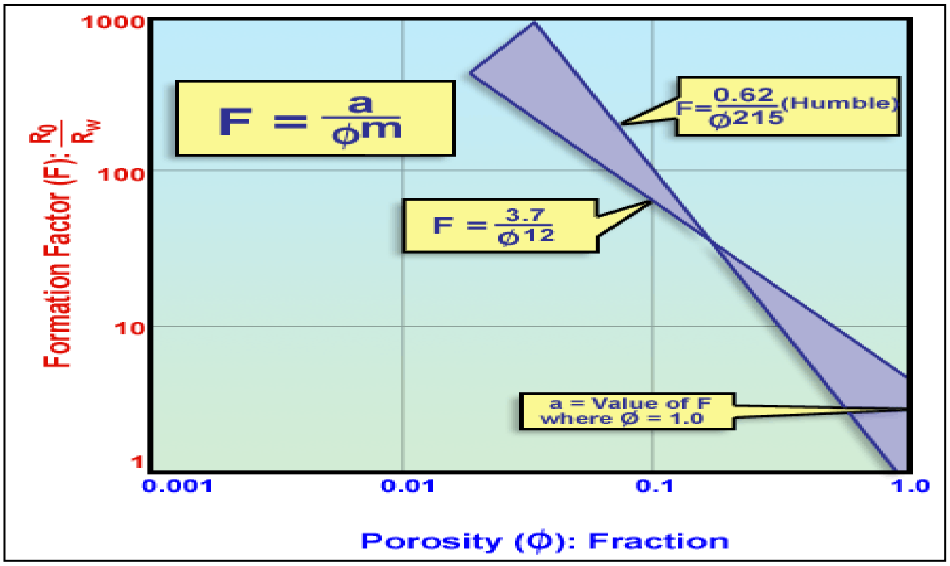

Figure 3-5: Plot between Formation Factor versus porosity with the change of intercept"a"(Serra, Oberto, 1984).

Moreover, the actual resistivity increases with the reduction of water saturation in a given sample. This is due to the fact that fewer ions are available for flow path of electricity. The ratio of true resistivity (R_t) at given saturation to the resistivity at 100% saturation (R_o) is defined as resistivity index (RI). The Figure (3-6) illustrates the relationship between the resistivity index and water saturation to calculate the range of slope "n."

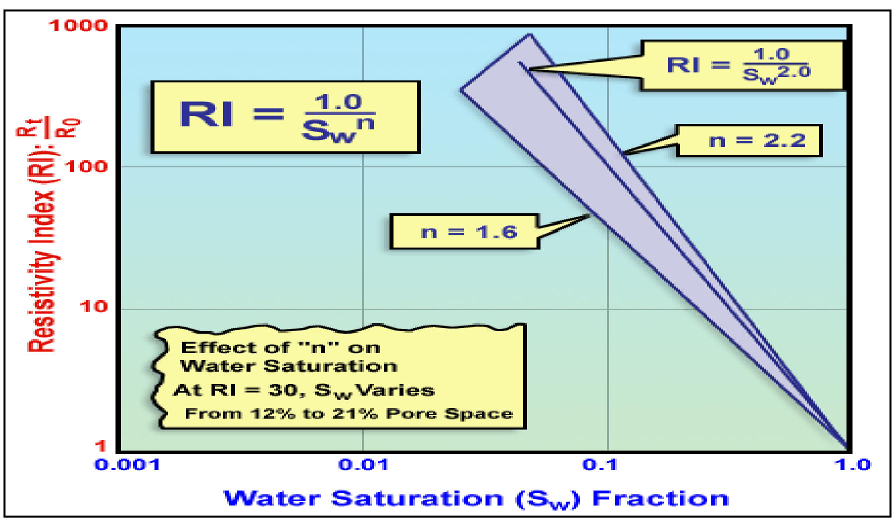

Figure 3-6: Plot between water saturation and resistivity index to calculate the range of slope "n"(Serra, Oberto, 1984).

Chapter 4 : Laboratory Methods for Core Plug Analysis

4.1 Core Analysis

Petrophysical analysis plays a vital role in reservoir evaluation. Coring is one of the major technique used for petrophysical analysis. Coring is a complete program which is designed for evaluation of hydrocarbon potential of the reservoir. Core samples are obtained from borehole through coring programs at specific depth intervals. The length of core ranges from 1.5-400 feet. Coring is characterized into two types: conventional coring and wireline log retrievable coring.

4.1 Core Sampling and Preparation

Proper core sampling and preparation procedure should be conducted, before core analysis. Core samples are prepared and evaluated for the following information.

a. Detail description and distribution of lithology
b. In lithology interval porosity and permeability variations
c. Hydrocarbon distribution

4.2.1 Plug Samples

From entire core sample (ranging from 1.5ft to 400ft in length), plug samples of 1inch to 3inch length is drilled out with respect to the bedding plane (horizontally or vertically). Drill press with diamond-edged core drills, capable of drilling cylinderical sample are used .These plug samples are drilled out with bit size of 1inch to 1.5inch from the core on specific points. To avoid the bending and deforming of bit or plug sample, excessive pressure should not be used during drilling.

4.2.2 Sample Cutting, Trimming, and Mounting

To prepare the core plug in proper cylindrical shape cutting, trimming and mounting is carried out (API Recommended Practice, 1988). In sample cutting and trimming operation, huge slab saw with a diamond blade and trim saw with a diamond blade instruments are used. Precautionary measures should be taken by user before cutting, trimming and mounting operations.

4.2.3 Core Cleaning and Drying

Before petrophysical analysis of core samples, it is essential to remove fluids (drilling mud and hydrocarbons) from pore spaces of core sample. Cleaning of core sample is accomplished through flushing of selected solvents to displace hydrocarbon, water, and brine. Genarlly distillation extraction method is applied for core cleaning. The color of siphons (due to solvent) intermittently in extractor can give an idea of core sample cleaning. This procedure of extraction constantly repeated until the extract becomes clear (API Recommended Practice, 1988). Extra care must be taken, while selecting solvent for solvent extraction technique. Solvent should not damage core sample. The table (4-1) illustrates major techniques for drying of conventional core sample.

Table 4-1: Various drying techniques of core samples

Rock Type	Method	Temperature, °C
Sandstone (low clay content)	Conventional oven	116
	Vacuum oven	90
Sandstone (high clay content)	Humidity oven, 40% relative humidity	63
Carbonate	Conventional oven	116
	Vacuum oven	90
Gypsum-bearing	Humidity oven, 40% relative humidity	60
Shale or other high clay rock	Humidity oven, 40% relative humidity Conventional vacuum	60

4.2 Porosity Measurement Method for Core Plug

Various methods can be used for porosity measurement. Grain volume method is more accurate as compared to volumetric method (API recommended practice., 1998). In grain volume measurement, absolute porosity is calculated using Boyle's Law. Boyle's law states that at constant temperature, volume of gas is inversely proportional to pressure.

$$\frac{V_1}{V_2} = \frac{P_1}{P_2} \qquad or \qquad P_1P_2 = P_2V_2 \tag{4.1}$$

For accurate volume measurement, the equation (4.1) can be modified to incorporate temperature and compressibility factor variations.

$$\frac{V_1}{Z_1}\frac{P_1}{T_1} = \frac{P_2}{Z_2}\frac{V_2}{T_2} \tag{4.2}$$

Grain volume (GV) of core sample is measured using equation (4.2). Helium porosimeter is used to measure porosity of core plug. A schematic diagram of helium porosimeter is shown in fig (4-1). In helium porosimeter, known volume of reference cell (V_r) is introduced with gas at fixed reference pressure (100 to 200 psi). Initially reference chamber volume (V_r) and sample chamber volume (Vc) are calibrated. In sample chamber, core plug is positioned. After calibration a pre-determined pressure of helium gas is applied in reference chamber, which is approximately 100 to 200 psi. Pressure is applied for 30 seconds approximately to achieve the equilibrium and P_1 (pressure indicated by the digital transducer readout) is noted. After, gas is allowed to expand and a lower pressure (P_2) is noted at equilibrium. Boyle's law is used to measure grain volume through initial pressure of reference chamber and final pressure system. The difference of grain volume and bulk volume is the pore volume. By using mass balance inside the reference chamber and sample chamber, an equation is derived from Boyle's law, for calculation of grain volume is given below:

$$\frac{P_1V_r}{Z_1T_{1r}} + \frac{P_a(V_c - V_g)}{Z_aT_{2c}} = \frac{P_2V_r}{Z_2T_{2r}} + \frac{P_2(V_c - V_g + V_v)}{Z_2T_{2c}} \tag{4.3}$$

For ideal gas and isothermal condition ($T_1 = T_2$):

$$V_g = V_c - V_r\left(\frac{P_1 - P_2}{P_2 - P_a}\right) + V_v\left(\frac{P_2}{P_2 - P_a}\right) \tag{4.4}$$

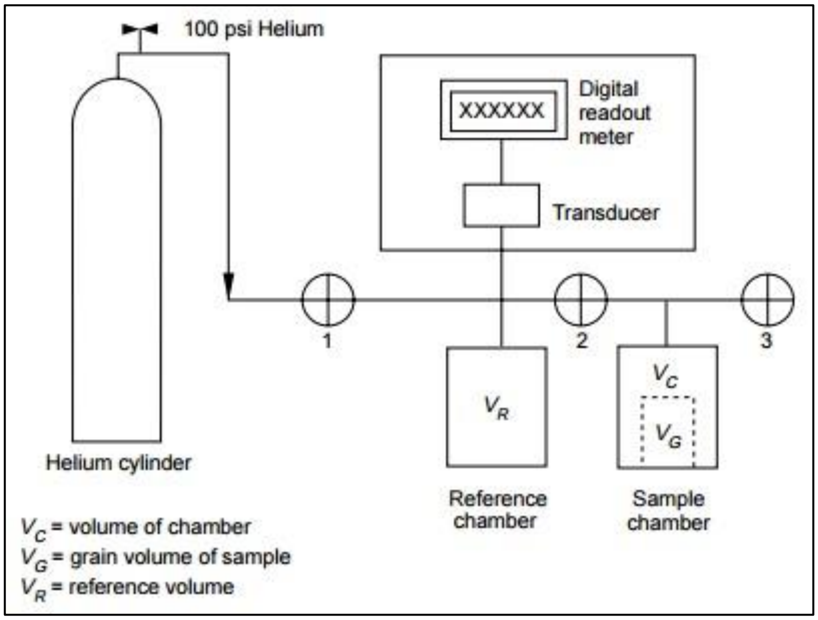

Figure 4-1: Schematic diagram of Helium Porosimeter (Koederitz L.F., et. al, 1989)

4.3 Permeability Measurement Method for Core Plug

The permeability of a porous medium is a measure of ease with which fluids may pass through the medium under the influence of driving pressure. The magnitude of permeability depends on size, shape and continuity of the pores within the rock. The permeability of a porous medium can be determined from core samples by laboratory testing (Koedertiz, et al., 1989). Gas permeameter is most commonly used for permeability determination of core samples. The figure (4-2) describes the mechanism of gas permeameter is given below:

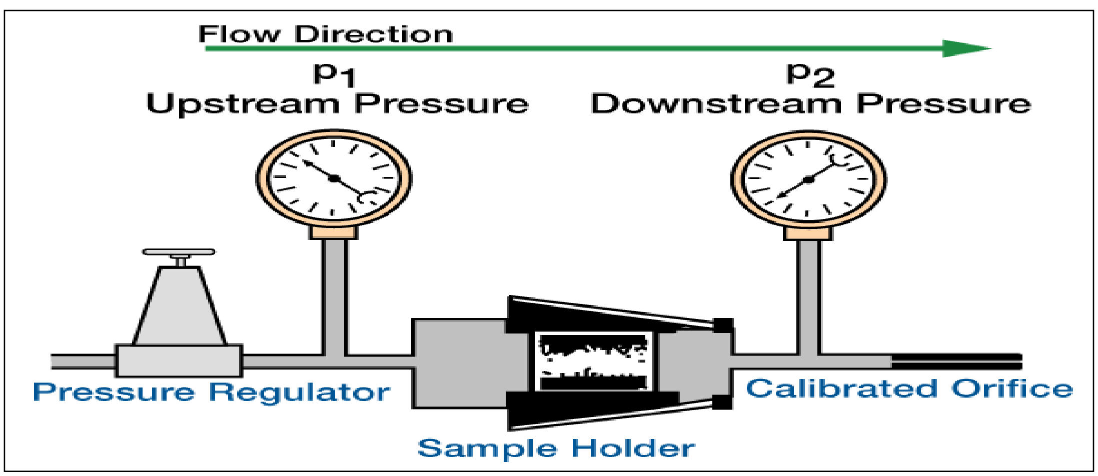

Figure 4-2: Gas Permeater flow diagram mention process of gas flow and differential pressure (Koederitz L.F., et. al, 1989).

The stepwise procedure for permeability measurement is given below:

1. Turn on the power, allow five minutes warm-up time. The led display should read "Zero" with valve V_2 in the "OPEN" position.
2. Measure and record the core sample area and cross-sectional area (A) and length (L).
3. Load the core into the core holder.
4. Attach the hydraulic pump to the confining pressure inlet, and adjust to obtain the desired confining pressure. Distilled water or a light oil can be used.
5. Open valve V_4. After the pressure has been applied as indicated by the confining pressure gauge, close valve V_4 to lock in the confining pressure.
6. For gas admission V_1(Core Inlet) and V_3(inlet metering) will be at close position while V_2(Zero) will be at open position
7. To admit gas, open V_1 and opening the upstream metering valve, V_3.
8. If permeability to be determined against an atmospheric back pressure, no pressure should be applied to the dome of the back-pressure regulator. Gas rates are regulated by adjusting the gas supply pressure regulator (inlet metering) and observed on the appropriate mass flow meter read out. V_2 is closed (handle in the right position) to establish a P across the core.
9. If permeabilities are to be determined at elevated core pressure, apply the desired pressure to the dome of the back-pressure setting, if desired. The back-pressure regulator will regulate the back pressure to approximately the same pressure as is applied to its dome.

To determine the gas permeability, Darcy's equation is used. It requires measurement of the core cross-sectional area, core length, pressure drop across the core, and the gas flow rate at that pressure drop. The accuracy can be increased by measuring flowing gas ambient pressure and temperature. Darcy equation for isothermal steady-state gas flow is given below:

$$K_a = \frac{2\mu Q_b P_b L}{A(P_1^2 - P_2^2)} \tag{4.7}$$

4.4 Relative Permeability Method for Core Plug

Relative permeability is the most significant parameter describing multiphase flow and is the ratio of effective permeability to the absolute permeability. The unsteady-state experiment of oil-water relative permeability was conducted both at ambient and simulated reservoir conditions using mineral oil (viscosity 20 cp at 75 °F). The procedure of the relative permeability measurement is given below:

- The cleaned, dried out crop sample saturated with an aqueous phase was placed in Hassler core holder.
- Core holder was then connected with the main core flooding unit.
- Confining pressure of 2000 psig was applied to the annulus of the core holder with Haskel pump.
- In case of simulated temperature experiment, the temperature of the system was stabilized at 180°F equivalent to the reservoir condition;
- The aqueous phase was allowed to flow for sufficient time till the differential pressure was stabilized. Then three concordant reading of flow rates were recorded to calculate the absolute permeability.
- Kerosene was used for displacement purpose, and the relative volumes of effluents (produced fractions of oil and water) were measured to determine oil-water relative permeability data as well as the average in situ fluid saturation at any interval along the test sample during an experiment.
- When water production from the out crop sample becomes zero, then it was saturated with oil at irreducible water saturation. At this stage, differential pressure was also stabilized.
- Fluids displacement rates were kept low to minimize the variation in relative permeability data sets due to fines migration effects.

Relative permeability measurement system can be varied according to the circumstances. A figure (4-3) shows the complete concept of relative permeability system. The relative permeability system is composed of stainless steel for both reservoir and ambient conditions. At ambient condition, fluid flow pressures and confining pressure ranges upto 100psi and 1500psi respectively.

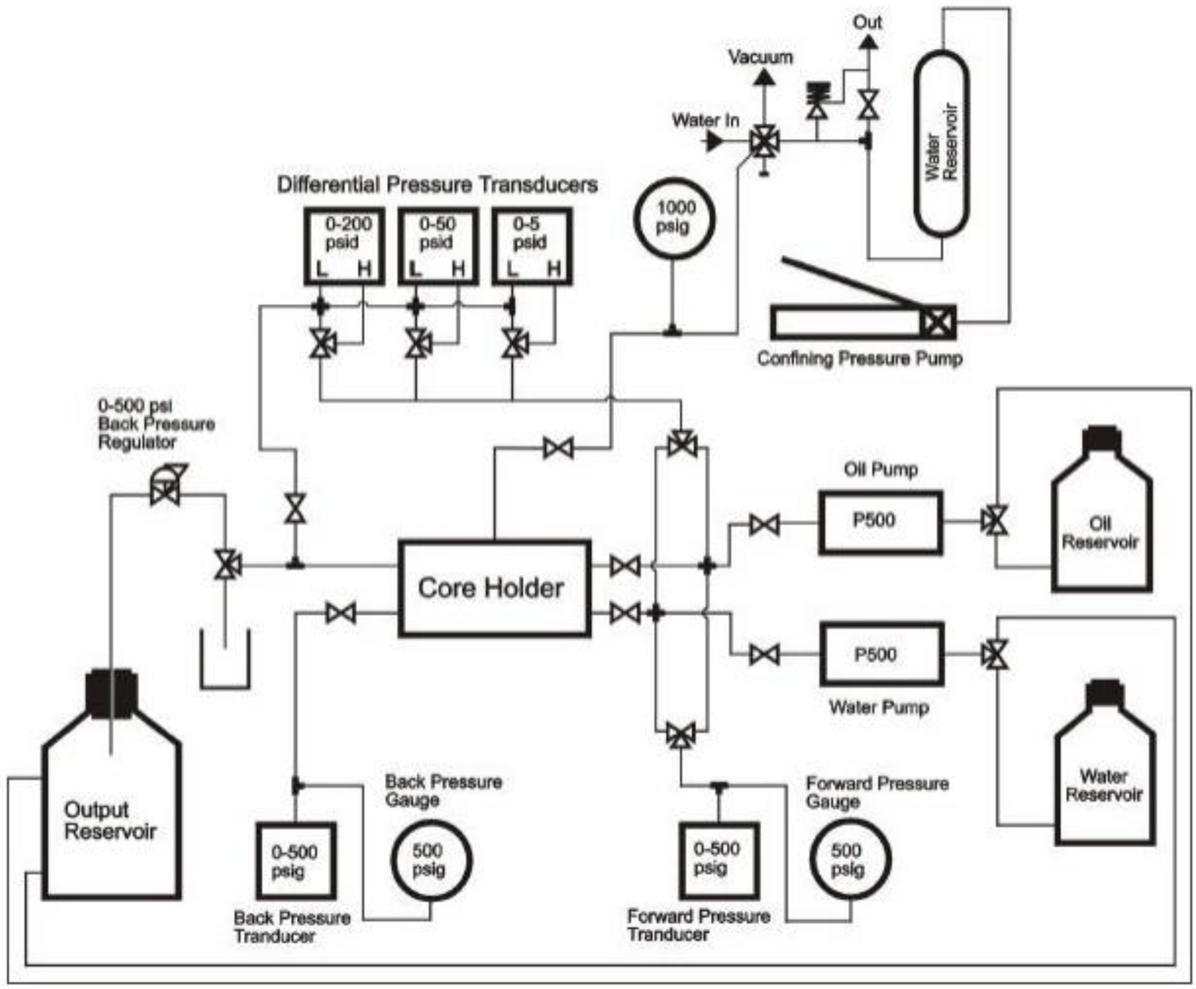

Figure 4-3: Schematic diagram of relative permeability system ((Honarpour et al., 1982)

4.5 Capillary Pressure Measurement Method for Core Plug

Capillary pressure apparatus is used to calculate the capillary pressure of core sample. It is also used to calculate height of transition zone from plot of saturation versus capillary pressure. (Hassler G.L. & Brunner E., 1945).

1. A cleaned, dried core sample bulk volume and pore volume is calculated. Then measured the weight of dry core sample.
2. The core sample is saturated with known brine/water density. The weight of core sample is measured.
3. After saturating the core sample, it is placed in the centrifuge and start the centrifuge at the rotation rate of 500 RPM.

4. Observe the displaced fluid volume in the tube and calculate it.
5. Collected volume is noted through graduated tube, when the volume of collected fluid represents no advance alterations.
6. The Same procedure of 4 and 5 step is repeated for higher rotational speed.

The following step will be involved to calculate the capillary pressure:

1. The pore volume of the core sample is calculated as: $V_p = \frac{W_{sat} - W_{dry}}{\rho_w}$
2. RPM is converted in rad/s as $\omega = \frac{2\pi(\mathrm{RPM})}{60}$
3. Capillary pressure is calculated as: $P_{cL} = \frac{1}{2}\rho_w \omega^2 (r_2^2 - r_1^2)$
4. Measure average water saturation S_w in the core sample established on the volume of the water collected at resultant capillary pressure: $S_w = 1 - \frac{V_{coll}}{V_p}$
5. Draw a plot S_{PcL} versus P_{cL}
6. Draw tangents to the plot of the curve at every point and measure the slope of every tangent. These slopes are the water saturation data S_w at the resultant capillary pressure.
7. Draw the capillary pressures as a function of the water saturations.

4.6 Resistivity Measurements Method for Core Plug

To calculate the major electrical characteristics of porous rock such as resistivity, formation factor, tortuosity, cementation factor, resistivity index and saturation exponent a resistivity experiment is conducted. Resistance is measure of voltage reduction between a reference resistor and a sample (to be measured) in series as shown in figure (4-4) (Wyllie M.R. & Spangler M.B., 1952). Formerly, resistance of sample is measured, and resistivity of the sample can be established from sample size.

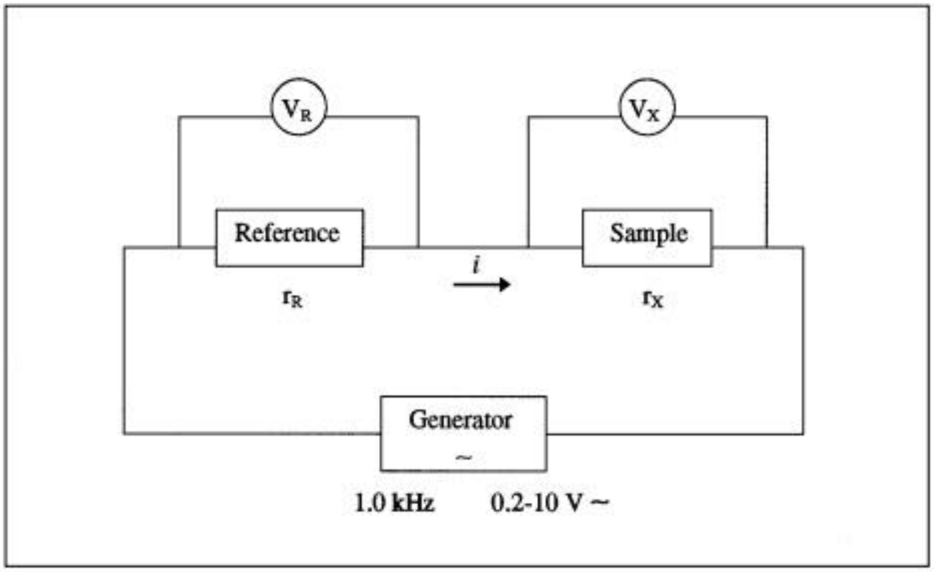

Figure 4-4: Flow diagram which shows the process of rock resistance measurement

Chapter 5 : Case Study of Integration of Core Analysis and Log Interpretation

5.1 Introduction

Core analysis and wireline log interpretation methods are considered as an essential part of formation evaluation. In this study, Core-Log Integration of Datta Sandstone (Upper Indus Basin) of Pakistan is carried out to investigate the petrophysical parameters. Conclusive core analysis results have been determined under standard laboratory conditions on core plug which is derived from the reservoir rock. Moreover, log interpretation of wells A, B, C and D intervals of the reservoir rock is carried out to investigate petrophysical parameters (Porosity and Permeability). The objective of this study is to integrate the derived log and core data to minimize the uncertanity of tools and borehole environment. The objective is acheived by integration of measurements by depth matching the core plug samples to the logs and calibration of logs using the core plug measurements. Finally, a review of the basic principles and techniques is presented, along with some of the uncertainties, assumptions, and errors.

5.2 Data Analysis and Corrections

It is important to evaluate the quality of data and corrections. In this regard following methods or techniques can be applied:

5.1.1 Depth Calibration on Log

Depth log calibration is used to overcome the probable errors of exact depth interval measurement. This error is placed due to high tension cable, over pull, improper calibration, inappropriate deviation reading. To fix this depth error, different techniques can be used such as by matching gamma ray log of well borehole and core, by matching the petrophysical log with drilling log depth and by matching the formation tops evaluated by geologists. In this study, log depth is matched in the limit of 0.2 m.

5.1.2 Correction of Well Deviation

This technique is applied to minimize borehole deviation, correction and vertical depth. A relationship has been developed by Yangjian (1995), as described in equation 5.1 to find out precise and actual vertical depth value.

$$Z_2 - Z_1 = \int_{\phi_1}^{\phi_2} \frac{b_1 - b_2}{\phi_2 - \phi_1} \cos\phi \, d\phi = \frac{b_1 - b_2}{\phi_2 - \phi_1} (\sin\phi_1 - \sin\phi_2) \qquad (5.1)$$

In this equation b_1 and b_2 are initial and end point of well/ borehole. Moreover, Z_1 and Z_2 are relative vertical depth intervals, whereas, ϕ_1 and ϕ_2 are angle deviation factor.

5.1.3 Rebuilding of Logs Curves

It has been observed that, during well logging, there are some abnormal variations and loss of data at certain depth intervals. Sometimes log data gives abnormal variations or loss of data at certain depth. These problems are overcome by developing a new relationship between erroneous log data and other logs (porosity, shale content and other log curves). Abnormal interval is replaced by new log curves (log*) based on following relationship (Schlumberger 1994).

$$log^* = f(Por, Vsh, log1, log2 \ldots) \qquad (5.2)$$

5.1.4 Normalization of Log Curve

For multi-well data, it is very common to have different log readings for the same formation or rock types in the same area. A standard formation (normally, a shale formation) is defined to compare with the same log data in the same formation, and a normalization method is then used to correct log readings.

5.1.5 Core and Log data Calibration

In this method, density is calculated at specific depth through core analysis and log interpretation. On the basis of core and log data, graph is prepared to check the relation between core density and log density. The same method has been applied for wells A, B, C and D. The results showed that core density matches with log density as shown in figure (5-1):

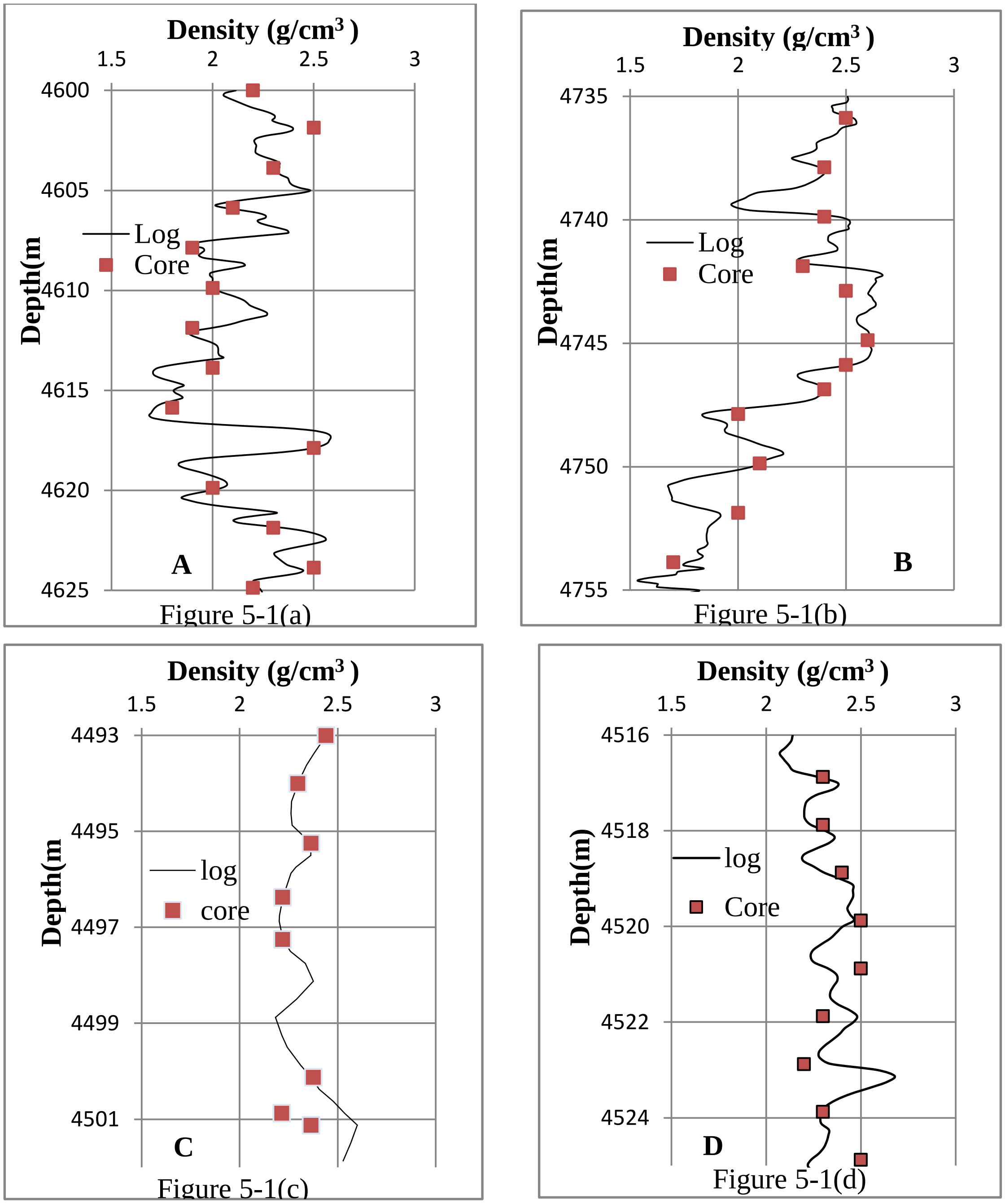

Figure 5-1: Cross plot developed between density of core and log data of wells A, B, C and D with depth interval

5.1.6 Matching of Core Data

Log data has more discrepancy than core data. This issue is resolved by comparison of vertical resolution and distance from source to receiver of log equipment (Khalid P., et. al., 2015).

5.3 Lithological Analysis

Depth intervals of wells A, B, C and D of 30m (4595m-4625m), 50m (4710m-4760m), 50m (4451m-4501m) and 30m (4510m-4540m) respectively are selected for wireline log interpretation. These intervals lie in Datta formation. After log data corrections, interpretation of these logs is carried out. From spontaneous potential log, it is found that Datta contains clean sandstone on major portion of reservoir intervals. Gamma ray log show high values on upper portions and low at bottom. Moreover, it also showed that Datta formation has shale in upper portion. Details representation of wireline logs interpretations is shown on figures (5-2,5-3, 5-4 and 5-4) given below:

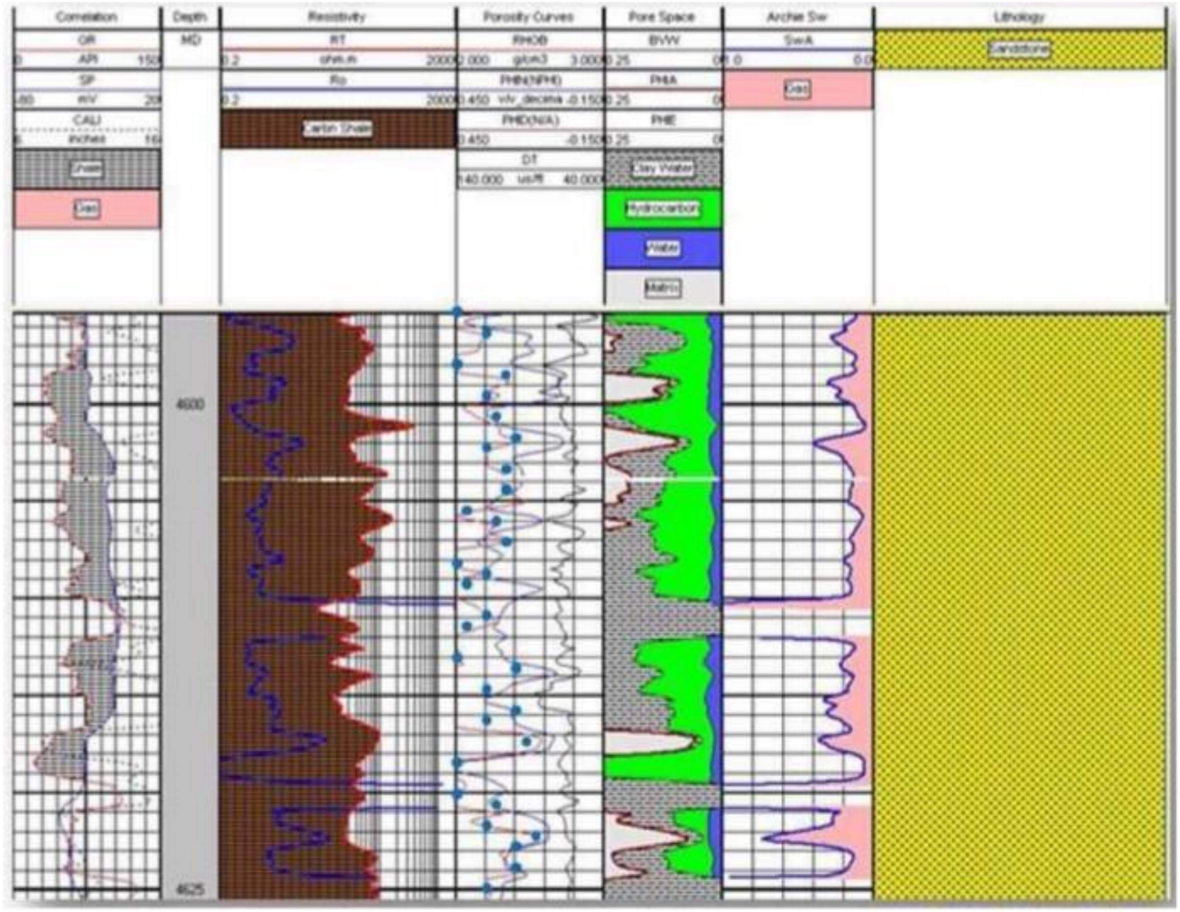

Figure 5-2 : Graphical log interpretation of well A

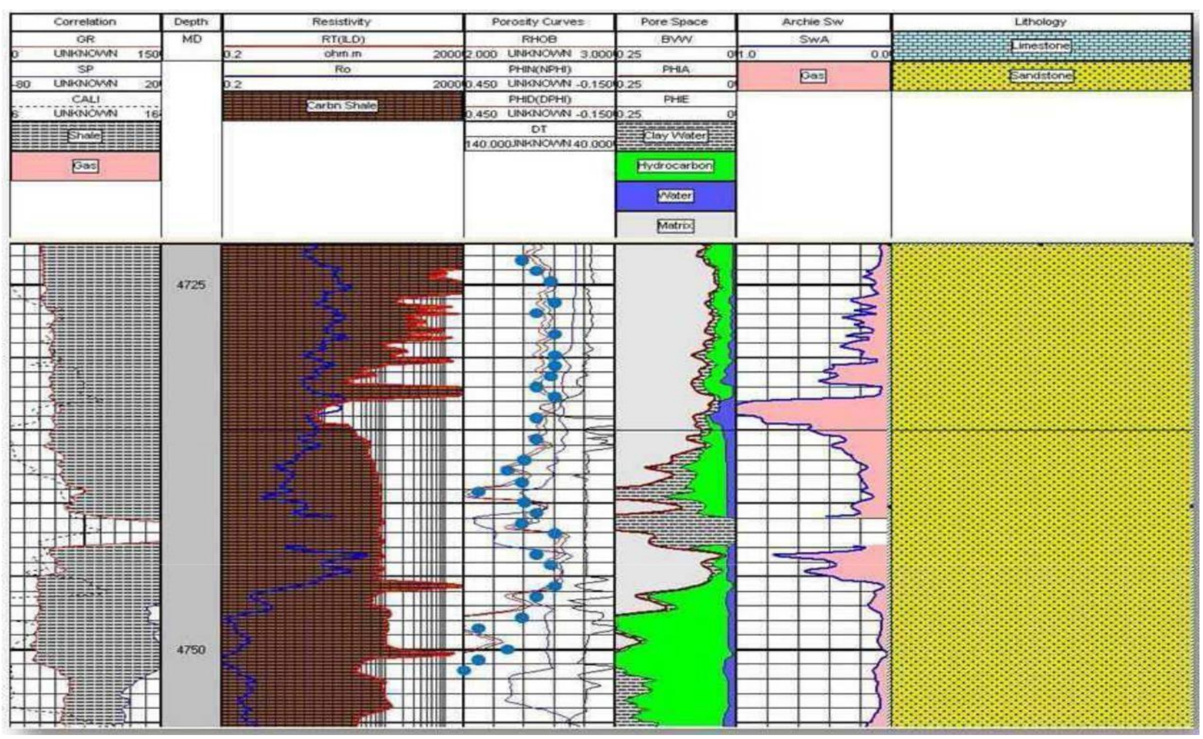

Figure 5-3: Graphical log interpretation of well B

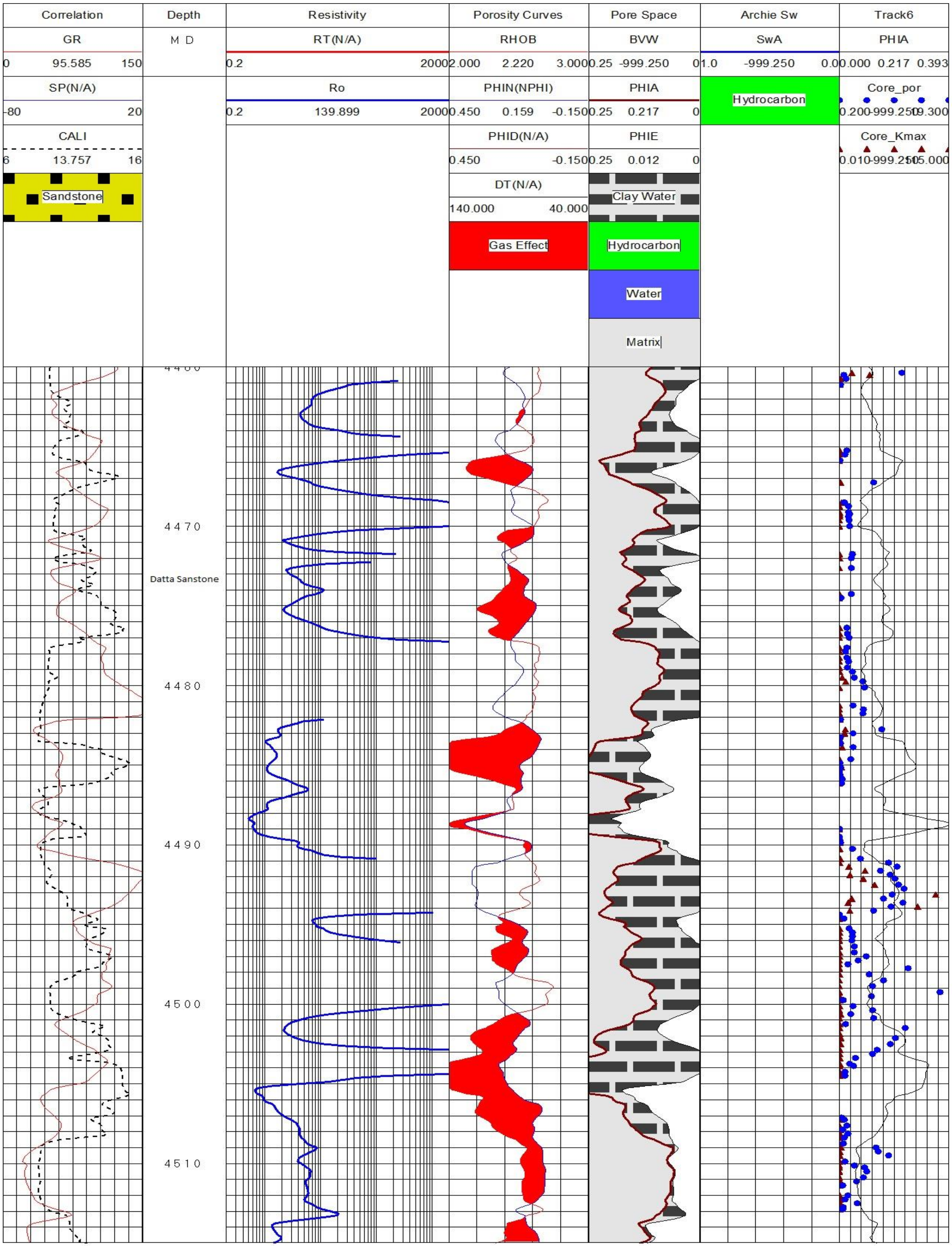

Figure 5-4: Graphical log interpretation of well C

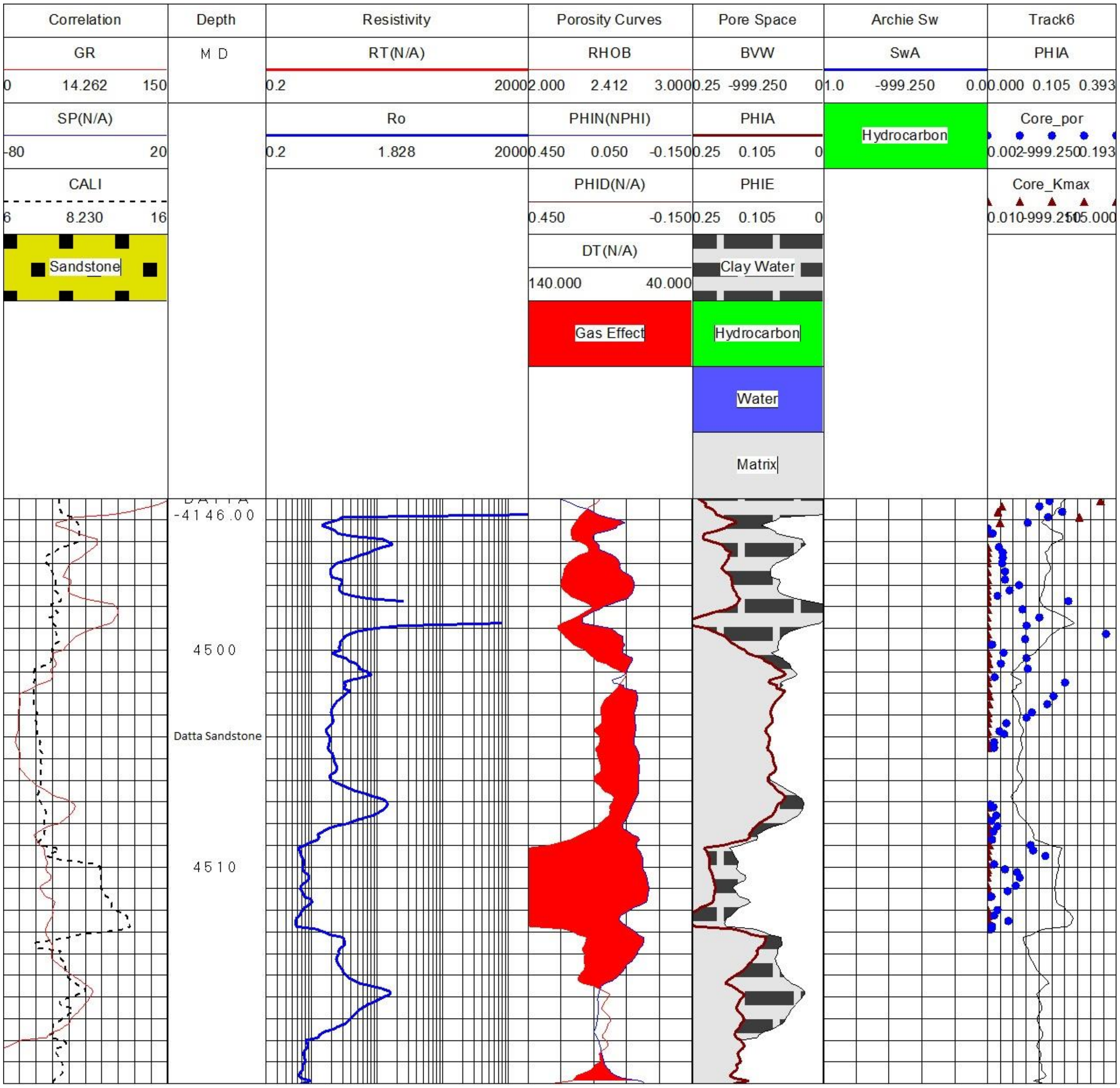

Figure 5-5: Graphical log interpretation of well D

The graphical representations showed that major portion of Datta formation having wells (A, B, C and D) consist of sandstone. Moreover, presence of clean sandstone is also validated from core analysis. Resistivity values are increasing in hydrocarbon bearing zones and decreases in water bearing zones. The detailed analysis of coring and log data showed that Datta formation has good matrix porosity and permeability.

5.4 Porosity and Permeability from Cores and Logs

After lithological analysis of Datta formation, porosity logs (sonic, density and neutron) are applied to find out porosity. These logs showed that porosity values are increasing from top to bottom. In wells A, B, C and D porosity values obtained from wireline log interpretation, ranges from 16 to 21%, 18 to 22%, 6 to 13% and 6 to 11% accordingly. Porosity analysis is also conducted on five to ten samples from wells A, B, C and D. From core samples, average porosity ranges from 19 to 23%, 8 to 13%, 10 to 11% and 6 to 12% in wells A, B, C and D respectively, as shown in table (5-1). The porosity value from core samples showed similar results to wireline log.

Table 5-1: *Core and log data average porosity and permeability of well A, B, C and D are presented.*

Well Name	Age/ Formation	Depth Interval(m)	Average ϕ , from Wireline Logs (%)	Average K, from Wireline Logs(md)	Core Interval (m)	ϕ From Core (%)	K from Core(md)
Well A	Jurrasic/Datta	4595-4625	16-21	0.1-299	Core-1: 4595-4605	17-22	0.3-130
					Core-2: 4609-4618		
					Core-3: 4620-4627		
Well B	Jurrasic/Datta	4710-4760	18-22	0.1-300	Core-1: 4709-4718	19-23	0.2-180
					Core-2: 4725-4735		
					Core-3: 4740-4751		
Well C	Jurrasic/Datta	4451-4501	6-13	1-213	Core-1: 4408-4460	8-13	10-220
					Core-2:4460-4516	10-11	2-117
Well D	Jurrasic/Datta	4510-4540	6-11	1-210	Core-1:4516-4524	6-12	1-170

Linear regression of figure (5-4) showed that porosity results (core & logs) are in accordance with each other. The permeability can be calculated from SP, resistivity and porosity log. The table (5-1) showed that calculated value of permeability ranges from 0.1md to 299md, 0.1md to 300md, 1md to 213md and 1md to 210md in wells A, B, C and D respectively. Moreover, permeability analysis is also conducted on five to ten samples from wells A, B, C and D. Permeability ranges from 0.3md to 130md, 0.2md to 180md, 2md to 220md and 1md to 170md in wells interval of A, B, C and D. Permeability values from core and log data shows large variation in well C and D than in well A and B. Linear relationship has been observed in a cross plot of well A and B, but variations are detected in well C and D which are shown in figure (5-6).

Graph has been plotted between log porosity and log permeability of well A.

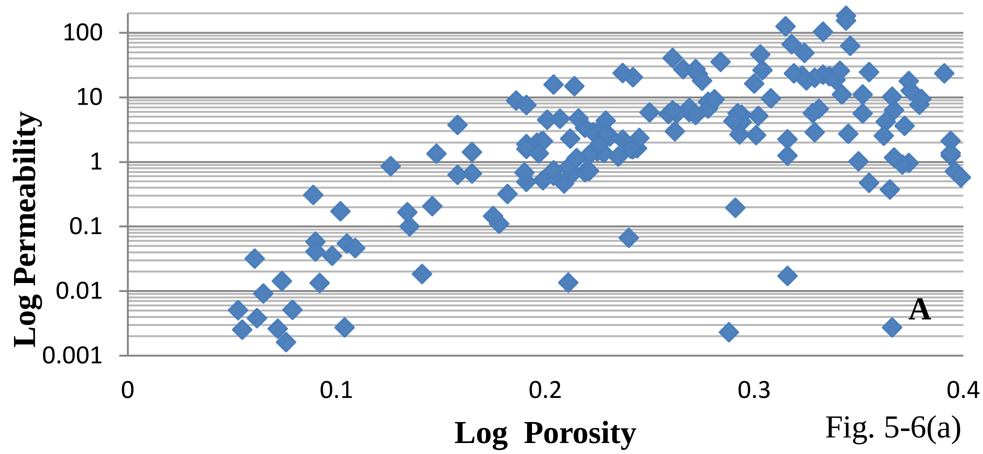

Fig. 5-6(a)

Porosity verses permeability graph has been plotted on the basis of values obtained from core analysis.

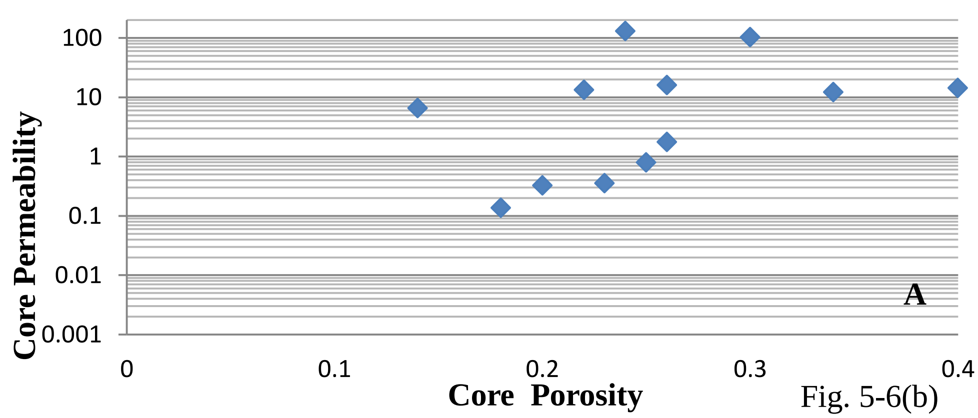

Fig. 5-6(b)

Between log porosity and log permeability graph has been present below of Well B.

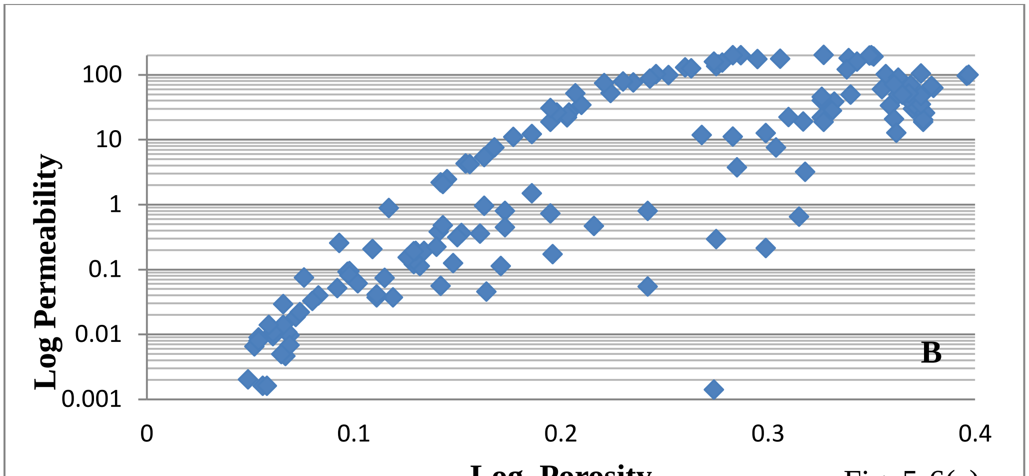

Fig. 5-6(c)

A graph has been plotted between core porosity and core permeability of Well B.

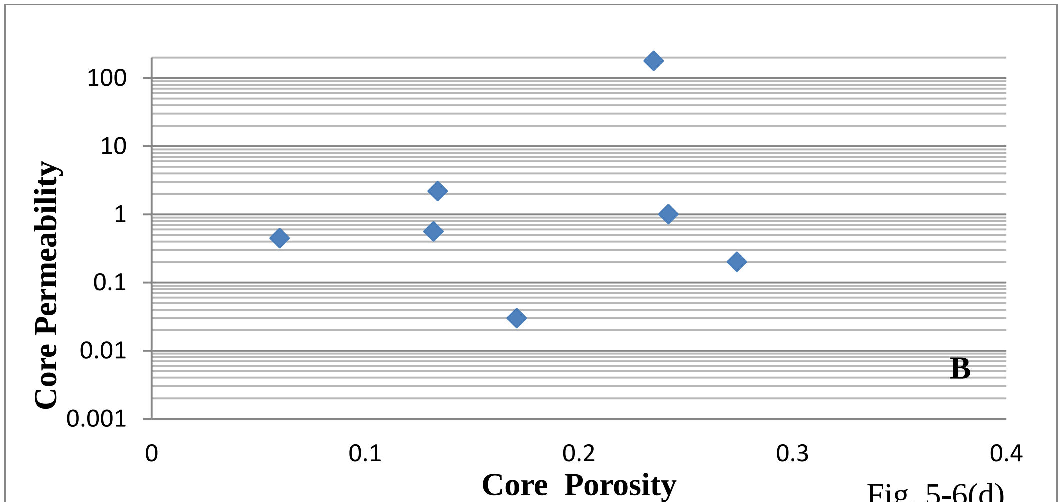

Fig. 5-6(d)

Graph between log porosity and log permeability of well C has been presented below.

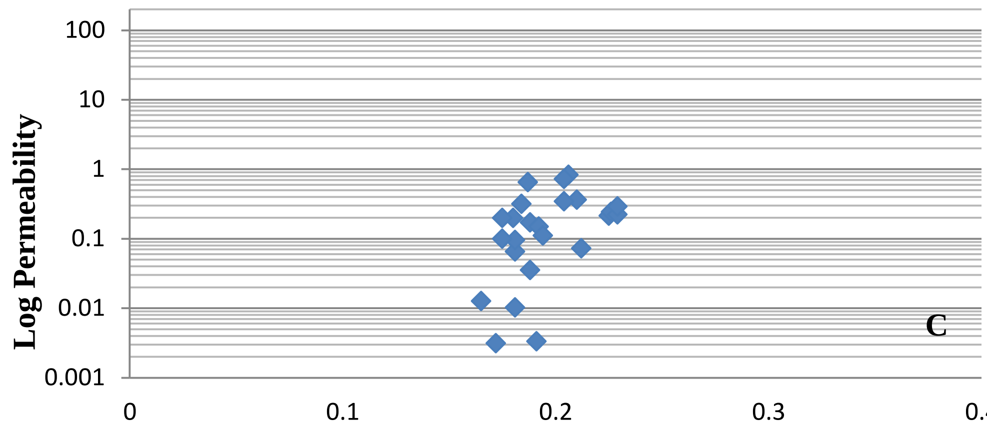

Fig. 5-6(e)

Core porosity verses core permeability graph of well C is presented below.

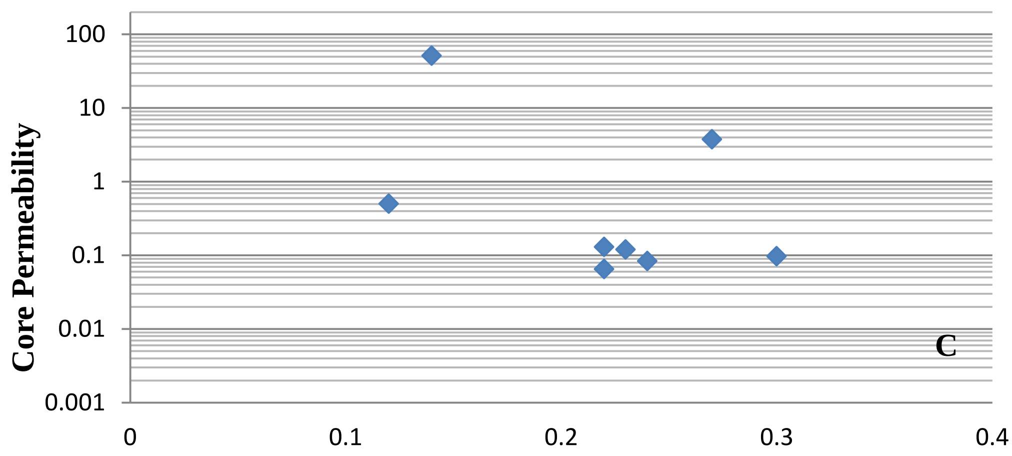

Fig. 5-6(f)

Graph between log porosity and log permeability of well D is presented below.

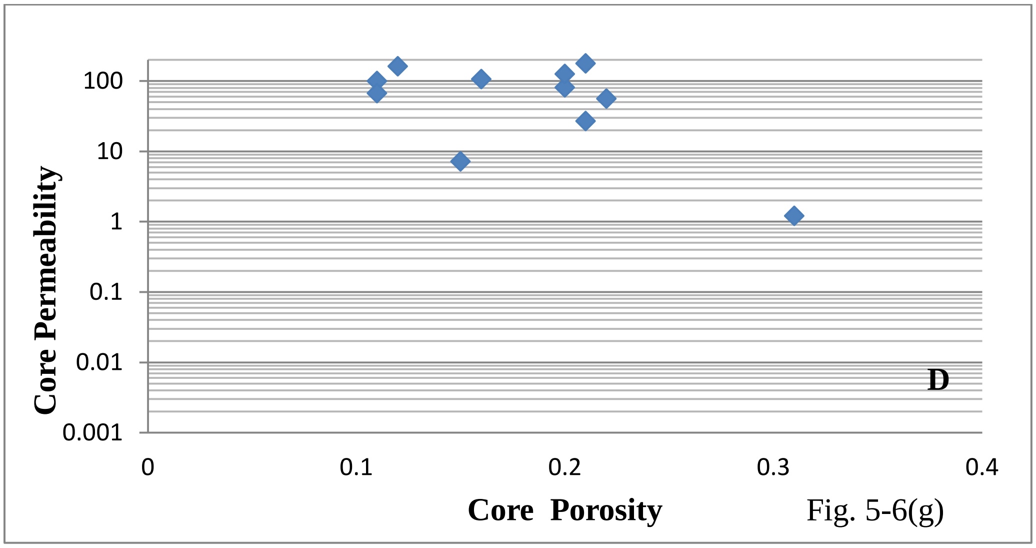

Well D core porosity verses core permeability graph is presented below.

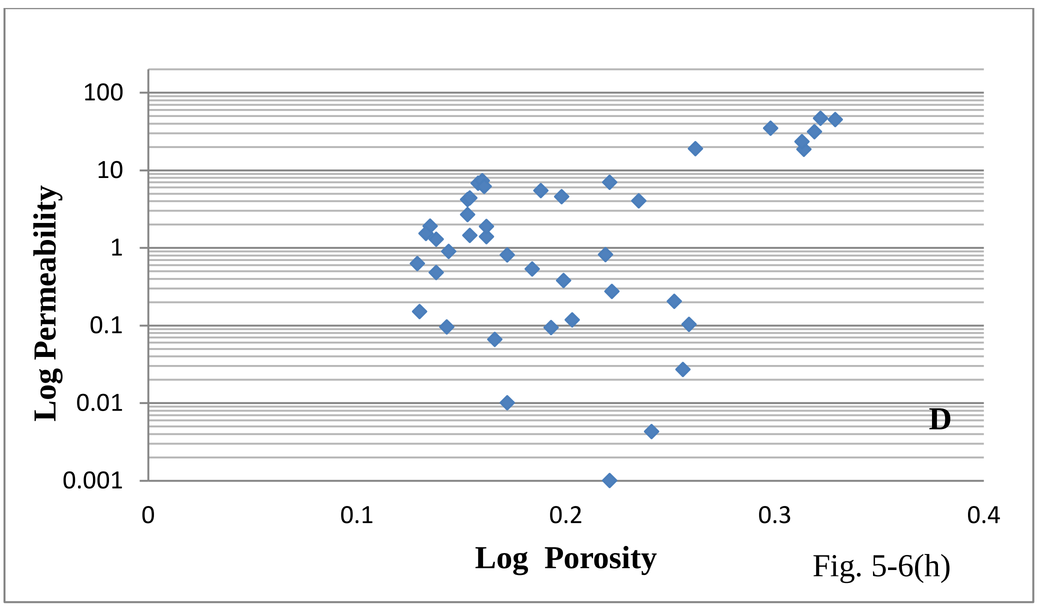

Figure 5-6: Cross plot between core porosity and permeability and plot of log porosity and permeability are shown of well A, B, C and D (a,b,c,d,e,f,g,h)

The detailed porosity and permeability (log and core) for different wells are referred in appendix-I. The relationship between core and log porosity has been derived from well A, B, C and D in given equations.

$$\phi_{Log} = 0.9613\phi_{Core} + 0.0131 \qquad (Porosity\ Core - Log\ Relationship\ of\ Well\ A) \quad (5.3)$$

$$\phi_{Log} = 0.9695\phi_{Core} + 0.0028 \qquad (Porosity\ Core - Log\ Realtionship\ of\ Well\ B) \quad (5.4)$$

$$\phi_{Log} = 0.9031\phi_{Core} + 0.0267 \qquad (Porosity\ Core - Log\ Relationship\ of\ Well\ C) \quad (5.5)$$

$$\phi_{Log} = 0.802\phi_{Core} + 0.0505 \qquad (Porosity\ Core - Log\ Relationship\ of\ Well\ D) \quad (5.6)$$

From integration of core porosity and log porosity of Well A a relationship has been developed which is presented below.

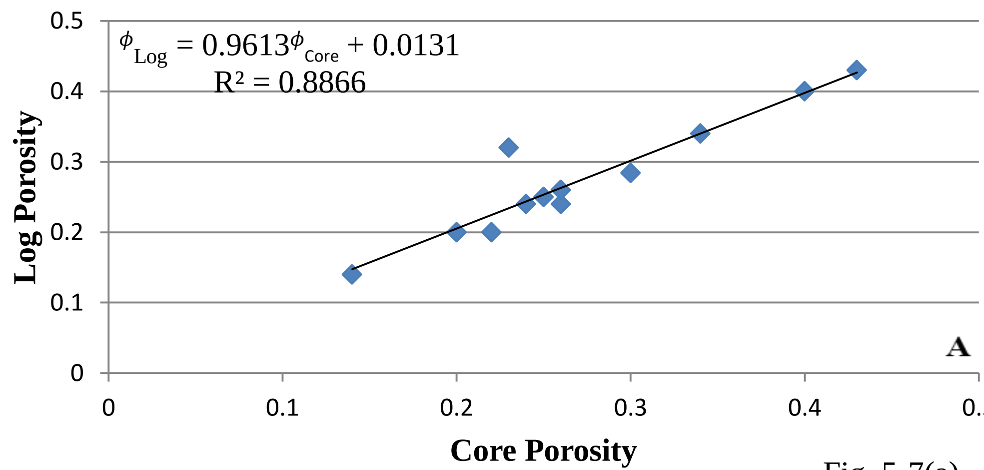

Fig. 5-7(a)

A relationship from the linear plot between core porosity and log porosity has been presented below.

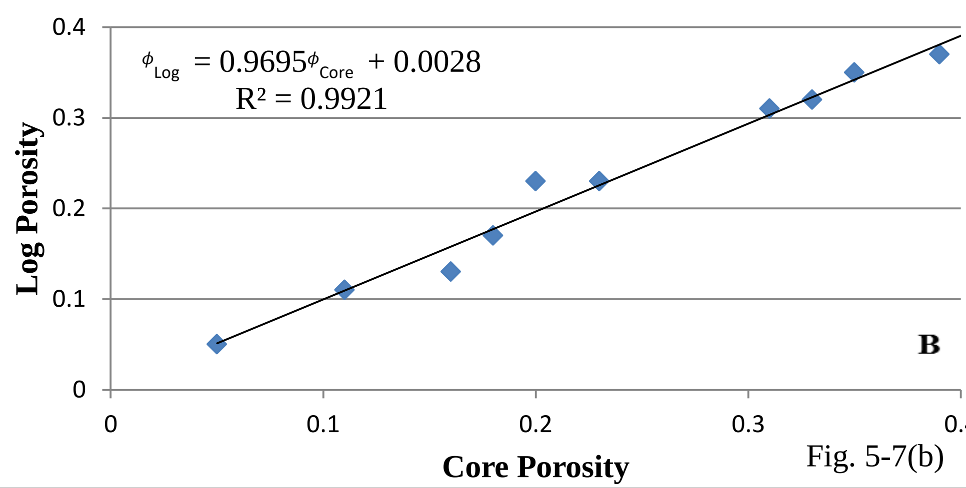

Fig. 5-7(b)

Cross plot between log porosity and core porosity of well C has been plotted and develops a linear relationship which is shown below.

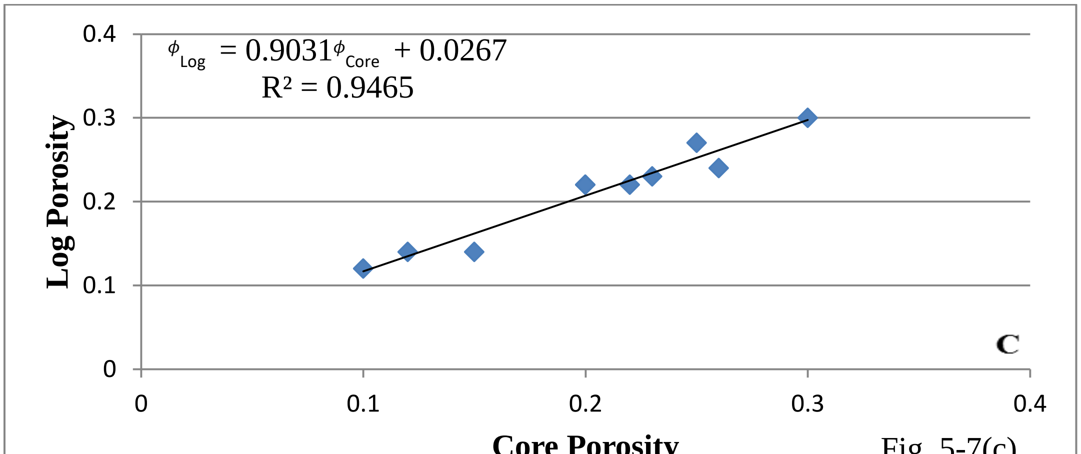

Fig. 5-7(c)

Linear relationship between core porosity and log porosity of well D has been plotted which is presented below.

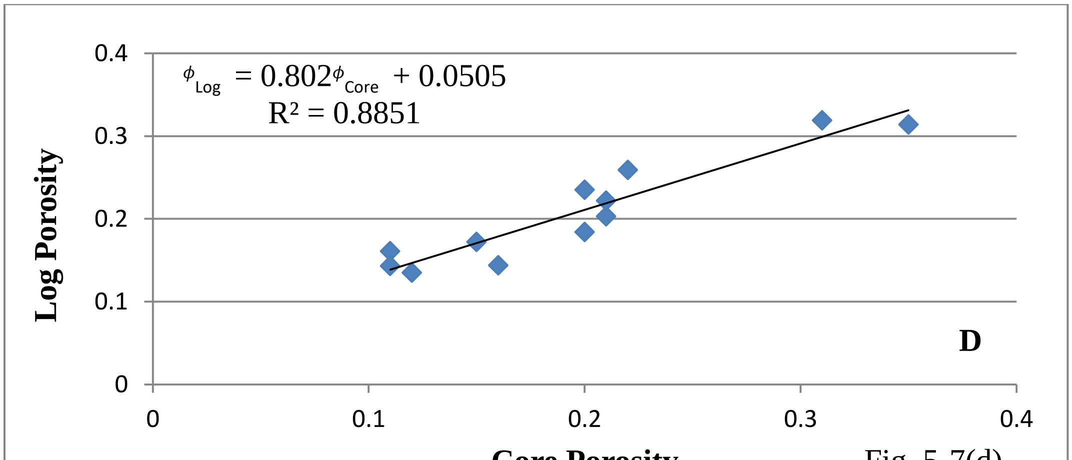

Fig. 5-7(d)

Figure 5-7: Well A, B, C and D core and log porosity linear relationship has been developed (a, b, c, d)

Porosity values evaluated from core and log analyses of well A, B, C and D is plotted on graphs with respect to depth.

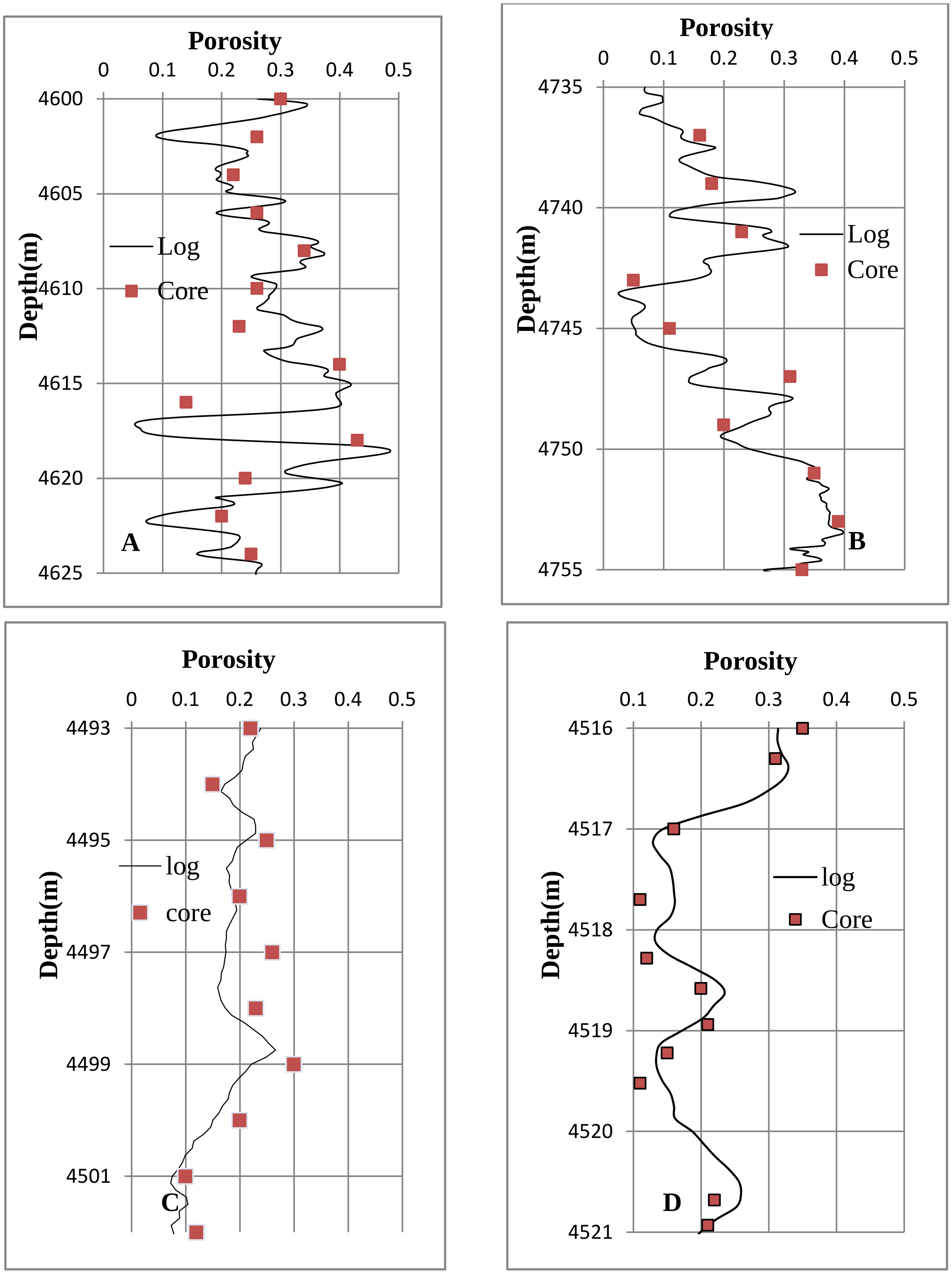

Figure 5-8: Well A, B, C and D correlation of porosity from core and log data with reference to same interval

Permeability values obtained from log interpretation and lab analysis of well A, B, C and D are plotted on graph.

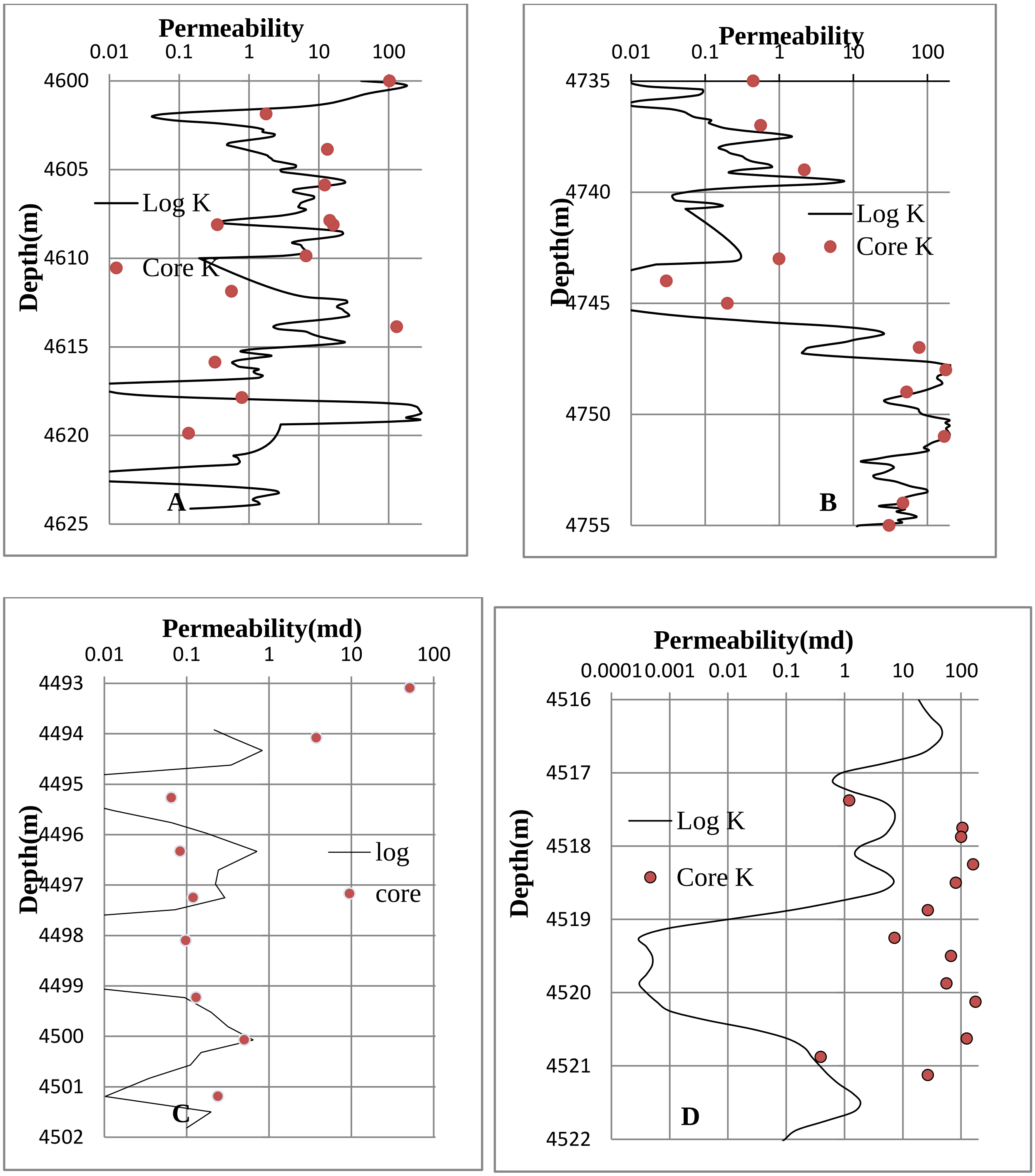

Figure 5-9 : Plot of well A, B, C and D has been developed to show the relation of permeability from core and log with respect to depth.

5.5 Porosity and Permeability Trend

Porosity and permeability trends of Datta formation (Jurassic Sandstone) of Upper Indus Basin of Pakistan have been developed on the basis of porosity and permeability data derived from different wells. According to the contours different horizons of porosity and permeability are presented on contour maps in figures (5-10 and 5-11). Porosity values ranges from 5 to 32% on porosity contour map which is scaled with colors of red, blue and green as represented in figure (5-10). Red color represents highest value of porosity and decreases from green to blue.

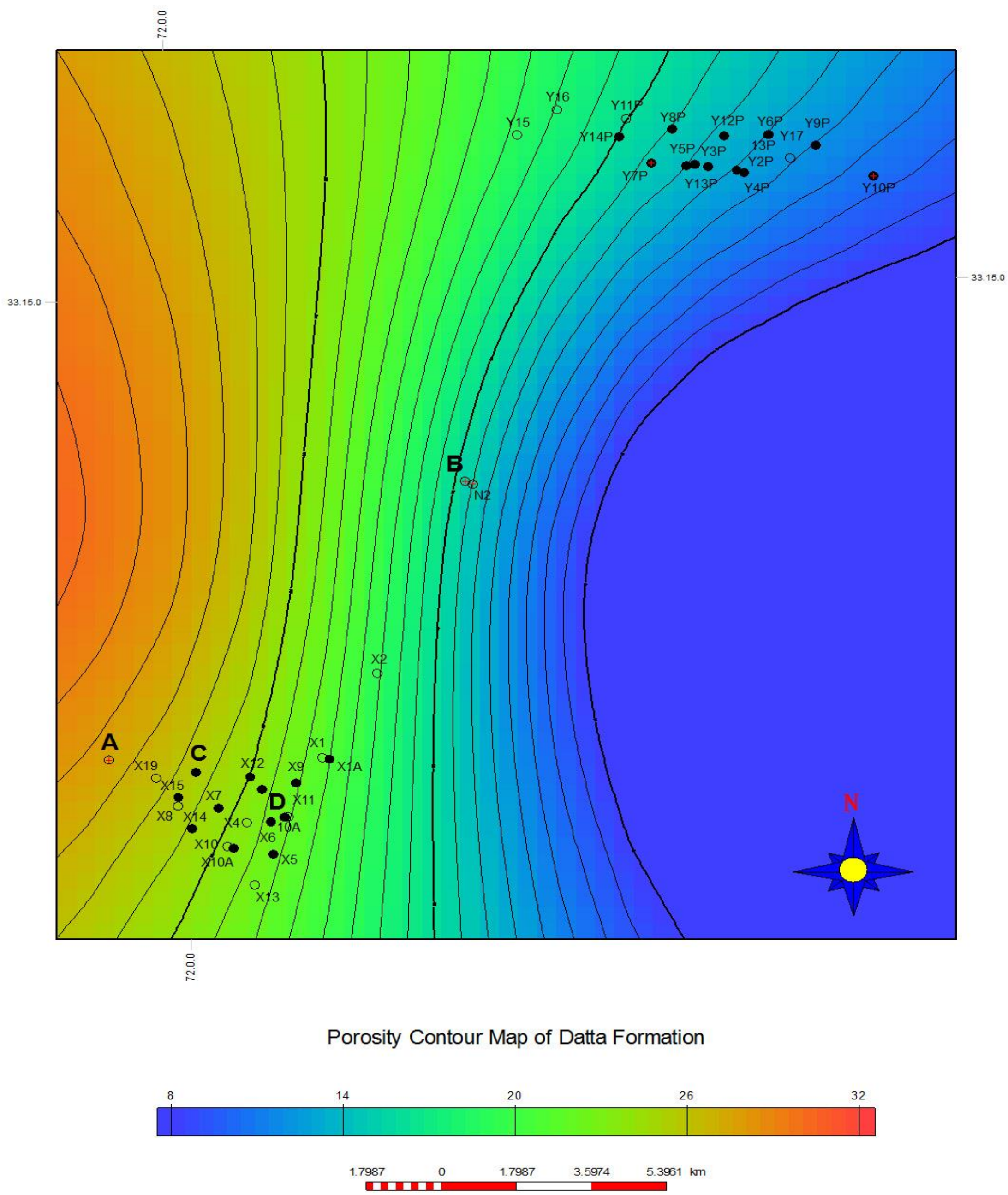

Figure 5-10: Porosity trend contour map of Datta Formation

Permeability values ranges from 0.1md to 300md and map is presented with red, green and blue color as a trend. In this trend highest value of permeability is lies in red color and decreases from green to blue figure 5-11.

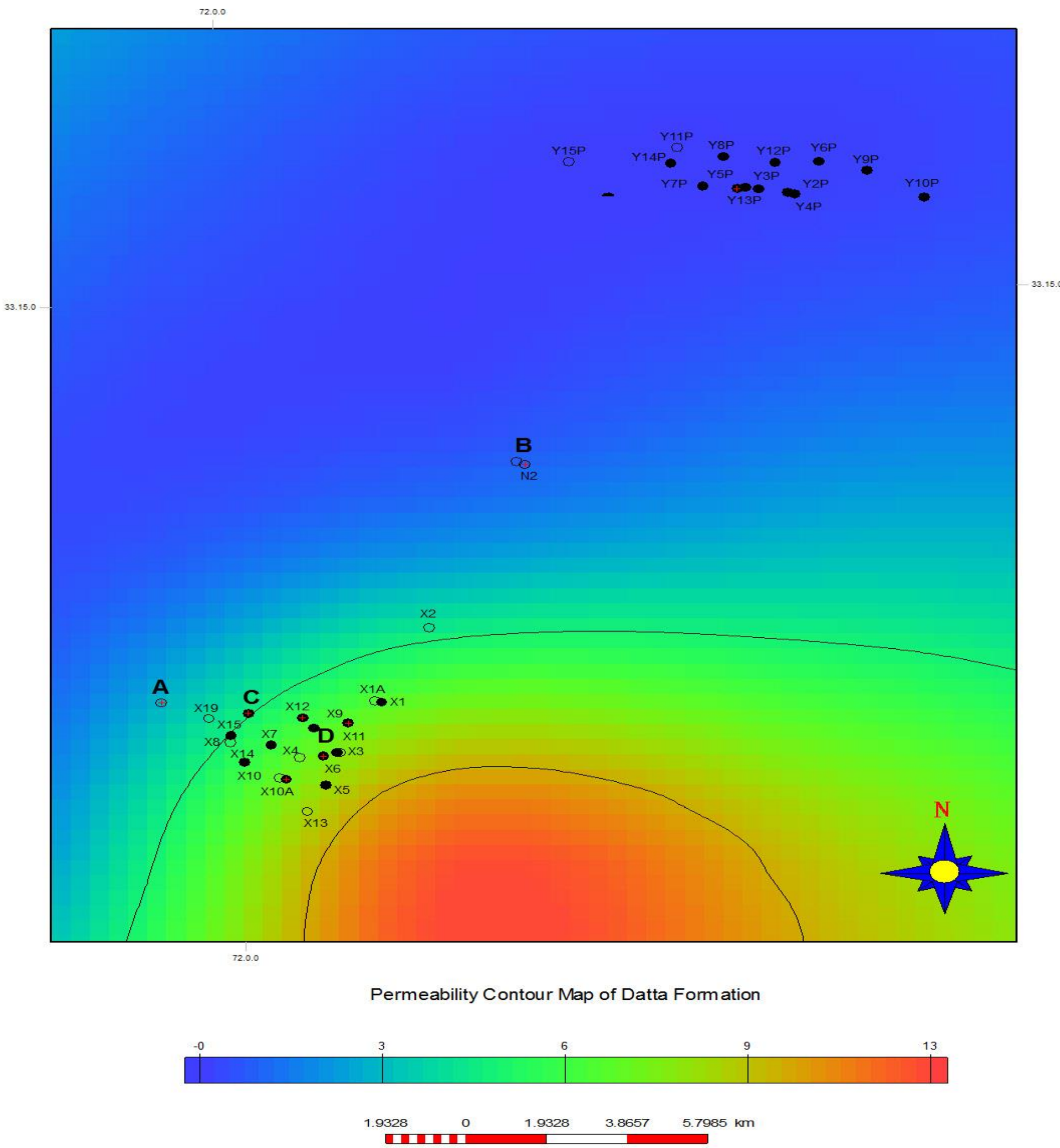

Figure 5-11: Permeability trend contour map of Datta Formation

Chapter 6 : Case Study of Multiphase Fluid Flow Through Porous Media

6.1 Introduction

Multiphase fluids flow through porous media effects reservoir potential and recovery mechanism. This study is focused on determining the flow behavior of Datta sandstone through relative permeability, capillary pressure and resistivity analysis of core plugs selected from wells C and D of Western Potowar area of Pakistan.

6.2 Relative Permeability Analysis

Five samples are selected for relative permeability and residual gas analysis. These five samples (now at immobile water saturation) have been evacuated under a surfactant free mineral oil of around 20 cp viscosity at ambient conditions. By applying back-pressure, samples have been cleaned through oil to eject remaining gas or mobile water in the pore spaces. At immobile water saturation, effective permeabilities of oil is determined for each sample to work as “base” permeabilities for later relative permeability measurement. As a function of time incremental effluents gas and oil volume is collected under constant pressure for each sample by injecting gas. At the excess of 30 in gas-oil relative permeability ratio the experiment is terminated. The tabulated data of each sample is given in appendix-II. Moreover, graphical representation of each sample is shown in figures given below:

Gas-oil relative permeability test of core sample no.1 of well A is conducted and found that 37 percent oil is recovered from the pore space, graphical representation is given below.

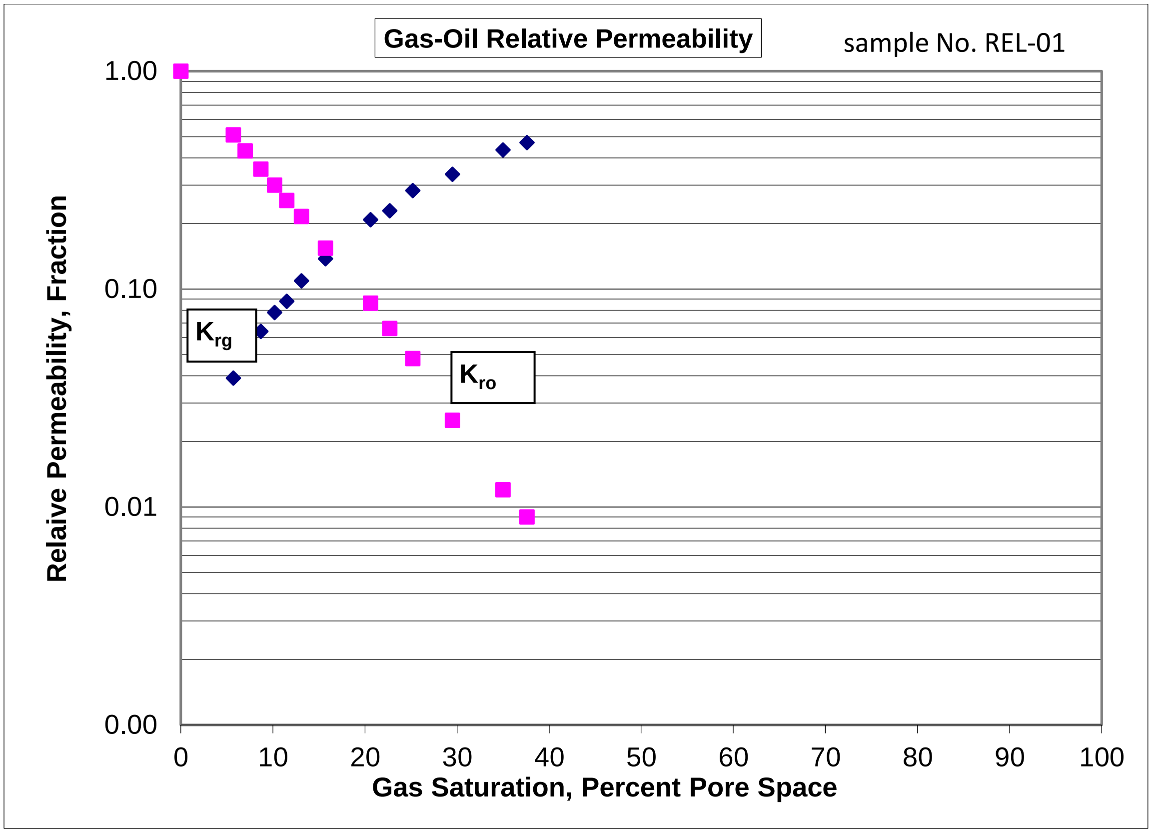

Figure 6-1: Gas-Oil relative permeability curves of Well C, Sample No. REL-01

Graphical results of sample no.2 of well C show that 49 percent oil is recovered from pore space.

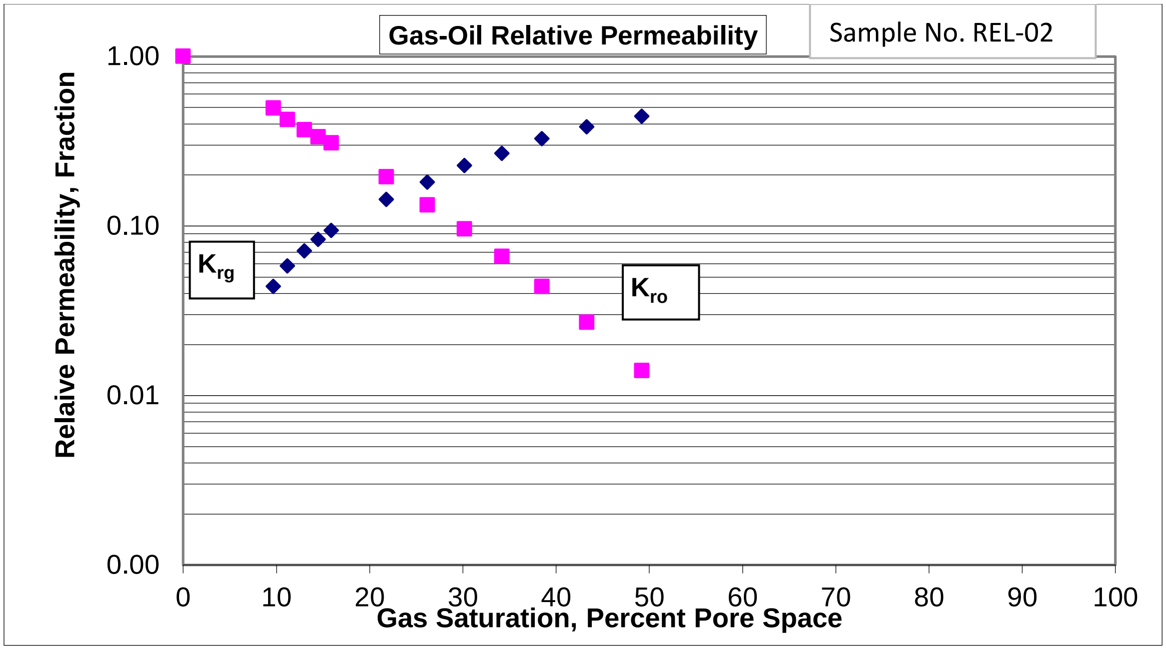

Figure 6-2: Gas-Oil relative permeability curves of Well C, Sample No. REL-02

Gas-oil relative permeability result of sample no. 3 shows that 40 percent oil is recovered from pore space.

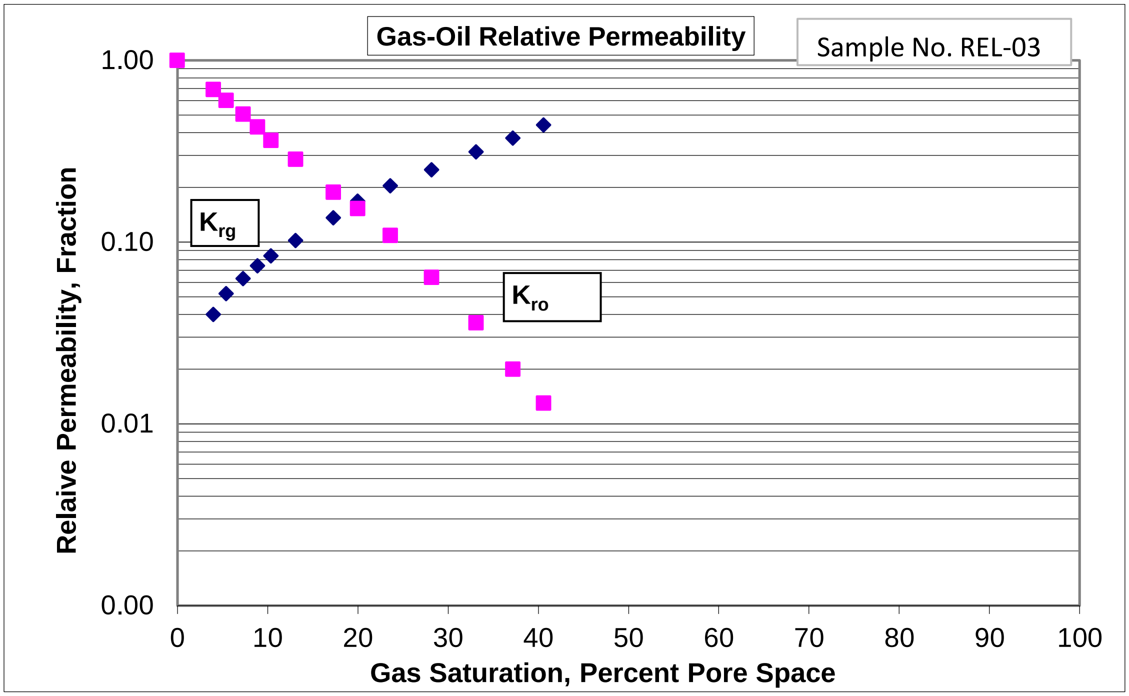

Figure 6-3: Gas-Oil relative permeability curves of Well C, Sample No. REL-03

Gas-oil relative permeability test of sample no. 4 of well D show that 40 percent oil is recovered from the pore space.

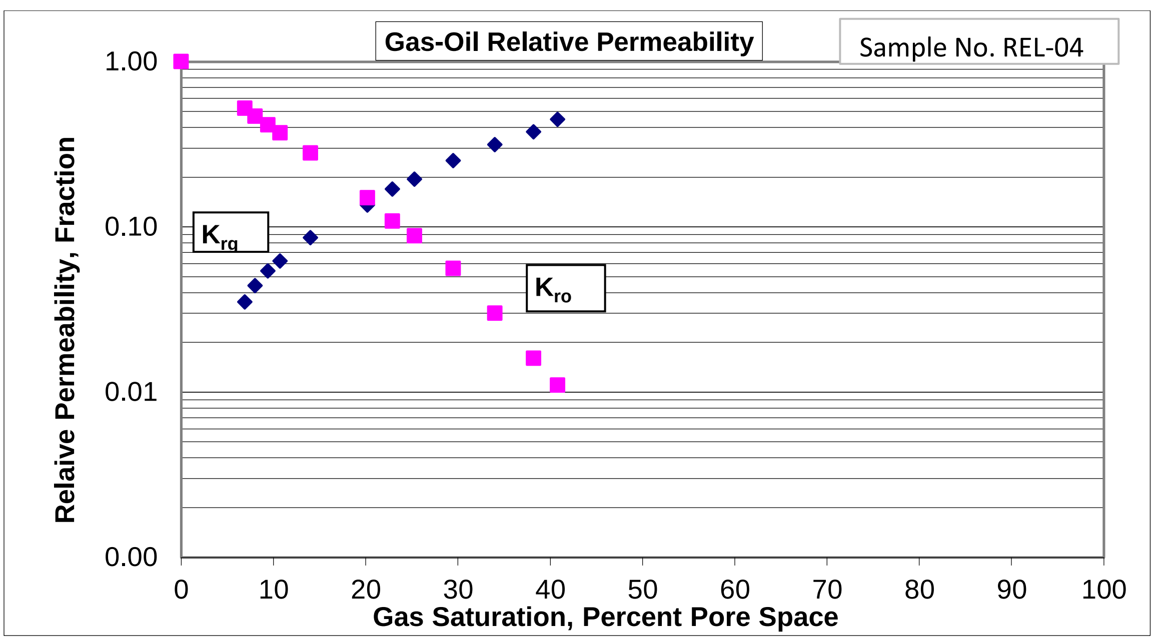

Figure 6-4: Gas-Oil relative permeability curves of Well D, Sample No. REL-04

Sample no. 5 of well D gas-oil relative permeability results shows that 45 percent oil is recovered from the pore space.

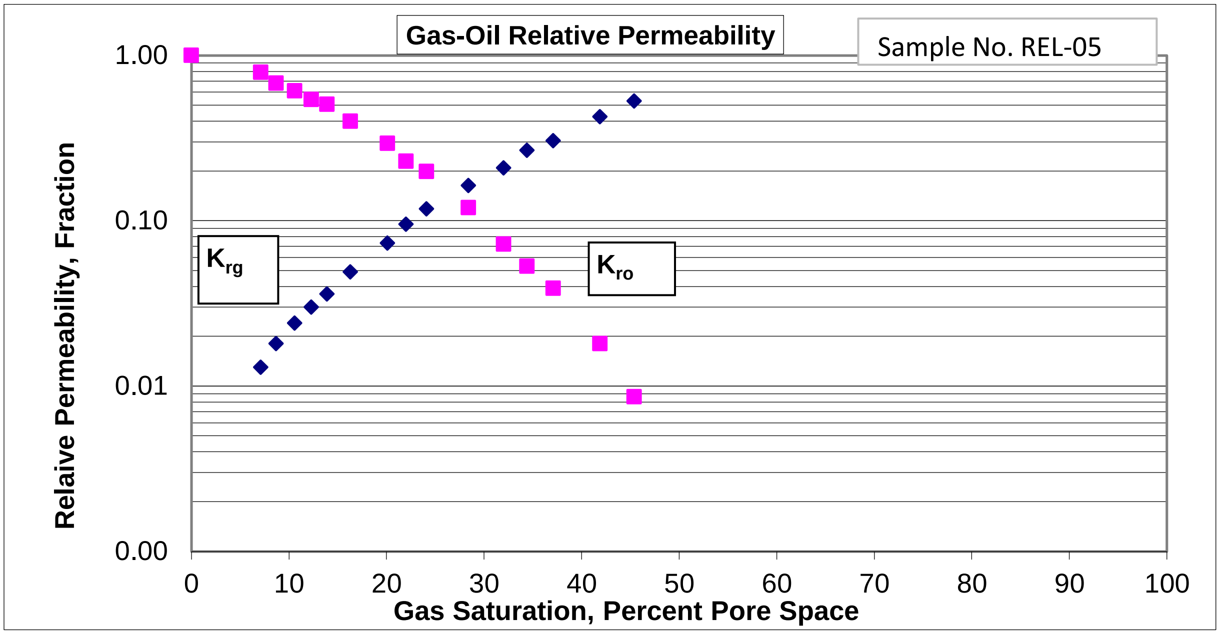

Figure 6-5: Gas-Oil relative permeability curves of Well D, Sample No. REL-05

Gas-oil ratio has been obtained from gas-oil relative permeability analysis. From these five analyses of well C and D it is observed that maximum oil recovery is 49 percent of sample no. 2 of well C and minimum oil recovery is 37 percent of sample no. 1 of well C.

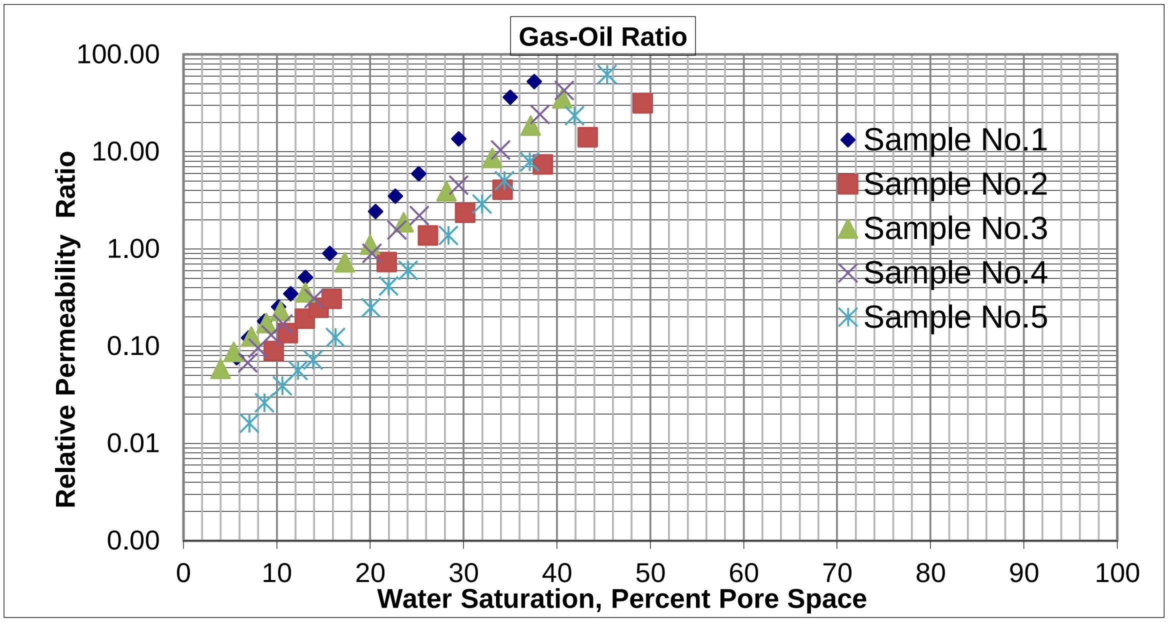

Figure 6-6: Gas-Oil relative permeability ratio curves of Well C and D, Sample No. REL-(01-05)

The similar tests are also performed for oil-water relative permeability but meaningful results could not be attained. The tabulated data for oil-water relative permeability is given in appendix-II. Moreover, graphical representation is given below:

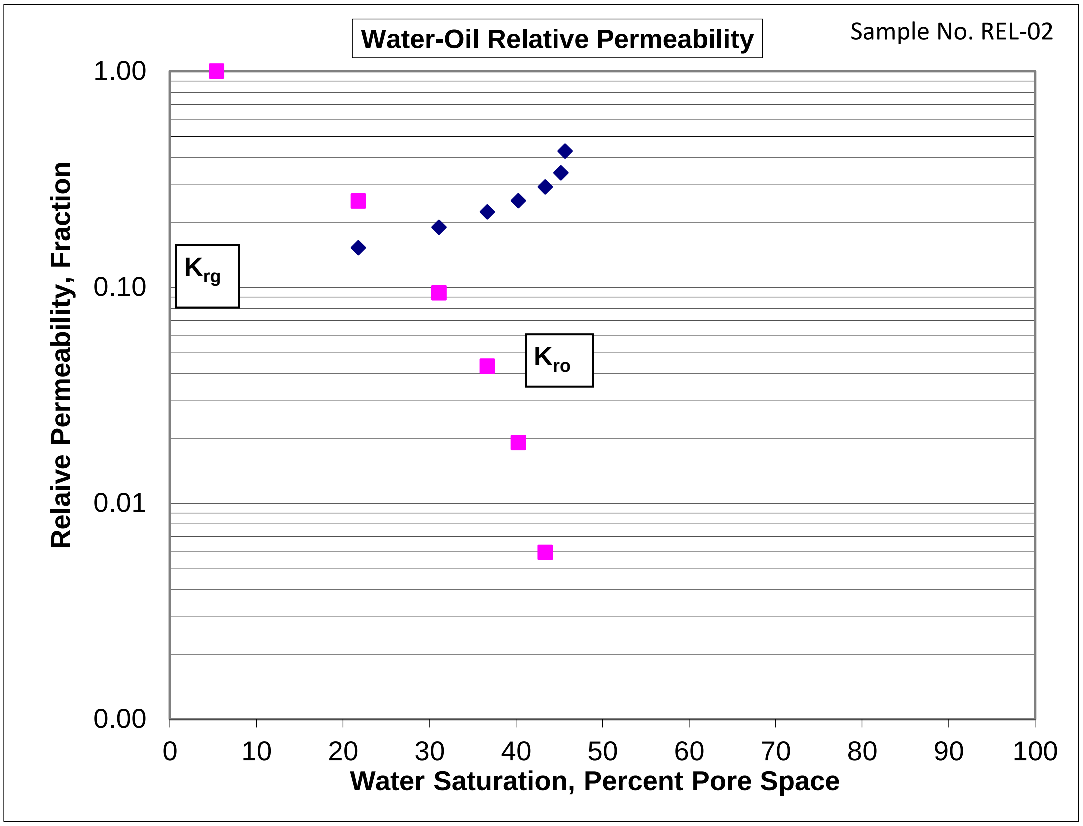

Figure 6-7: Water-oil relative permeability curves of Well C, Sample No. REL-02

Through Gas-Oil relative permeability test it is observed that oil recovered ranges from 37 to 49 percent as shown in table 6-1.

Table 6-1: Summary of oil, gas and water recovery

Sample ID		Depth in Meters	Permeability to Air Milidarcey	Porosity Percent	Initial Conditions: Water saturation, Percent Pore Space	Initial Conditions: Effective Permeability to Oil Milidarcys	Terminal Conditions: Oil Saturation, Percent Pore Space	Terminal Conditions: Effective Permeability to Gas Milidarcys	Oil Recovered: Percent Pore Space	Oil Recovered: Percent Oil in Place
Well C	REL-01	4451.45	63	10.1	11.7	57	50.7	27	37.6	42.6
	REL-02	4456.57	220	12.6	5.4	82	45.4	80	49.2	52
	REL-03	4456.84	9.4	8.4	7.1	6	52.3	2.6	40.6	43.7
Well D	REL-04	4492.81	117	10.6	3.1	110	56.1	49	40.8	42.1
	REL-05	4501.82	2.1	10.7	19.9	0.68	34.7	0.36	45.4	56.7

Water-oil test is performed and recovery of oil ranges from 36 to 66 percent as shown in table (6-2) given below:

Table 6-2: Summary of water-oil relative permeability Test Results

Sample ID		Depth in Meters	Permeability to Air Milidarcey	Porosity Percent	Initial Conditions		Terminal Conditions		Oil Recovered	
					Water saturation, Percent Pore Space	Effective Permeability to Oil Milidacys	Oil Saturation, Percent Pore Space	Effective Permeability Water Milidarcys	Percent Pore Space	Percent Oil in Place
Well C	REL-01	4451.45	63	10.1	11.7	57	55.8	18	32.5	36.8
	REL-02	4456.57	220	12.6	5.4	182	54.3	78	40.3	42.6
	REL-03	4456.84	9.4	8.4	7.1	6	53.5	1.6	39.4	42.4
Well D	REL-04	4492.81	117	10.6	3.1	110	67.5	17	29.4	30.3
	REL-05	4501.82	2.1	10.7	19.9	0.68	27.2	0.04	52.9	66

6.3 Capillary Pressure Analysis

For centrifuge capillary pressure tests, plug samples are cleaned in methanol, dried at 80 ^oC. The selected five samples for residual gas tests are evacuated and pressure saturated with toluene. Each sample is then allowed to imbibe toluene by being submerged in the fluid, and the residual gas saturation determined gravimetrically. Results founded from the capillary pressure analysis it is observed that the samples are strongly wetting characteristics which will readily allow imbibition. From capillary pressure test it is observed that as pressure increases from 0 to 1000psi the brine saturation level also decreases ranges from 100 to 3.3 percent. Sample No. 5 of well C highest brine saturation ranges from 100 to 13 percent at pressures ranges from o to 1000psi. The graphical representation of capillary pressure data is given below:

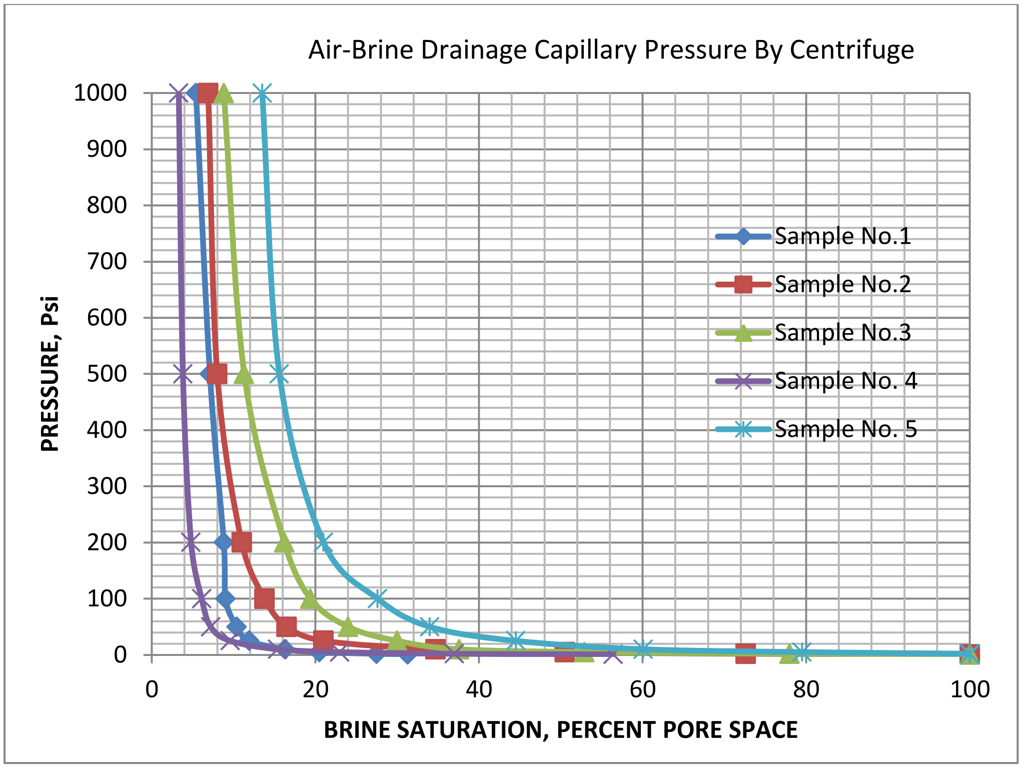

Figure 6-8: Air-Brine Drainage Capillary Pressure

The results showed that values achieved for immobile water saturation are unexpectedly low considering the rather low permeability of many of the samples.

6.4 Formation Factor as a Function of Overburden Pressure

Five samples were evacuated and saturated by pressure with simulated formation brine approximately 65,000 mg/1 concentration. On consecutive overburden pressure of 200, 3700 and 7400 psi the electrical resistivity of brine-saturated samples is determined. On direct observation of incremental brine displacement, porosity reduction is calculated. The calculated formation factor values are shown below:

From graph given below it is observed that an intercept “a” of unity, the composite plots yields values for the cementation exponent, “m,” is 1.69 at effective overburden pressures of 0 psi.

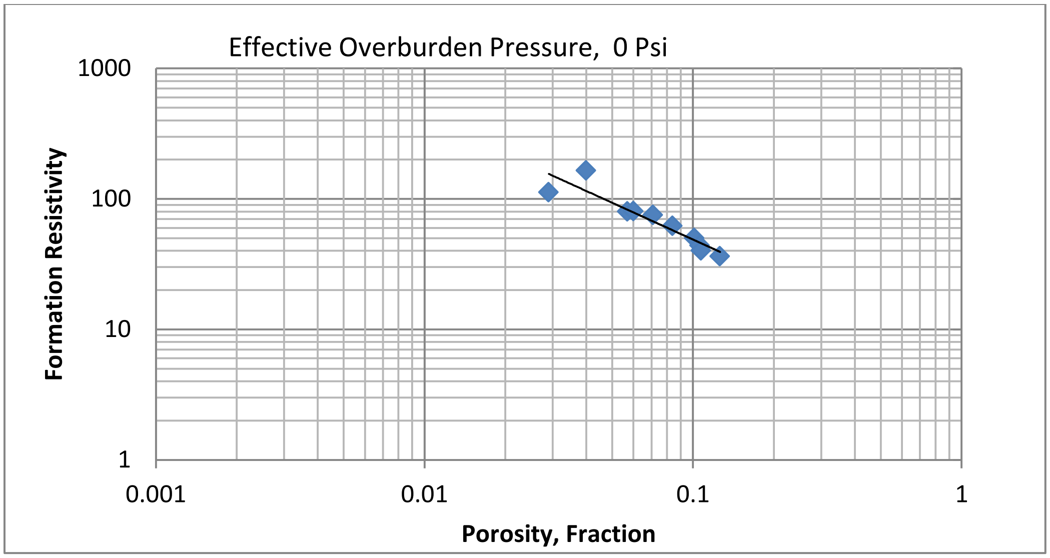

Figure 6-9: Effective Overburden Pressure at 0 Psi

It is observed that an intercept "a" of unity, the composite plots yields values for the cementation exponent, "m," is 1.72 at effective overburden pressures of 200 psi.

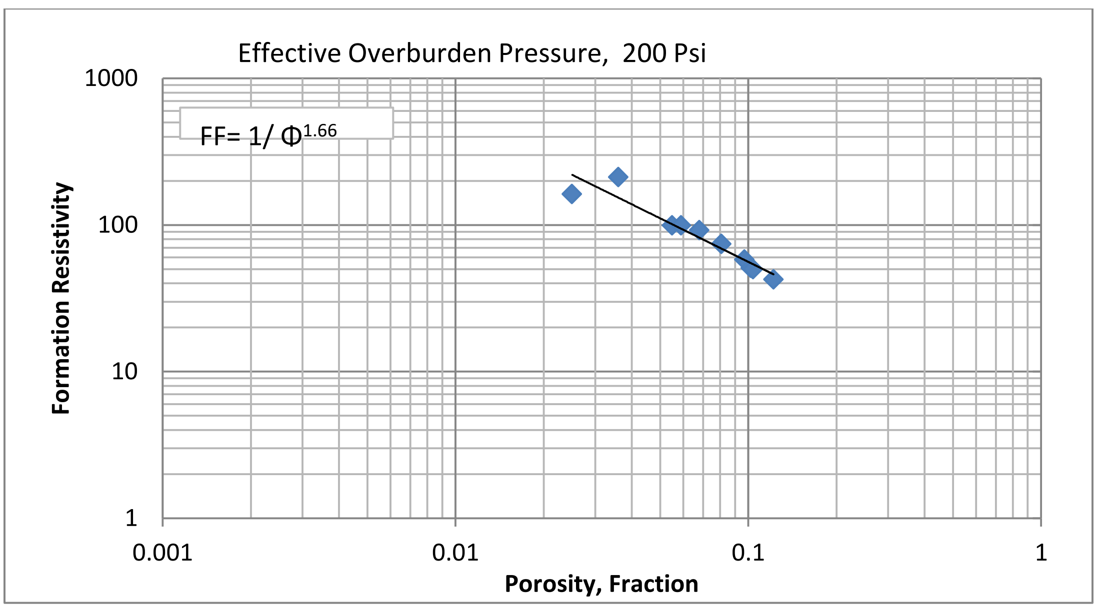

Figure 6-10: Effective Overburden Pressure at 200 Psi

It is observed that an intercept "a" of unity, the composite plots yields values for the cementation exponent, "m," is 1.91 at effective overburden pressures of 3700 psi.

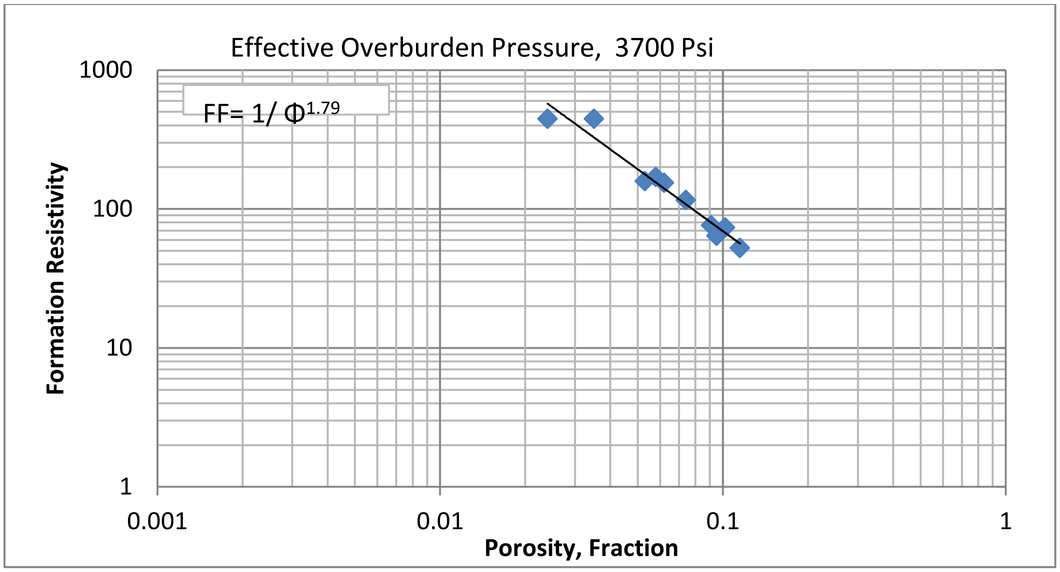

Figure 6-11: Effective Overburden Pressure at 3700 Psi

6.5 Formation Resistivity Index

After cleaning with hot methanol and drying at 80 ^{0}C, these five samples were tested for formation resistivity index. From these resistivity determinations on samples of known water saturation, resistivity index values were calculated. The graphical data is shown on figure (6-13 to 6-17). The composite figure (6-18) yields an average saturation exponent, “n,” of 1.80 for the samples from well C and D.

The graphical representation of sample (1) is given below:

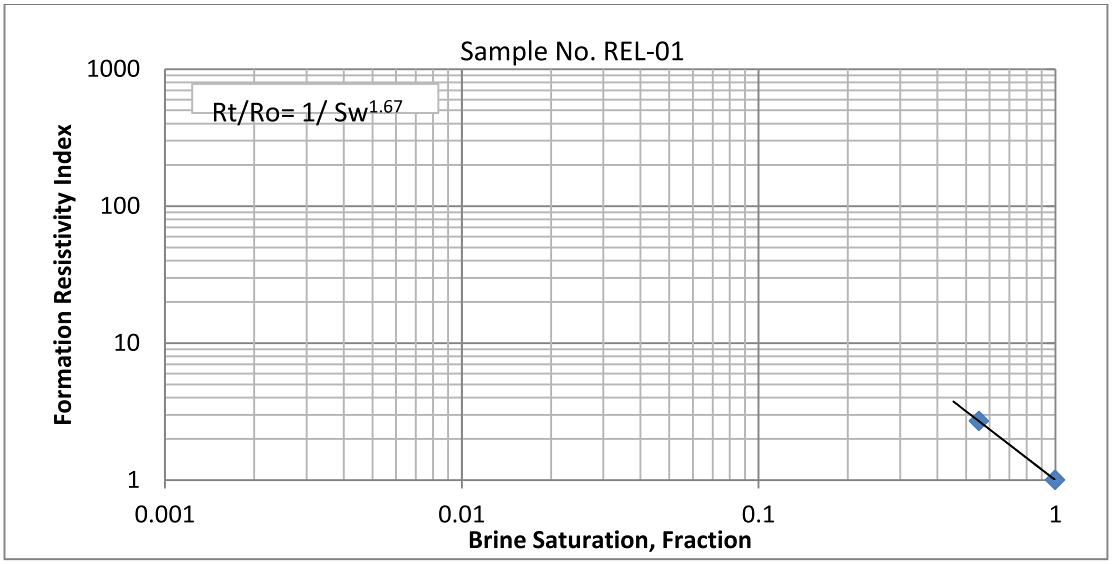

Figure 6-12: Formation Resistivity Factor and Resistivity Index of Well C, Sample No. REL-01

The graphical representation of sample (2) is given below:

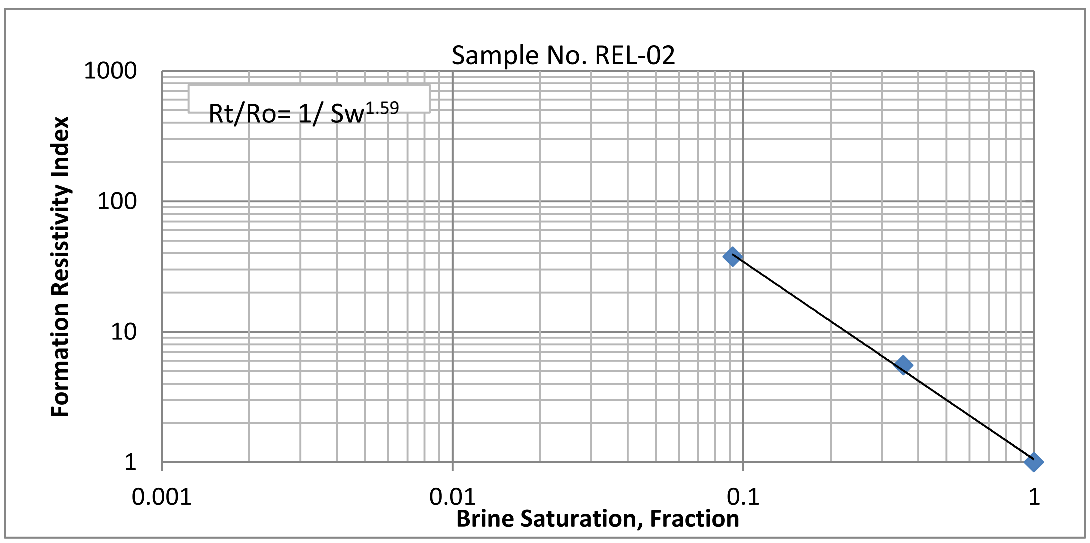

Figure 6-13: Formation Resistivity Factor and Resistivity Index of Well C, Sample No. REL-02

The graphical representation of sample (3) is given below:

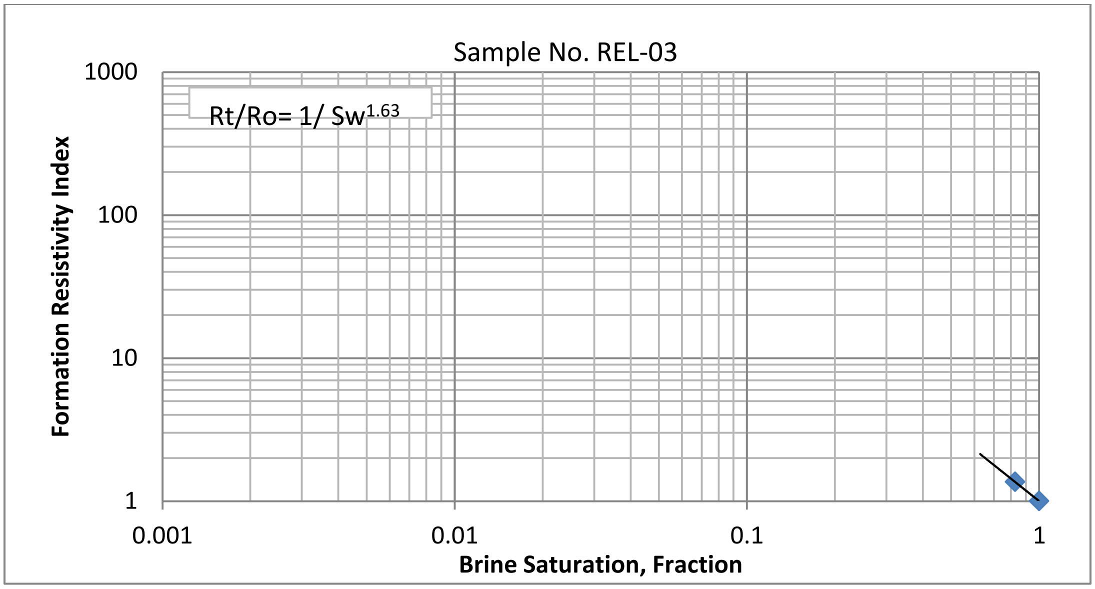

Figure 6-14: Formation Resistivity Factor and Resistivity Index of Well C, Sample No. REL-03

The graphical representation of sample (4) is given below:

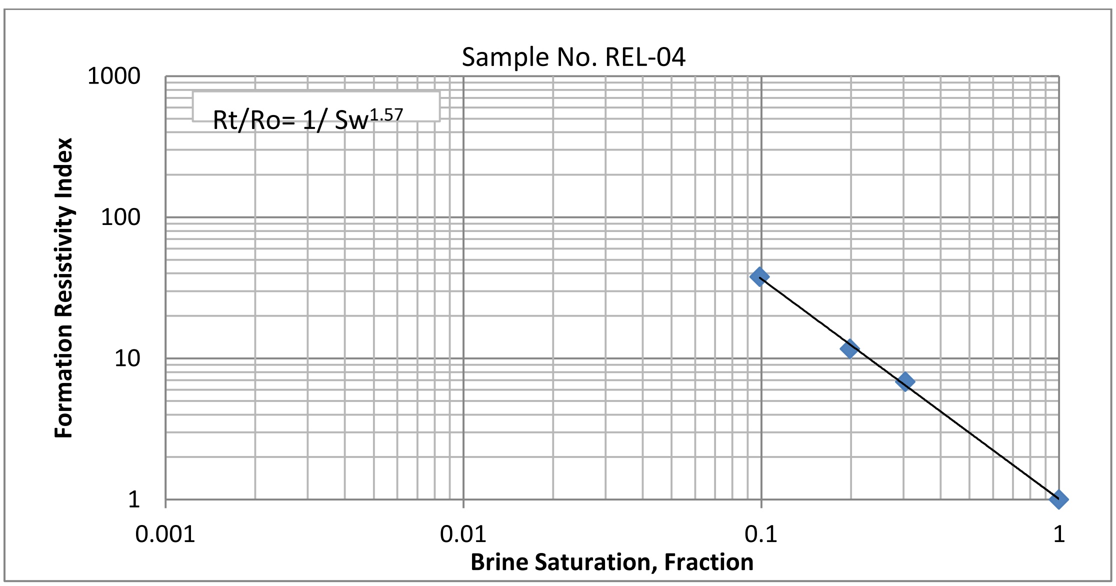

Figure 6-15: Formation Resistivity Factor and Resistivity Index of Well D, Sample No. REL-04

The graphical representation of sample (5) is given below:

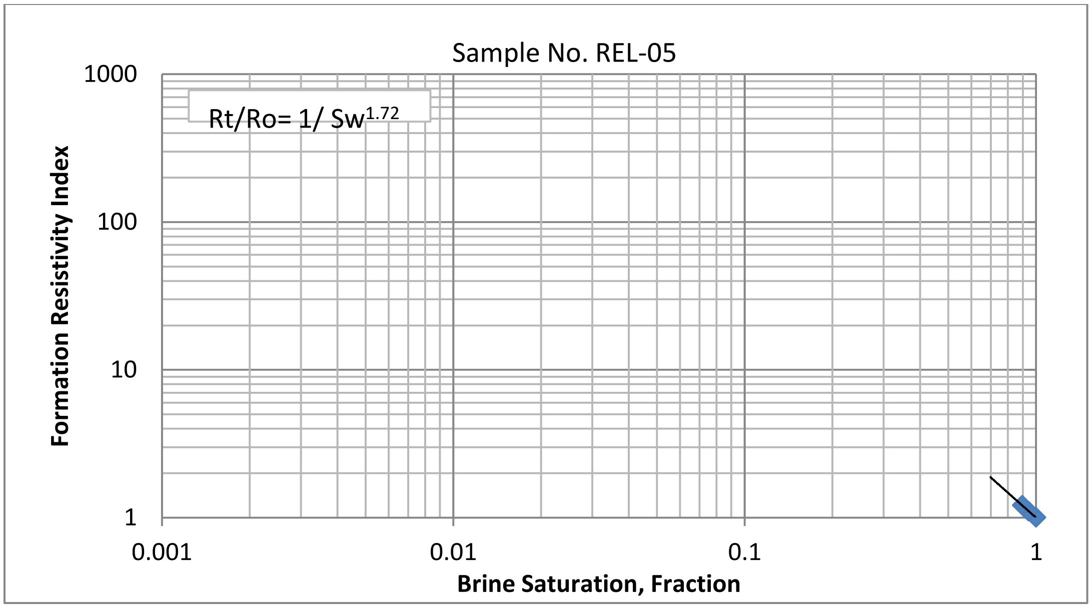

Figure 6-16: Formation Resistivity Factor and Resistivity Index of Well D, Sample No. REL-05

The graphical representation of composite is given below:

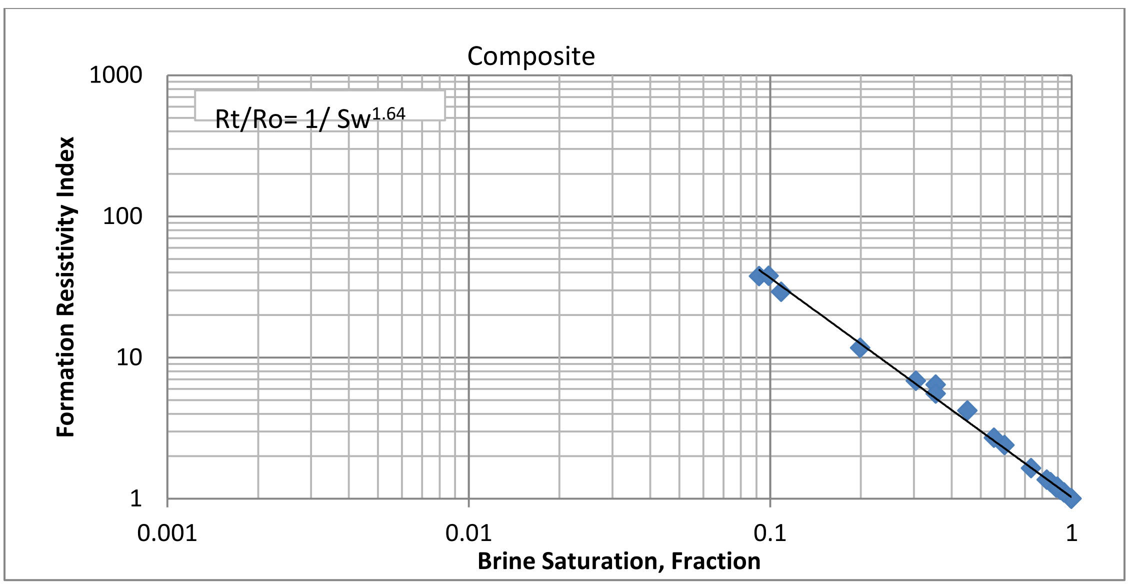

Figure 6-17: Formation Resistivity Factor and Resistivity Index

6.6 Multiphase Flow Behavior of Datta Sandstone

The results showed that oil recovery is greater from water-oil relative permeability test as compare to gas-oil relative permeability tests. It represents the greater efficiency of the water-drive system in the reservoir. Contrary to this, observations made on the end-point data showed less recoverable oil from water-oil system as compare to gas-oil system. This uncharacteristic data for oil-water system is due to lithological heterogeneities. Moreover, these heterogeneities may also affect gas-oil data. The data obtained is not consistent either with the type of deleterious rock-brine interaction, that often results in low oil recovery and unrepresentative incremental data for water-oil relative permeability tests. The data produced is affected by core contamination (drilling/coring fluid). By conducting gas-oil and water-oil relative permeabilities analysis, oil flow rate ranges from 2.59 to 790 cc/sec and gas flow rate ranges from 1.5 to 347cc/sec. It can be observed that oil flow rate is higher than gas flow rate. The details of oil and gas flow rates are shown in table (6-7). The flow rate of oil and gas has been derived from equation 6.1.

$$Q = \frac{A\Delta P}{K\mu L} \ (Darcy's\ Law) \qquad (6.1)$$

Table 6-3: Oil and Gas Flow rates and permeabilities

Sample ID		Depth in Meters	Effective Permeability to Oil (Milidacys)	Effective Permeability to Gas (Milidarcys)	Permeability to Air (Milidarceys)	Viscosity(cp)	Length (cm)	Area (cm^2)	Change In Pressure (Psi)	Flow Rate Q_o(cc/sec)	Flow Rate Q_g(cc/sec)
Well C	REL-01	4451.45	57	27	63	20	7.62	11.39	1	247.4682	117.2218
	REL-02	4456.57	182	80	220	20	7.62	11.39	1	790.1617	347.3238
	REL-03	4456.84	6	2.6	9.4	20	7.62	11.39	1	26.04929	11.28802
Well D	REL-04	4492.81	110	49	117	20	7.62	11.39	1	477.5703	212.7358
	REL-05	4501.82	0.68	0.36	2.1	20	7.62	11.39	1	2.952252	1.562957

A linear relation has been observed between the permeability of oil and gas to flow rate of oil and gas which is shown in Figure no. (6.19).

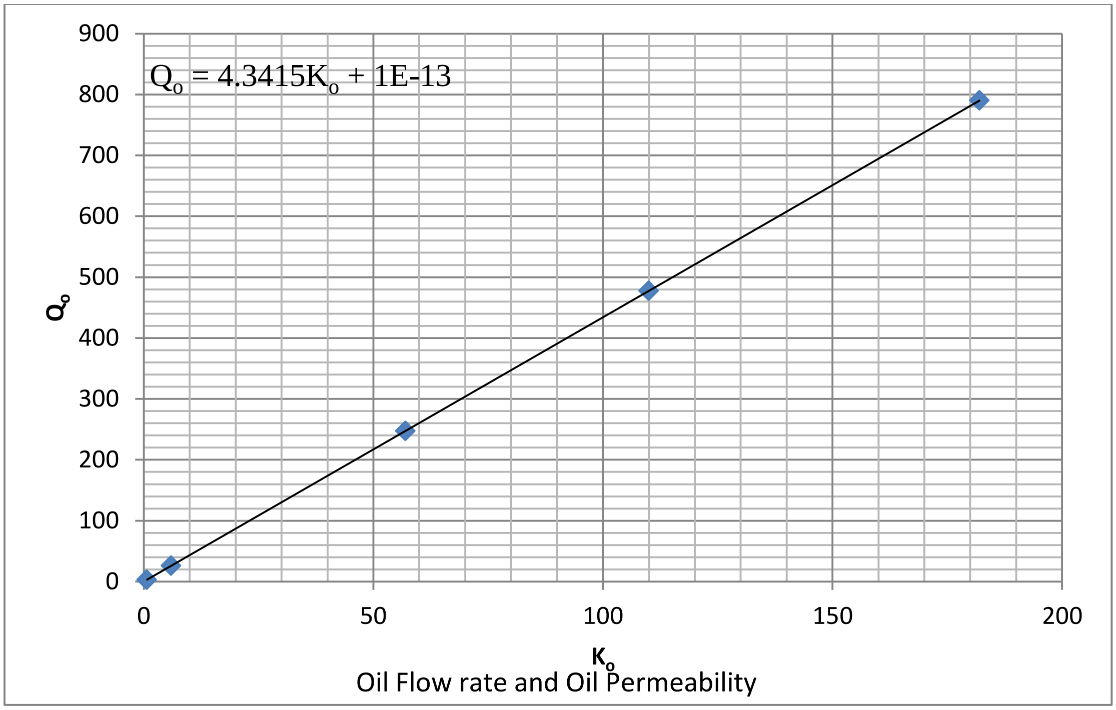

Figure 6-18: Oil flow rate and oil permeability

A similar trend is also observed between gas flow rate and permeability as shown below:

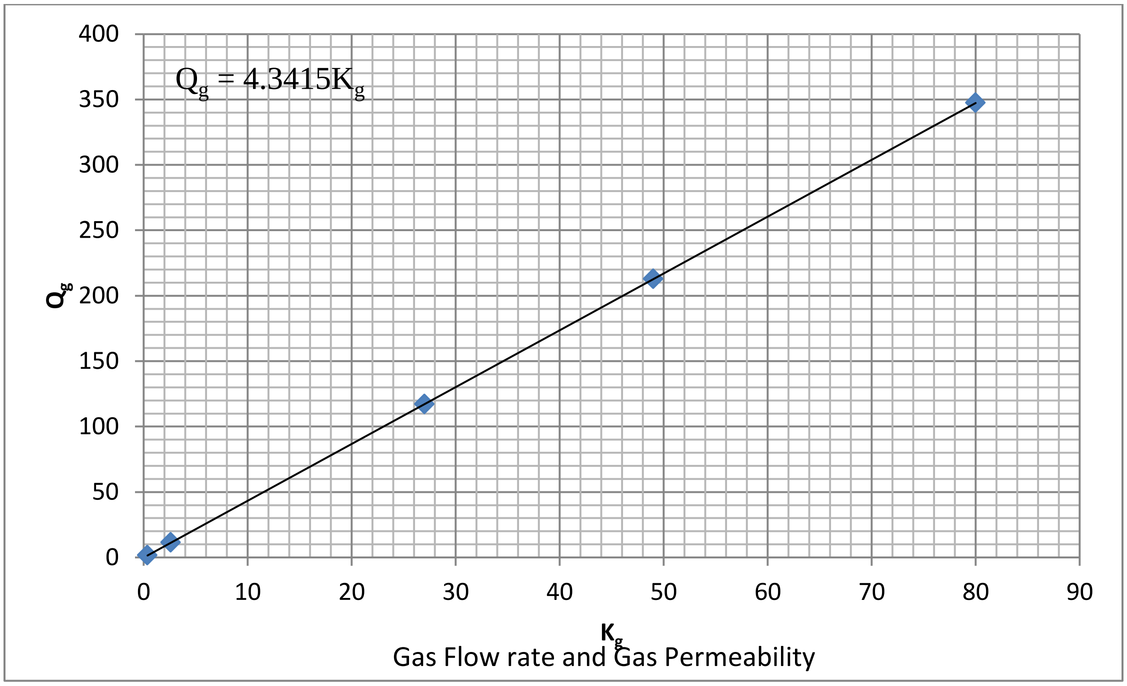

Figure 6-19: Gas flow rate and gas permeability

Correlation of oil flow rate with oil permeability has been developed which is explained in equation no. 6.2. Similarly, correlation of gas flow rate with gas permeability is defined in equation no. 6.3.

$$Q_o = 4.3415K_o + 1E - 13 \quad (Relationship\ of\ oil\ flow\ rate\ and\ oil\ permeability) \quad (6.2)$$

$$Q_g = 4.3415k_g \quad (Relationship\ of\ gas\ flow\ rate\ and\ gas\ permeability) \quad (6.3)$$

Core samples of Datta Sandstone from different wells have been selected for measurement of oil and gas flow rate. After selection of core samples and flow rate measurement oil and gas flow rate trends have been developed through contour map as shown in figure (6-20 & 6-21).

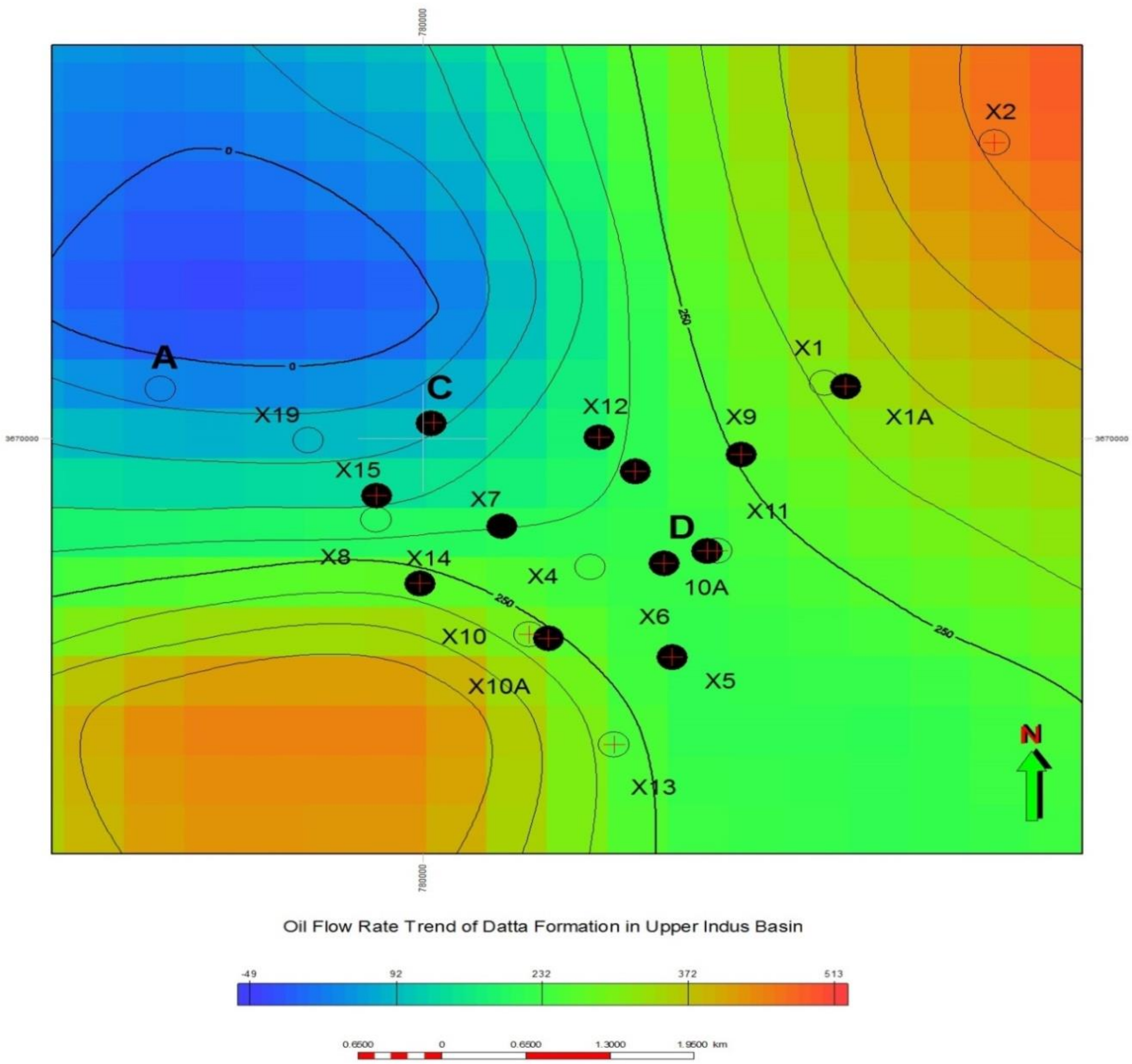

Figure 6-20: Oil flow rate trend contour map of Datta Formation of Upper Indus Basin

Blue color depicts minimum flow rate but green and red colors are specified for medium to maximum flow rates. The contour map for gas flow rate is given below:

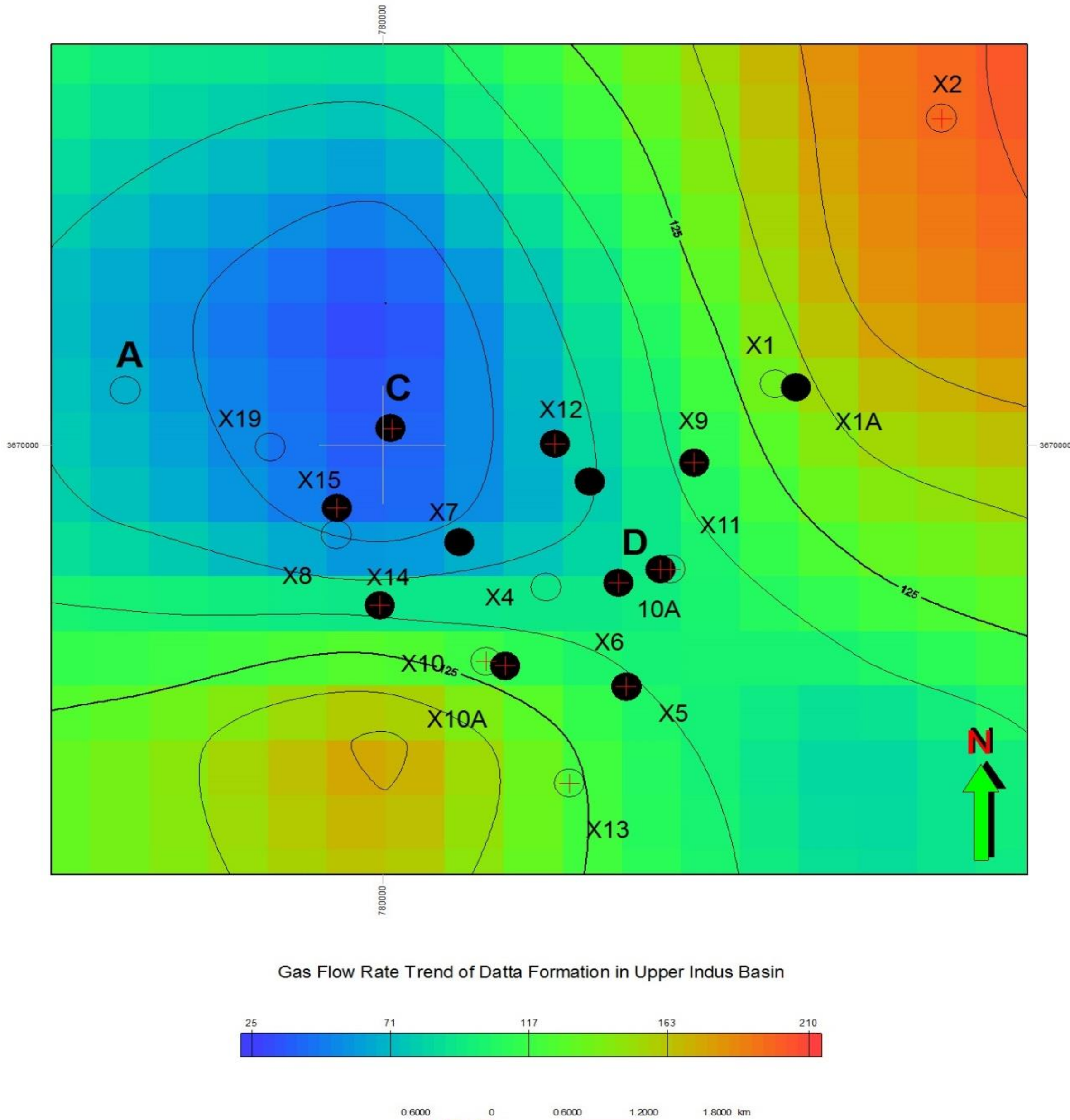

Figure 6-21: Gas flow rate trend contour map of Datta Formation of Upper Indus Basin

Chapter 7 : Conclusion and Recommendations

7.1 Conclusion

- The density results from logs and core are in close relationship for all major intervals in all wells. Similarly, results of porosity and permeability from log and core are similar for major intervals of the wells (A, B, C, and D).

- Based on the research, linear relationship exists between core and log porosity. For wells A, B, C and D regression coefficient R^2 values are 0.8866, 0.9921, 0.9465 and 0.8851 respectively. Porosity values vary in all wells. The porosity value for well B is greater as compared to well A, C and D.

- The porosity and permeability contour maps of Upper Indus Basin of Pakistan have been developed based on porosity and permeability data. Porosity values ranges from 0.324% to 20% and permeability values ranges from 0.0035 md to 1284 md.

- From the core samples of well C and D of Datta Sandstone it is concluded that oil recovery is less in water-oil as compared to gas-oil tests. By conducting gas-oil and water-oil relative permeabilities analysis, oil flow rate ranges from 2.59 to 790 cc/sec and gas flow rate ranges from 1.5 to 347cc/sec. It can be observed that oil flow rate is higher than gas flow rate.

- From capillary pressure test of core samples of well C and D, it has been observed that the samples have strong wetting characteristics, which readily allow imbibition.

- Based on the resistivity analysis, cementation factor “m” of well C and D of core samples ranges from 1.69 to 1.91.

7.2 Recommendations

- Enhance Oil Recovery study can be conducted to recover the remaining potential of the reservoir.

- Simulation study can be conducted on this available lab analysis and results.

References

Alam, E. D. (2008). Wettability. Texas: Gulf Publishing company.

Adamson A.W.: “Physical Chemistry of Surfaces,” John Wiley & Sons, 1982.

Archie, G.E.: “The Electrical Resistivity Log as an Aid in Determining Some Reservoir Characteristics,” AIME, 1942, p. 54.

Archie, G.E.: “Classification of Carbonate Reservoir Rocks and Petrophysical Considerations,” Bull., AAPG(Feb 1952) 36, No. 2.

Blanchard, A. and Dewan, J.T. (1953), “Calibration of Gamma Ray Log.”

Bear J.C.: “Dynamic of Fluids in Porous Media,” American Elsevier, 1972.

Buckley, S.E.: “Mechanisms of Fluid Displacement in Sands,” AIME, 1942, vol. 146, 107.

Boxiao Li and Sally M. Benson:“Small-scale Heterogeneities and Buoyancy-driven CO_2 Migration in Geological Storage” Energy Procedia 63 (2014) 3608 – 3615

Bannert, D., Raza H.A., 1992.The segmentation of the Indo-Pakistan Plate. Pakistan Journal of Hydrocarbon Research, 4(2), 5-18.

Brooks, R.H., and Corey, A.T., 1964, Hydraulic properties of porous media: Hydrology Papers, Colorado State University, 24 p

Collins R.E.: “Flow of Fluid through Porous Materials,” Reinhold Pub. Co., 1961.

Cosse R.: “Basics of Reservoir Engineering,” Editions Technip, Paris, 1993.

Craig F.: “The Reservoir Engineering Aspects of Waterflooding,” Monograph Volume 3, AIME, 1971.

ChineduAgbalaka, S. O., Abhijit Y. Dandekar, S. S., & and James R. Hemsath, A. E. (2008, October). The Effect Of Wettability On Oil Recovery: A Review. Society of Petroleum Engineers.

Charles Robert Smith, G. W. (1992). Applied Reservoir Engineering (Vol. 1). Pennsylvania: OGCI publications.

Dullien, F. (1992).Porous Media (Fluid Transport and Pore Structure) 2nd Edition. United States: Academic Press.

Djebbar, T., & Donaldson, E. C. (2004).Petrophysics - Theory and Practice of Measuring Reservoir Rock and Fluid Transport Properties (2nd Edition). USA: Elsevier Gulf Professional Publishing.

Djebbar, T., & Donaldson, E. C. (2004).Petrophysics(SeondEDition).

Donnez P. (2007). Essentials of Reservoir Engineering, 387 pp., Paris, Technip. [A modern and concise handbook on hydrocarbon reservoir engineering and reservoir modeling]

Doll H.G. (1948). American Institute of Mining, Metallurgical, and Petroleum Engineers AIME, “The SP Log: Theoretical Analysis and Principles of Interpretation”.

Doll H.G. (1950) “The SP Log in Shaly Sands” Trans, AIME.

Gaymard, J. and Poupon, A. (1968), “Response of Neutron and Formation Density Log in Hydrocarbon-Bearing Formation,” The Log Analyst.

Gee, E. R. (1980) Pakistan geological Salt Range series: Directorate of Overseas Surveys, United Kingdom, for the Government of Pakistan and Geological Survey of Pakistan, 6 sheets, scale 1:50,000.

Gee, E. R. (1989) Overview of the geology and structure of the Salt Range with observations on related areas of northern Pakistan. In: L.L. Malinconico Jr. and R.J. Lillie (Eds.), Tectonics of the western Himalayas. Geol. Soc. Amer. Spec. Paper, no.232, pp.95-111.

Honarpour Mehdi, Koederitz Leonard and Harve A. Herbert 1982, “Relative Permeability of Petroleum Reservoirs”, Boca Raton, Florida: CRC Press, Inc.

Hassler G.L. and Brunner E.: “Measurement of Capillary Pressure in Small Core Samples”, AIME, 1945 Vol. 160, 114.

Hjelmeland O. and Torsæter O.: “Coring and Core Analysis”, SINTEF Report, Trondheim, 1984.

Iqbal, M.W.A. and Shah, S.M.I. (1980) A guide to the stratigraphy of Pakistan, Quetta. Geol. Surv. Pakistan Rec., v.53, pp.34

Johnson E.F.: “Calculation of Relative Permeability from Displacement Experiments”, AIME, 1959, vol. 216, 370.

Jaswal, T., R.J. Lillie and R.D. Lawrence, 1997. Structure and evolution of northern Potwar deformed zone, Pakistan. Am.Assoc. Geol. Bull., v.81, p. 308-318.

Koederitz L.F., Harvey A.H. and Honarpour M.: “Introduction to Petroleum Reservoir Analysis; Laboratory Workbook”, Gulf Pub. Co., 1989.

Kobesh, F. P. and Blizard, R. B., 1959, Geometric Factors in Sonic Logging: Geophysics, v.24, pp. 64-76.

Khalid Perveiz, QamarYasin, GmdSohail, and Jam Muhammad Kashif."Integrating core and wire-line log data to evaluate porosity of Jurassic formations of Injra-1 and Nuryal-2 wells, Western Potwar, Pakistan", Journal of the Geological Society of India ,2015.

Khan, M.A., R. Ahmed, H.A. Raza and A. Kemal, 1986, Geology of petroleum in Kohat-Potwar depression, Pakistan.Bull.Amer.Assoc.Petrol. Geol., v. 70, no.4.p.369-414.

Kemal, A., 1992, Geology and New trends for petroleum exploration in Pakistan; In: Ahmad, G (ed.). Proceedings of an Int. petroleum seminar on new directions and strategies for accelerating petroleum exploration and production in Pakistan.p.16-57.

Lyons, W. C. (1996). Standard Handbook of Petroleum & Natural Gas Engineering Volume1. Houston, Texas: Gulf Publishing Company.

Lawrence M. Anovitz and David R. Cole, January 2015, Characterization and Analysis of Porosity and Pore Structures, Mineralogical Society of America.

Norman R. Morrow, S. N. (1990, December). Wettability and Its Effect on Oil Recovery. Journal of Petroleum Technology, 42(12), 1476-1484.

Muhammad Kaleem A.Q., Shahid Ghazi and Aftab Ahmed Butt Geology Of The Lower Jurassic Datta Formation, Kala Chitta Range, PakistanGeol. Bull. Punjab Univ. Vol. 40-41, 2005-6, pp 27-44

Park, A., “Improved Oil Saturation Data Using Sponge Core Barrel,” SPE Production Operations Symposium, February 27 - March 1, 1983, Oklahoma City, OK, p. 87-91.

Pettijohn, F. F. (1987). Sand and Sandstone.Springer.

Paul F. Worthington, August 1994, Effective integration of core and log data, Marine and Petroleum Geology, Publisher Elsevier.

Qadri, I.B. (1995) Petroleum Geology of Pakistan, Pakistan Petroleum Limited Publication, pp.18-35.

R.Worden, S. M. (2009).Quartz Cementation in Sandstones; Special Publication 29 of the IAS.Wiley.

Sattler, A. R., Heckes, A. A., and Clark, J. A., “Pressure Core Measurements in Tight Sandstone Lenses During the Multiwell Experiment,” SPE Formation Evaluation Journal (1988), 645-650

Serra, Oberto1984, “Fundamentals of Well Log Interpretation” Elsevier Science Publishing Company INC 52, Vanderbilt Avenue New York, NY 10017, U.S.A

Shah, S.M.I., Ahmed, R., Cheema, M.R., Fatmi, A.N., Iqbal, M.W.A., Raza, H.A. and Raza, S.M. (1977) Stratigraphy of Pakistan. Geol. Surv. Pakistan, Mem., no.12, pp.137

Scheidegger, A. E. (1974). The Physics of flow through porous media. Toronto, Canada: University of Toronto Press.

Skopec, R. A., Mann, M. M., Jeffers, D., and Grier, S. P., “Horizontal Core Acquisition and Orientation for Formation Evaluation,” Society of Petroleum Engineers Drilling Journal, Vol. 7, No. 1, p. 47-54, 1992

Tiab, Djebbar Donaldson, Erle C.. (2004). Petrophysics - Theory and Practice of Measuring Reservoir Rock and Fluid Transport Properties (2nd Edition). Elsevier.

Treiber, L.E., D.L. Archer, and W.W.Owens, 1972, A Laboratory Evaluation of the Wettability of Fifty Oil producing reservoirs, Presented at the Society of Petroleum Engineers 46th Annual Fall Meeting, October 3-6, New Orleans, SPE Journal, SPE Paper 3526, v.12, no.6, p. 531-540.

Tracy, H. B. (1996). Petrology(Second Edition); (Igneous, Sedeimentary, and Metamorphic). New York: W.H Freeman and Company.

Tarek Ahmed, P. P. (2001). Reservoir Engineering Handbook. Texas: GUlf Professional Publishing.

Welge, H.J.: "Simplified Method for Computing Oil Recovery by Gas or Water Drive", AIME, 1952, Vol. 195, 91.

Wyllie M.R.J. and Spangler M.B.: "Application of Electrical Resistivity Measurements to Problem of Fluid Flow in Porous Media", Bull. AAPG, Feb. 1952, p. 359.

Wandrey, C.J., Law, B.E. and Shah, H. A. (2004a) Patala-NammalCompositeTotal Petroleum System, Kohat-Potwar Geologic Province, Pakistan. USGS Bull.b2208-b.http://pubs.usgs.gov/bul/b2208-c/

Wilson, J. R. (1995). A Collector's Guide to Rock, Mineral, & Fossil Localities of Utah. Utah: Utah Geological Survey Miscellanous Publication 95A.

Yeats, R.S. and Lawrence, R.D. (1984) Tectonics of the Himalayan thrust belt in northern Pakistan. In:B.U. Haq and J.D. Milliman (Eds.), Marine geology and oceanography of the Arabian Sea and coastal Pakistan. New York, Van Nostrand Reinhold, pp.117-198.

Yu-shu wu, Karsten Pruess and Peter Persoff (23 February 1998), Gas Flow in Porous Media with Klinkenberg Effects, Transport in Porous Media 32: 117–137, 1998, Kluwer Academic Publishers. Printed in the Netherlands.

Appendix-I

Details of well A Core and Log values at similar depth

Depth (m)	Log Density (RHOB)	Core Density (RHOB)	Log Porosity (Fraction)	Core Porosity (Fraction)	Log Permeability (md)	Core Permeability (md)
4600	2.115	2.2	0.261	0.3	40.5481	103
4600.125	2.063		0.315		124.4256	
4600.25	2.054		0.344		182.1879	
4600.375	2.077		0.344		153.4224	
4600.5	2.107		0.333		102.7532	
4600.625	2.137		0.318		65.6803	
4600.75	2.167		0.303		45.5188	
4600.875	2.201		0.284		35.1081	
4601	2.246		0.266		27.1971	
4601.125	2.283		0.242		20.4402	
4601.25	2.306		0.214		14.7364	
4601.375	2.307		0.186		8.7966	
4601.5	2.295		0.158		3.7219	
4601.625	2.323		0.126		0.8523	
4601.75	2.37		0.102		0.1699	
4601.875	2.397	2.5	0.09	0.26	0.0579	1.7589
4602	2.393		0.09		0.0406	
4602.125	2.351		0.105		0.0539	
4602.25	2.271		0.135		0.0995	
4602.375	2.222		0.182		0.3167	
4602.5	2.206		0.213		0.6593	
4602.625	2.209		0.235		1.1992	
4602.75	2.216		0.244		1.608	
4602.875	2.214		0.242		1.5638	
4603	2.212		0.245		2.3203	
4603.125	2.214		0.237		2.2104	
4603.25	2.236		0.225		1.4472	
4603.375	2.271		0.211		0.8141	
4603.5	2.308		0.199		0.5185	
4603.625	2.331		0.191		0.487	
4603.75	2.33		0.19		0.6753	
4603.875	2.33	2.3	0.198	0.22	0	13.2622
4604	2.316		0.198		2.031	
4604.125	2.323		0.196		1.9661	
4604.25	2.343		0.191		1.8845	
4604.375	2.371		0.199		2.0846	

Depth (m)	Log Density (RHOB)	Core Density (RHOB)	Log Porosity (Fraction)	Core Porosity (Fraction)	Log Permeability (md)	Core Permeability (md)
4604.5	2.377		0.212		2.2823	
4604.625	2.383		0.219		3.3382	
4604.75	2.398		0.216		4.6599	
4604.875	2.433		0.207		4.5927	
4605	2.483		0.223		2.8486	
4605.125	2.438		0.262		2.9692	
4605.25	2.336		0.294		5.2646	
4605.375	2.231		0.308		9.6133	
4605.5	2.134		0.3		16.2535	
4605.625	2.056		0.273		22.7523	
4605.75	2.013		0.237		23.5575	
4605.875	2.062	2.1	0.204	0.34	15.6201	12.1595
4606	2.149		0.191		7.552	
4606.125	2.223		0.201		4.4742	
4606.25	2.261		0.229		4.2889	
4606.375	2.26		0.269		5.8524	
4606.5	2.223		0.28		8.4167	
4606.625	2.234		0.278		8.4506	
4606.75	2.274		0.269		6.7709	
4606.875	2.326		0.263		5.5865	
4607	2.369		0.272		5.2922	
4607.125	2.374		0.302		5.1345	
4607.25	2.253		0.331		6.5493	
4607.375	2.115		0.352		5.5947	
4607.5	1.993		0.363		4.17	
4607.625	1.913		0.362		2.5076	
4607.75	1.895		0.35		1.0154	
4607.875	1.95	1.9	0.355	0.26	0.4706	16.09
4608	1.959		0.365		0.3707	
4608.125	1.945		0.374		0.959	
4608.25	1.932		0.372		3.6089	
4608.375	1.957		0.352		11.0041	
4608.5	2.052		0.336		21.1595	
4608.625	2.145		0.333		22.2602	
4608.75	2.16		0.339		18.4734	
4608.875	2.111		0.342		10.94	
4609	2.04		0.328		5.6361	
4609.125	1.99		0.294		4.1239	
4609.25	1.987		0.259		5.4599	
4609.375	1.999		0.25		5.7735	

Depth (m)	Log Density (RHOB)	Core Density (RHOB)	Log Porosity (Fraction)	Core Porosity (Fraction)	Log Permeability (md)	Core Permeability (md)
4609.5	2		0.261		6.1997	
4609.625	1.996		0.278		6.6648	
4609.75	1.996		0.292		5.6158	
4609.875	2.002	2	0.293	0.23	2.6425	0.3547
4610	2.021		0.291		0.1933	
4610.125	2.054		0.288		0.0023	
4610.25	2.093		0.284		0	
4610.375	2.128		0.28		0	
4610.5	2.155		0.28		0	
4610.625	2.171		0.276		0	
4610.75	2.185		0.272		0	
4610.875	2.213		0.266		0	
4611	2.246		0.26		0	
4611.125	2.269		0.262		0	
4611.25	2.266		0.283		0	
4611.375	2.213		0.303		0	
4611.5	2.156		0.311		0	
4611.625	2.113		0.317		0	
4611.75	2.064		0.327		0	
4611.875	1.996	1.9	0.344	0.4	0	14.4535
4612	1.922		0.366		0.0027	
4612.125	1.884		0.371		0.9015	
4612.25	1.896		0.366		10.1847	
4612.375	1.928		0.355		24.3718	
4612.5	1.966		0.341		25.5983	
4612.625	1.999		0.329		19.8685	
4612.75	2.02		0.325		18.2073	
4612.875	2.027		0.323		21.5217	
4613	2.028		0.319		23.4164	
4613.125	2.028		0.304		26.0753	
4613.25	2.034		0.272		27.0011	
4613.375	2.052		0.275		17.9812	
4613.5	1.954		0.281		9.2967	
4613.625	1.865		0.29		4.2589	
4613.75	1.784		0.301		2.5712	
4613.875	1.729	2	0.316	0.14	2.2281	6.5664
4614	1.709		0.345		2.7046	
4614.125	1.705		0.367		6.2562	
4614.25	1.713		0.379		7.6284	
4614.375	1.741		0.38		9.3726	

Depth (m)	Log Density (RHOB)	Core Density (RHOB)	Log Porosity (Fraction)	Core Porosity (Fraction)	Log Permeability (md)	Core Permeability (md)
4614.5	1.782		0.375		12.6217	
4614.625	1.827		0.374		17.8229	
4614.75	1.858		0.391		23.3965	
4614.875	1.827		0.409		12.0648	
4615	1.807		0.418		3.7837	
4615.125	1.816		0.418		1.1857	
4615.25	1.84		0.409		0.7534	
4615.375	1.851		0.401		1.1924	
4615.5	1.811		0.394		2.1001	
4615.625	1.759		0.394		1.2388	
4615.75	1.73		0.396		0.7133	
4615.875	1.714	1.8	0.399	0.43	0.5733	0.56509
4616	1.704		0.402		0.6322	
4616.125	1.696		0.402		0.7387	
4616.25	1.686		0.394		1.3616	
4616.375	1.703		0.367		1.1658	
4616.5	1.773		0.316		1.249	
4616.625	1.907		0.241		1.5793	
4616.75	2.106		0.148		1.3355	
4616.875	2.351		0.089		0.3044	
4617	2.492		0.061		0.0316	
4617.125	2.557		0.053		0.005	
4617.25	2.581		0.055		0.0025	
4617.375	2.584		0.062		0.0038	
4617.5	2.577		0.065		0.0091	
4617.625	2.569		0.074		0.0142	
4617.75	2.545		0.098		0.0351	
4617.875	2.502	2.5	0.146	0.24	0.2038	130.6283
4618	2.426		0.225		2.822	
4618.125	2.306		0.324		48.636	
4618.25	2.139		0.42		185.7754	
4618.375	1.978		0.466		250.1592	
4618.5	1.88		0.485		270.0615	
4618.625	1.836		0.484		281.21	
4618.75	1.833		0.466		293.7671	
4618.875	1.859		0.437		237.1511	
4619	1.905		0.401		178.3009	
4619.125	1.951		0.37		276.7851	
4619.25	1.991		0.346		62.3188	
4619.375	2.027		0.329		2.8442	

Depth (m)	Log Density (RHOB)	Core Density (RHOB)	Log Porosity (Fraction)	Core Porosity (Fraction)	Log Permeability (md)	Core Permeability (md)
4619.5	2.056		0.316		0.017	
4619.625	2.07		0.307		0	
4619.75	2.07		0.31		0	
4619.875	2.045	2	0.33	0.2	0	0.326575
4620	1.992		0.359		0	
4620.125	1.926		0.388		0	
4620.25	1.87		0.404		0	
4620.375	1.846		0.394		0	
4620.5	1.884		0.373		0	
4620.625	1.936		0.34		0	
4620.75	2.013		0.295		0	
4620.875	2.119		0.24		0.0663	
4621	2.239		0.191		1.5883	
4621.125	2.319		0.204		0.6069	
4621.25	2.226		0.219		0.6854	
4621.375	2.138		0.221		0.7165	
4621.5	2.102		0.204		0.7376	
4621.625	2.131		0.165		0.659	
4621.75	2.237		0.134		0.1652	
4621.875	2.352	2.3	0.109	0.25	0.0458	0.7957
4622	2.436		0.092		0.0132	
4622.125	2.494		0.079		0.0051	
4622.25	2.533		0.072		0.0026	
4622.375	2.557		0.076		0.0016	
4622.5	2.558		0.104		0.0027	
4622.625	2.518		0.141		0.0183	
4622.75	2.459		0.178		0.109	
4622.875	2.396		0.209		0.4609	
4623	2.341		0.228		1.3612	
4623.125	2.306		0.231		2.4522	
4623.25	2.308		0.229		2.6714	
4623.375	2.322		0.226		1.845	
4623.5	2.338		0.221		1.2681	
4623.625	2.354		0.215		1.1333	
4623.75	2.375		0.197		1.3417	
4623.875	2.418	2.5	0.165	0.18	1.4073	0.1368
4624	2.449		0.158		0.6248	
4624.125	2.427		0.175		0.1441	
4624.25	2.358		0.211		0.0134	
4624.375	2.269		0.249		0	

Depth (m)	Log Density (RHOB)	Core Density (RHOB)	Log Porosity (Fraction)	Core Porosity (Fraction)	Log Permeability (md)	Core Permeability (md)
4624.5	2.204		0.267		0	
4624.625	2.199		0.267		0	
4624.75	2.213		0.262		0	
4624.875	2.229	2.2	0.259	0.23	0	0
4625	2.24		0.258		0	
4625.125	2.246		0.259		0	
4625.25	2.245		0.268		0	
4625.375	2.224		0.274		0	
4625.5	2.208		0.276		0	
4625.625	2.204		0.271		0	
4625.75	2.215		0.262	0.24	0	0
4625.875	2.24	2.2			0	

Details of well B Core and Log values at similar depth

Depth (m)	Log Density (RHOB)	Core Density (RHOB)	Log Porosity (Fraction)	Core Porosity (Fraction)	Log Permeability (md)	Core Permeability (md)
4735	2.507	2.53	0.069	0.06	0.0096	0.446
4735.125	2.51		0.068		0.0107	
4735.25	2.5		0.072		0.0183	
4735.375	2.436		0.097		0.0914	
4735.5	2.439		0.098		0.0933	
4735.625	2.443		0.098		0.081	
4735.75	2.486		0.083		0.0393	
4735.875	2.534		0.066		0.0139	
4736	2.547	2.36	0.061	0.132	0.0093	
4736.125	2.545		0.061		0.0106	
4736.25	2.488		0.08		0.0326	
4736.375	2.469		0.092		0.0509	
4736.5	2.457		0.102		0.0604	
4736.625	2.431		0.115		0.0733	
4736.75	2.391		0.129		0.1199	
4736.875	2.365		0.132		0.112	
4737	2.364	2.37	0.129	0.134	0.1389	0.561
4737.125	2.363		0.13		0.1921	
4737.25	2.341		0.141		0.3779	
4737.375	2.294		0.163		0.9528	
4737.5	2.249		0.186		1.4825	
4737.625	2.283		0.173		0.792	
4737.75	2.337		0.152		0.362	
4737.875	2.379		0.134		0.1904	
4738	2.398	2.1	0.126	0.242	0.1516	
4738.125	2.399		0.129		0.19	
4738.25	2.383		0.14		0.2216	
4738.375	2.362		0.15		0.3113	
4738.5	2.333		0.161		0.3551	
4738.625	2.299		0.173		0.445	
4738.75	2.24		0.195		0.719	
4738.875	2.102		0.242		0.7901	
4739	2.056	2.46	0.275	0.171	0.2919	2.184
4739.125	2.03		0.299		0.2118	
4739.25	1.994		0.315		0.6449	
4739.375	1.968		0.318		3.1556	
4739.5	1.992		0.304		7.5367	
4739.625	2.068		0.285		3.7327	

Depth (m)	Log Density (RHOB)	Core Density (RHOB)	Log Porosity (Fraction)	Core Porosity (Fraction)	Log Permeability (md)	Core Permeability (md)
4739.75	2.322		0.216		0.4619	
4739.875	2.463		0.171		0.1119	
4740	2.512	2.42	0.142	0.274	0.0552	
4740.125	2.519		0.119		0.0367	
4740.25	2.51		0.111		0.0366	
4740.375	2.511		0.111		0.0409	
4740.5	2.456		0.148		0.1237	
4740.625	2.423		0.196		0.1701	
4740.75	2.417		0.242		0.0543	
4740.875	2.42		0.274		0.0014	
4741	2.444	2.43	0.279	0.235	0	0
4741.125	2.46		0.265		0	
4741.25	2.456		0.27		0	
4741.375	2.395		0.286		0	
4741.5	2.308		0.303		0	
4741.625	2.274		0.306		0	
4741.75	2.29		0.279		0	
4741.875	2.433		0.235		0	
4742	2.566	2.6	0.194	0.164	0	
4742.125	2.647		0.17		0	
4742.25	2.67		0.166		0	
4742.375	2.638		0.174		0	
4742.5	2.64		0.176		0	
4742.625	2.63		0.179		0	
4742.75	2.618		0.176		0	
4742.875	2.609		0.164		0.0453	
4743	2.603	2.56	0.143	0.056	0.4744	1
4743.125	2.619		0.109		0.2054	
4743.25	2.627		0.074		0.0218	
4743.375	2.638		0.043		0.0008	
4743.5	2.635		0.026		0	
4743.625	2.611		0.027		0	
4743.75	2.592		0.038		0.0002	
4743.875	2.56		0.056		0.0016	
4744	2.55	2.6	0.067	0.049	0.0046	0.03
4744.125	2.551		0.069		0.0068	
4744.25	2.56		0.065		0.0049	
4744.375	2.581		0.058		0.0016	
4744.5	2.601		0.05		0.0003	

Depth (m)	Log Density (RHOB)	Core Density (RHOB)	Log Porosity (Fraction)	Core Porosity (Fraction)	Log Permeability (md)	Core Permeability (md)
4744.625	2.608		0.047		0.0002	
4744.75	2.608		0.047		0.0005	
4744.875	2.605		0.049		0.002	
4745	2.602	2.52	0.052	0.117	0.0065	0.2
4745.125	2.612		0.054		0.0089	
4745.25	2.619		0.054		0.0079	
4745.375	2.615		0.059		0.0139	
4745.5	2.609		0.066		0.029	
4745.625	2.598		0.076		0.0744	
4745.75	2.573		0.093		0.2542	
4745.875	2.527		0.117		0.8743	
4746	2.423	2.41	0.154	0.156	4.2472	
4746.125	2.329		0.186		12.0686	
4746.25	2.279		0.203		21.8416	
4746.375	2.279		0.204		25.9344	
4746.5	2.307		0.195		18.581	
4746.625	2.355		0.177		10.9621	
4746.75	2.391		0.168		7.5267	
4746.875	2.411		0.156		4.1612	
4747	2.406	1.83	0.145	0.314	2.4457	77.8016
4747.125	2.377		0.142		2.1836	
4747.25	2.351		0.143		2.0503	
4747.375	2.292		0.163		5.3146	
4747.5	2.185		0.203		23.4572	
4747.625	2.039		0.252		97.5986	
4747.75	1.898		0.295		172.5128	
4747.875	1.835		0.314		276.8507	
4748	1.847	2.03	0.308	0.246	250.0554	178.1695
4748.125	1.911		0.287		197.9386	
4748.25	1.946		0.276		142.3318	
4748.375	1.948		0.275		135.3804	
4748.5	1.938		0.278		152.1253	
4748.625	1.945		0.274		157.697	
4748.75	1.985		0.26		128.1151	
4748.875	2.032		0.246		101.7126	
4749	2.072	2.1	0.235	0.23	75.4251	52.6334
4749.125	2.111		0.224		51.9392	
4749.25	2.162		0.21		34.2481	
4749.375	2.201		0.198		25.9622	

Depth (m)	Log Density (RHOB)	Core Density (RHOB)	Log Porosity (Fraction)	Core Porosity (Fraction)	Log Permeability (md)	Core Permeability (md)
4749.5	2.208		0.195		30.5177	
4749.625	2.164		0.207		51.1798	
4749.75	2.121		0.221		74.117	
4749.875	2.101		0.23		77.6787	
4750	2.065	1.67	0.243	0.35	86.9787	
4750.125	2.003		0.263		124.524	
4750.25	1.923		0.283		197.2637	
4750.375	1.837		0.306		174.9891	
4750.5	1.765		0.327		199.753	
4750.625	1.718		0.339		178.7915	
4750.75	1.677		0.351		188.5763	
4750.875	1.679		0.35		198.9182	
4751	1.683	1.91	0.349	0.359	195.2437	168.7243
4751.125	1.689		0.343		157.9175	
4751.25	1.694		0.338		120.3754	
4751.375	1.696		0.357		101.9714	
4751.5	1.745		0.363		89.5329	
4751.625	1.798		0.374		104.1489	
4751.75	1.863		0.369		68.9426	
4751.875	1.911		0.359		33.428	
4752	1.919	1.85	0.361	0.375	20.5678	
4752.125	1.906		0.362		12.6897	
4752.25	1.889		0.37		29.5943	
4752.375	1.871		0.37		35.2976	
4752.5	1.86		0.372		31.2376	
4752.625	1.857		0.376		25.4952	
4752.75	1.854		0.375		18.6407	
4752.875	1.854		0.375		20.2988	
4753	1.855	1.76	0.374	0.368	34.9374	
4753.125	1.859		0.374		46.7507	
4753.25	1.846		0.38		61.8889	
4753.375	1.814		0.396		95.6256	
4753.5	1.817		0.397		99.0919	
4753.625	1.837		0.379		66.8461	
4753.75	1.817		0.363		49.1248	
4753.875	1.763		0.368		51.0862	
4754	1.748	1.62	0.365	0.326	49.2555	46.7093
4754.125	1.841		0.31		22.1857	
4754.25	1.723		0.34		49.1415	

Depth (m)	Log Density (RHOB)	Core Density (RHOB)	Log Porosity (Fraction)	Core Porosity (Fraction)	Log Permeability (md)	Core Permeability (md)
4754.375	1.708		0.332		38.3718	
4754.5	1.588		0.355		59.1098	
4754.625	1.534		0.361		70.5834	
4754.75	1.628		0.326		40.0102	
4754.875	1.625		0.326		45.017	
4755	1.815	1.62	0.268	0.327	11.751	30.4243
4755.125	1.766		0.283		11.0824	
4755.25	1.715		0.299		12.5942	
4755.375	1.654		0.317		18.9579	
4755.5	1.496		0.365		48.7899	
4755.625	1.613		0.331		27.7761	
4755.75	1.624		0.326		21.7847	
4755.875	1.624		0.327		18.6588	

Details of well C Core and Log values at similar depth

Depth (m)	Log Density (RHOB)	Core Density (RHOB)	Log Porosity (Fraction)	Core Porosity (Fraction)	Log Permeability (md)	Core Permeability (md)
4493.09	2.441	2.5	0.239	0.22	0	51.32
4493.34	2.378		0.231		0	
4493.65	2.341		0.223		0	
4493.92	2.311		0.225		0.2135	
4494.08	2.298	2.32	0.21	0.14	0.3611	3.74
4494.33	2.265		0.206		0.829	
4494.62	2.262		0.204		0.344	
4494.87	2.268		0.191		0.0033	
4495.27	2.364	2.64	0.172	0.27	0.0031	0.065
4495.52	2.363		0.165		0.0126	
4495.76	2.286		0.181		0.0653	
4495.97	2.262		0.188		0.1707	
4496.33	2.22	2.32	0.204	0.22	0.7166	0.083
4496.7	2.203		0.226		0.2418	
4496.98	2.201		0.229		0.2227	
4497.25	2.22	2.42	0.229	0.24	0.2899	0.12
4497.49	2.258		0.212		0.0722	
4497.78	2.335		0.195		0.0003	
4498.1	2.376	2.4	0.19	0.23	0	0.097
4498.46	2.289		0.186		0	
4498.84	2.182		0.175		0.0005	
4499.23	2.215	2.2	0.181	0.3	0.0947	0.13
4499.52	2.243		0.18		0.1983	
4499.81	2.311		0.184		0.3166	
4500.07	2.364	2.64	0.187	0.22	0.6459	0.5
4500.32	2.405		0.192		0.1493	
4500.57	2.476		0.194		0.1106	
4500.83	2.535		0.188		0.035	
4501.19	2.6	2.65	0.181	0.12	0.0102	0.24
4501.5	2.566		0.175		0.1978	
4501.82	2.527		0.175			

Details of well D Core and Log values at similar depth

Depth (m)	Log Density (RHOB)	Core Density (RHOB)	Log Porosity (Fraction)	Core Porosity (Fraction)	Log Permeability (md)	Core Permeability (md)
4516	2.507	2.53	0.314	0.35	18.6492	
4516.125	2.51		0.313	0.31	23.4035	
4516.25	2.5		0.319		31.2644	
4516.375	2.436		0.329		44.7554	
4516.5	2.439		0.322		46.548	
4516.625	2.443		0.298		34.6024	
4516.75	2.486		0.262		18.9436	
4516.875	2.534		0.198		4.5366	
4517	2.547	2.36	0.144	0.16	0.8968	
4517.125	2.545		0.129		0.6275	
4517.25	2.488		0.138		1.2938	
4517.375	2.469		0.153		4.1844	1.2
4517.5	2.457		0.158		6.7756	
4517.625	2.431		0.16		7.2997	
4517.75	2.391		0.161	0.11	6.1774	106
4517.875	2.365	2.38	0.154		4.3842	100
4518	2.364		0.135		1.895	
4518.125	2.363		0.133	0.12	1.5227	
4518.25	2.341		0.153	0.2	2.689	161
4518.375	2.294		0.188		5.4565	
4518.5	2.249		0.221		6.9631	81
4518.625	2.283		0.235		4.0417	
4518.75	2.337		0.219		0.8137	
4518.875	2.379		0.203	0.21	0.1182	27
4519	2.398	2.1	0.172		0.0101	
4519.125	2.399		0.141		0.0009	
4519.25	2.383		0.134	0.15	0.0003	7.2
4519.375	2.362		0.135		0.0004	
4519.5	2.333		0.143	0.11	0.0005	67
4519.625	2.299		0.155		0.0005	
4519.75	2.24		0.16		0.0004	
4519.875	2.102		0.162		0.0003	56
4520	2.056	2.53	0.187		0.0004	
4520.125	2.03		0.204		0.0006	177
4520.25	1.994		0.221		0.001	
4520.375	1.968		0.241		0.0043	
4520.5	1.992		0.256		0.0269	
4520.625	2.068		0.259	0.22	0.1028	125
4520.75	2.322		0.252		0.2035	

Depth (m)	Log Density (RHOB)	Core Density (RHOB)	Log Porosity (Fraction)	Core Porosity (Fraction)	Log Permeability (md)	Core Permeability (md)
4520.875	2.463		0.222	0.21	0.2728	0.39
4521	2.512	2.42	0.199		0.3782	
4521.125	2.519		0.184	0.2	0.5339	27
4521.25	2.51		0.172		0.8119	
4521.375	2.511		0.162		1.3884	
4521.5	2.456		0.162		1.8827	
4521.625	2.423		0.154		1.4376	
4521.75	2.417		0.138		0.4789	
4521.875	2.42		0.13		0.1508	
4522	2.444	2.43	0.143		0.0953	
4522.125	2.46		0.166		0.0659	
4522.25	2.456		0.193		0.0935	

Appendix-II

Gas-Oil relative permeability			
Sample No. REL-01 **(Depth:** 4451 m**)**			
Sg (Percent Pore Space)	**Krg/Kro** (Fraction)	**Krg** (Fraction)	**Kro** (Fraction)
0	0	0	1
5.7	0.08	0.04	0.51
7.0	0.121	0.052	0.43
8.7	0.18	0.064	0.355
10.2	0.25	0.08	0.30
12.0	0.30	0.10	0.30
13.1	0.51	0.11	0.22
15.7	0.90	0.14	0.15
20.6	2.42	0.21	0.09
23.0	3.50	0.20	0.10
25.2	5.90	0.28	0.05
29.5	13.5	0.337	0.025
35.0	36.3	0.435	0.012
37.6	52.6	0.471	0.009
Sample No. REL-02 **(Depth:** 4456 m)			
Sg (Percent Pore Space)	**Krg/Kro** (Fraction)	**Krg** (Fraction)	**Kro** (Fraction)
0	0	0	1
9.7	0.09	0.04	0.5
11.2	0.136	0.058	0.424
13.0	0.191	0.071	0.369
14.5	0.25	0.08	0.34
16.0	0.30	0.10	0.30
21.8	0.73	0.14	0.20
26.2	1.37	0.18	0.13
30.2	2.35	0.23	0.10
34.0	4.10	0.30	0.10
38.5	7.37	0.33	0.04
43.3	14.0	0.384	0.027
49.2	31.3	0.442	0.014
Sample No. REL-03 (**Depth:** 4457m**)**			
Sg (Percent Pore Space)	**Krg/Kro** (Fraction)	**Krg** (Fraction)	**Kro** (Fraction)
0	0	0	1
4.0	0.06	0.04	0.69
5.4	0.087	0.052	0.601
7.3	0.125	0.063	0.505
8.9	0.17	0.07	0.43
10	0.20	0.10	0.40
13.1	0.36	0.10	0.29
17.3	0.72	0.14	0.19
20.0	1.1	0.17	0.15
24.0	1.9	0.20	0.10
28.3	3.91	0.25	0.06
33.1	8.58	0.313	0.036
37.2	18.4	0.373	0.02
40.6	35.2	0.441	0.013
Sample No. REL-04 (**Depth:** 4492m)			
Sg (Percent Pore Space)	**Krg/Kro** (Fraction)	**Krg** (Fraction)	**Kro** (Fraction)
0	0	0	1
6.9	0.07	0.04	0.52
8.0	0.095	0.044	0.446
9.4	0.13	0.054	0.414
10.7	0.17	0.06	0.37
14	0.30	0.10	0.30
20.2	0.90	0.14	0.15
22.9	1.56	0.17	0.11
25.3	2.20	0.19	0.09
30.0	4.50	0.30	0.10
34.0	10.4	0.31	0.03
38.2	24.1	0.375	0.016
40.8	42.4	0.447	0.011

Water-Oil relative permeability			
Sample No. REL-05 (**Depth:** 44501m)			
Sg (Percent Pore Space)	**Krg/Kro** (Fraction)	**Krg** (Fraction)	**Kro** (Fraction)
0	0	0	1
7.10	0.02	0.01	0.79
8.70	0.026	0.018	0.68
10.6	0.039	0.024	0.61
12.3	0.06	0.03	0.54
14.0	0.10	0	0.50
16.3	0.12	0.05	0.40
20.1	0.25	0.07	0.29
22.0	0.41	0.10	0.23
24.0	0.60	0.10	0.20
28.4	1.37	0.16	0.12
32.0	2.88	0.208	0.072
34.4	5.01	0.266	0.053
37.1	7.82	0.305	0.039
41.9	23.3	0.426	0.018
45.4	618	0.529	0.0086

Residual Gas Saturation by Imbibition

Sample ID		**Depth in Meters**	**Permeability to Air Milidarcey**	**Porosity Percent**	**Initial Liquid saturation, Perecent Pore Space**	**Residual Gas Saturation, Percent Pore Space**	**Gas Displaced Percent Pore Space**
Well D	REL-04	4492.81	117	10.6	3.3	52.5	44.2
	REL-05	4501.82	2.1	10.7	13.5	38	48.5
Well C	REL-01	4451.45	63	10.1	4.4	49.3	46.3
	REL-02	4456.57	220	12.6	5.4	61.8	32.8
	REL-03	4456.84	9.4	8.4	6.9	53	40.1

Formation Resistivity as a Function of Overburden Pressure

Formation Resistivity as a Function of Overburden Pressure								
Saturant		Simulated Formation Brine			**Effective Over Burden Pressure, Psi**			
Resistivity of Saturant: 0.115 Ohem-meters at 77^{O}F					0	200	3700	7400
Sample ID		Depth in Meters	Permeability to Air Milidarcey	Porosity Percent	**Formation Resistivity Factor**			
Well C	REL-01	4451.45	63	10.1	50.2	57.9	76.3	81.5
	REL-02	4456.57	220	12.6	36.4	42.5	52.2	54.7
	REL-03	4456.84	9.4	8.4	62.1	74.1	116	141
Well D	REL-04	4492.81	117	10.6	44	50.8	63.9	68.5
	REL-05	4501.82	2.1	10.7	40.2	49.9	73.3	85.9
					Porosity, Percent			
Well C	REL-01	4451.45	63		10.1	9.7	9.1	8.9
	REL-02	4456.57	220		12.6	12.2	11.5	11.4
	REL-03	4456.84	9.4		8.4	8.1	7.4	7.3
Well D	REL-04	4492.81	117		10.6	10.2	9.5	9.4
	REL-05	4501.82	2.1		10.7	10.4	10.2	10.1

The summary of capillary pressure test data is shown below:

Summary of capillary pressure test

Fluid System		Air-Water(Drainage)											
Test Method		High Speed Centrifuge	Pressure, Psi	1	2	5	10	25	50	100	200	500	1000
Sample ID	Depth in Meters	Permeability to Air Milidarcey	Porosity Percent	Brine Saturation , Percent Pore Space									
Well C	REL-01	4451.45	63	10.1	67.5	52.1	33.3	22.6	15	13	10.4	7.8	5.4	4.4
	REL-02	4456.57	220	12.6	31.3	27.5	20.5	16.3	11.9	10.4	9	8.8	7.1	5.4
	REL03	4456.84	9.4	8.4	100	72.6	50.5	34.7	21	16.5	13.8	11	8	6.9
Well D	REL-04	4492.81	117	10.6	56.4	37	23	15.4	9.6	7.2	6.1	4.8	3.8	3.3
	REL-05	4501.82	2.1	10.7	100	100	79.5	60.1	44.5	34	27.6	21	15.6	13.5

The tabulated formation resistivity index is given below:

Formation Resistivity Factor and Resistivity Index

Saturant: Simulated Formation Brine							
Resistivity Of Saturant 0.115 Ohem-Metrs at 77 ^{o}F							
Sample ID		Depth in Meters	Permeability to Air Milidarcey	Porosity Percent	Formation Resistivity Factor	Brine Saturation, Percent Pore Sapce	Resistivity Index
Well C	REL-01	4451.45	63	10.1	50.2	100	1
	REL-02	4456.57	220	12.6	36.4	100	1
	REL-03	4456.84	9.4	8.4	62.1	100	1
Well D	REL-04	4492.81	117	10.6	44	100	1
	REL-05	4501.82	2.1	10.7	40.2	100	1